Effects of the Martian Environment on its Surface Materials: Experimental Studies

Thesis by

Albert Shih-Yueh Yen

In partial fulfillment of the requirements

for the degree of

Doctor of Philosophy

California Institute of Technology

Pasadena, California

1998

(Submitted May 14, 1998)

To Mom and Dad for all of the support and encouragement over the years

and, of course, to Yenot, Pea, and Garbonzo.

Acknowledgements

I would like to thank the people who have contributed to this thesis. Bruce Murray was my primary advisor and guided my thinking about Mars and martian surface processes. George Rossman was also a principal advisor and helped to develop my understanding of mineralogy and the weathering of minerals. Bruce and George concentrating on the "big picture" and the details, respectively, were an excellent combination of faculty advisors. The experiments described in Chapters III and IV would not have been possible without the help and support of Frank Grunthaner, Vic Nenow, and JPL's MicroDevices Laboratory. Many others have also helped in discussions and reviews over the past five years, and I thank all of you.

Abstract

The past and present weathering processes active at the martian surface control the chemical and mineralogical nature of the soils. Determining the current characteristics of martian surface materials can, therefore, provide clues about the surface history of Mars. The research in this thesis is based on three sets of experiments. First, reflectance spectra are collected from Mars analog mineral samples in the laboratory and compared with spacecraft data. The results indicate that the water content of the martian soil is consistent with the 2% value obtained by the Viking Lander analyses, and this suggests a drier, more dehydrated soil than implied by much modeling of early Mars conditions. Second, ultraviolet radiation-induced dehydration of minerals is investigated as a possible method to convert the postulated large initial supply of hydrated mineral phases on Mars to the current, relatively anhydrous state. These experiments indicate that water adsorbed onto the surfaces of mineral grains can be ejected by incident ultraviolet photons, but that the removal of bound water from minerals is unlikely to be a significant weathering process on Mars. Thus, the inventory of hydrous minerals at the surface today is likely representative of the quantity that formed in the past. Finally, the possibility that ultraviolet radiation can stimulate the oxidation of materials on the martian surface is studied experimentally. The data show that the oxidation rate of metallic iron increases upon exposure to UV photons but that this process is unlikely to be an effective way to oxidize minerals on Mars. Suggestions for future laboratory experiments and spacecraft instruments which can further test the conclusions of this thesis are described.

Table of Contents

Acknowledgements iv
Abstract v

Chapter I: Introduction 1
1.1 Water on Mars 2
1.2 The Color of Mars 4
1.3 Future Tests 5

Chapter II: Water Content of the Martian Soil 6
2.1 Introduction 6
2.1.1 Hydrated Minerals on the Martian Surface 6
2.1.2 Strong OH Absorption in Near-IR Reflectance 7
2.1.3 In-Situ Analyses 7
2.1.4 Focus of this Study 8
2.1.5 Past Work 9
2.2 Experiment Description 11
2.2.1 Overview 11
2.2.2 Sample Preparation 11
2.2.3 Particle Size Considerations 12
2.2.4 Sample Characterization 13
2.2.5 Thermal Analysis of Water Content 14
2.2.6 Infrared Spectroscopy 15
2.2.7 Conversion to Absorbance 16
2.2.8 Results 17
2.3 Discussion 38
2.3.1 Comparison with Spacecraft Data 38
2.3.2 Upper Limit for Water Content 40
2.3.3 Spectral Shapes 41
2.3.4 Liquid, Frozen, and Adsorbed Water 42
2.4 Conclusions 45

Chapter III: Ultraviolet Radiation-Induced Desorption of Water 46
3.1 Introduction 46
3.1.1 Ultraviolet Radiation at the Martian Surface 46
3.1.2 Possible Effects of UV 47
3.1.3 New Experiments 48
3.2 Experiment Description 49
3.2.1 Apparatus 49
3.2.2 Samples 49
3.2.3 Procedure 50
3.2.4 Results 51
3.3 Source of the Observed Water 57
3.3.1 Vacuum Chamber Contamination 57
3.3.2 OH from the Crystal Structure 57
3.3.3 Adsorbed Water 58
3.4 Mechanism 60
3.4.1 Thermal ? 60
3.4.2 Electronic Interactions 60

3.4.2.1 Substrate Interaction 61
3.4.2.2 Effects at the Grain Surface 61
3.5 Application to Mars 64
3.5.1 Water on Soil Surfaces 64
3.5.2 Interlayer Water 65
3.5.3 Bound OH 66
3.5.3.1 Surface Soil 67
3.5.3.2 Suspended Dust 68
3.5.3.3 Implications for the History of Water 69
3.6 Conclusions 71

Chapter IV: Investigations of Ultraviolet Radiation-Stimulated Oxidation 72
4.1 Introduction 72
4.1.1 Weathering Processes on Mars 72
4.1.2 Ultraviolet Radiation Weathering 74
4.1.3 New Experiments 75
4.2 Experiment Description 76
4.2.1 Thin-film Sensors 76
4.2.2 Apparatus 76
4.2.3 Samples 79
4.2.4 Procedure 79
4.2.5 Results 81
4.3 Interpretation 92
4.3.1 Purge Gases 92
4.3.2 Ultraviolet Lamp in a Vacuum 93
4.3.3 Ultraviolet Lamp under "Dry" Nitrogen 95
4.4 Postulated Mechanism 97
4.5 Application to Mars 100
4.5.1 UV Weathering of Minerals 101
4.5.2 Weathering of Meteoritic Iron 103
4.6 Conclusions 104

Chapter V: Synthesis and Ideas 106
5.1 Water on Mars 106
5.2 The Color of Mars 109
5.3 Summary 111

Chapter VI: Future Tests 112
6.1 Laboratory Experiments 112
6.1.1 Dehydration of Minerals 112
6.1.2 Ultraviolet-Induced Oxidation 114
6.1.2.1 Thermal Effects 115
6.1.2.2 Photochemical Effects 115
6.1.2.3 Oxidation Products 116
6.2 Spacecraft Instruments 116
6.2.1 Thermal Emission Spectrometer 117
6.2.2 Thermal/Evolved Gas Analyzer (TEGA) 117
6.2.3 Deep Space 2 118

References 120

Chapter I: Introduction

The chemical and mineralogical nature of the martian soils contain signatures of past and present weathering processes. Determining the current characteristics of martian surface materials can, therefore, provide clues and constraints about the surface history of Mars. The experiments and analyses in this thesis research investigate the possible weathering mechanisms for martian minerals. Contrary to much of the published literature, the results suggest that, unlike Earth, interaction between liquid water and primary igneous products has not been a significant chemical weathering process on Mars. Furthermore, the abundant ferric oxides, I speculate, might be formed from meteoritic materials rather than aqueous weathering of local minerals as would be inferred by analogy with Earth.

1.1 Water on Mars

Geologic interpretations of spacecraft images indicate that the early martian climate (during Noachian times) was once much different than it is today and that liquid water may have been stable at the surface at that time. In contrast, there is a sharp change in global erosion rates between Noachian and Hesperian geologic units. Craters a few hundred meters in diameter formed in the early Hesperian (3.5 to 3.8 Gyr surface age) show very little degradation while 100 *kilometer* craters formed during the Noachian have flat floors and barely retain their crater rims [*Carr,* 1996]. *Craddock and Maxwell* [1993] attribute the erosion of the Noachian units to fluvial processes following precipitation.

The presence of ancient "valley networks" carved into early Noachian units also is cited to support the idea that liquid water was once stable at the martian surface. These features have been widely interpreted as fluvial in origin and are believed to require warm (above freezing) surface temperatures to allow erosion over long distances and to resupply the water source by atmospheric or subsurface paths [*Carr,* 1996]. These valley networks on ancient geologic units are distinct from younger channels (e.g., the Ares Vallis region where Pathfinder landed) which are also of fluvial origin, but do not necessarily require the stability of liquid water at the martian surface. These younger features may have formed from a transient aqueous episode at low (sub-freezing) temperatures and rapidly developed a layer of protective ice.

The availability of liquid water at the surface has suggested to many that primary basaltic rocks and volcanic glasses could have been chemically altered to secondary, hydrated mineral phases. Weathering models have suggested that

palagonite, silicate clays, iron oxyhydroxides, jarosite, ferrihydrite, and other hydrous phases should be found in the martian soils [*e.g., Burns,* 1988; *Gooding and Keil,* 1978; *Zolotov*, 1983]. None of these hydrated minerals has yet been convincingly identified on Mars. Furthermore, in situ analyses of the surface materials by the Viking Landers indicate that they contain less than 2% water [*Biemann et al.*, 1977]. The recent evidence for relatively pristine, unweathered pyroxenes and plagioclase on Mars [*Christensen et al.,* 1998] also seems inconsistent with a global, aqueous, chemical weathering environment. Furthermore, climate models have difficulty explaining how temperatures consistent with liquid water at the surface could realistically be sustained [*Haberle et al.,* 1994]. Thus, a crucial question is whether Earth-like aqueous conditions and chemical weathering rates ever existed on Mars.

In this research, I confirm that the water content of the martian soil indicated by reflectance spectroscopy is consistent with the Viking Lander measurements (chapter II) and then explore the possibility that ultraviolet radiation could have converted the postulated abundant supply of hydrated minerals to the current, relatively anhydrous state (chapter III). I conclude that UV-stimulated dehydration of minerals has not been a significant weathering process on Mars. The inability to identify a mechanism in this work and other studies [*e.g., Pollack et al.,* 1970] for converting the hypothesized large initial abundance of hydrated minerals to the current state introduces the possibility that hydrous phases never formed in large quantities at the martian surface. The presence of liquid water at the martian surface may have been too brief, too localized, or occurred at too low of a temperature to result in appreciable chemical weathering.

1.2 The Color of Mars

Iron oxides exhibiting strong Fe^{3+} to O^{2-} charge transfer absorptions in the blue to near-ultraviolet are believed to give Mars its characteristic reddish-brown color. The formation mechanism of these ferric oxides is uncertain, but the small particle sizes of the dust grains (~2.5 μm [*Pollack et al.,* 1979]) implies that a chemical weathering process is responsible. *Burns* [1993] suggested that dissolution of basalts in acidic ground water, aqueous oxidation by dissolved oxygen, and subsequent precipitation of Fe^{3+} minerals formed the pigmenting agents in the soil. Other models are also based on the interaction between liquid water and surface materials [*Allen et al.*, 1981; *Newsom*, 1980]. However, for the reasons discussed above, abundant liquid water may not have been available at the martian surface to oxidize the soils.

In this thesis, I offer an alternative possibility for the formation of the ferric minerals, and the consequent color, of the martian soil. Chapter IV shows that ultraviolet radiation is capable of enhancing the rate of oxidation of metallic iron on Mars. Based on this observation, I postulate that meteoritic iron rather than surface minerals were oxidized to form the pigmenting agent on Mars. The oxidation product of metallic iron is largely maghemite [*Golden et al.*, 1995], and recent independent evidence from the Pathfinder magnetic properties experiment is consistent with ~6% γ-Fe_2O_3 in the soil [*Hviid et al.*, 1997].

1.3 Future Tests

The details of the laboratory experiments are described in chapters II, III, and IV. The speculative hypotheses described in this chapter and in chapter V are loosely based on the experimental results and are testable in the laboratory and with existing and future spacecraft instruments. Chapter VI provides specific possibilities for pursuing these ideas.

Chapter II: Water Content of the Martian Soil

2.1 Introduction

2.1.1 Hydrated Minerals on the Martian Surface

Geologic interpretations of spacecraft images indicate that liquid water was once abundant at the surface of Mars [*Carr*, 1996]. The availability of surface water early in Mars' history suggests that primary basaltic rocks and volcanic glasses could have been chemically altered to secondary, hydrated mineral phases in that time period. In particular, much published literature infers an abundance of palagonites on the surface based on spectroscopic evidence, thermodynamic calculations, laboratory experiments, and models of basalt erupting through ice [*Soderblom and Wenner*, 1978; *Gooding and Keil*, 1978; *Allen et al.*, 1981; *Singer*, 1982; *Morris et al.*, 1990, *Bell et al.*, 1993]. Other authors contend that smectite clays dominate the martian fine particles [*Toulmin et al.*, 1977; *Baird et al.*, 1977; *Zolotov et al.*, 1983; *Banin et al.*, 1983; *Bishop et al.*, 1993]. *Burns* [1988] argues that weathering models and visible spectral data are consistent with ferrihydrite, jarosite, opal, and silicate clays. The presence of iron oxyhydroxides also has been suggested [*Morris et al.*, 1983; *Banin et al.*, 1993, *Burns and Fisher*, 1993]. Such analyses and inferences about the mineralogy of the martian surface suggest that numerous hydrated phases plausibly are present.

2.1.2 Strong OH Absorption in Near-IR Reflectance

Interpretations suggesting that hydrated minerals are present on the surface of Mars are consistent with the broad absorption centered around 3 μm which has been observed in reflectance spectra from Mars since the early 1960's (see figure 2.1). This feature has been attributed to the OH stretch of adsorbed, bound, or frozen water in surface materials [*Moroz*, 1964; *Sinton*, 1967; *Houck et al.*, 1973; *Pimentel et al.*, 1974; *Calvin*, 1997]. Spectra collected by the imaging spectrometer (ISM) onboard the Soviet Phobos 2 spacecraft indicate that 3 μm band depths as large as ~0.62 are seen in the martian surface [*Murchie et al.*, in review]. These ISM observations at high spatial resolution (~25 km) also detected regional variability of up to 20% in the depth of the 3 μm feature [*Bibring et al.*, 1990; *Erard et al.*, 1991]. This variability of the OH signature in the ISM data is consistent with the reflectance spectra obtained from the infrared spectrometers (IRS) onboard Mariners 6 and 7 [*Erard and Calvin*, 1997]. The depth of the IRS absorptions measured at 3 μm, however, are ~15% larger than corresponding ISM data. This difference has been attributed primarily to the larger phase angles in the IRS observations which result in more scattering in the continuum [*Erard and Calvin*, 1997; *Murchie et al.*, in review].

2.1.3 In-Situ Analyses

The only direct measurement of the water content of the martian surface materials was performed by the gas chromatograph - mass spectrometer (GC-MS) instrument onboard the Viking Landers. The results from one of the landers (VL-2) indicate that less than 2% water[1] by weight was evolved from each of two

[1] Water (H_2O molecules) released from soil samples by heating can initially reside on the surfaces of soil grains (adsorbed), interlayer in clays, bound in mineral phases as H_2O, or held as OH within the structure. References to "water" content in this chapter refer to all forms of hydration which result in the evolution of H_2O upon heating.

samples heated in rapid (30 second) steps to 500°C [*Biemann et al.*, 1977]. The uncertainty in this value, however, is significant for the following reasons: (1) The instrument was not specifically designed to detect water; in fact, the gas chromatograph column was constructed to allow water to pass quickly through the system so it could be expelled prior to analysis of organic species. Laboratory simulations were necessary to understand the mass chromatograms obtained from the flight instrument, and "in the very worst case could be off by a factor of 5" [*Biemann et al.*, 1977]. (2) A temperature of 500°C is insufficient to dehydroxylate certain phyllosilicates such as montmorillonite [*De Bruyn and Van Der Marel*, 1954], and (3) adsorbed water could have been lost from the sample during exposure to the martian atmosphere at elevated temperatures (15°C) within the lander prior to the analyses [*Anderson and Tice*, 1979]. Some authors even suggest that the Viking Lander results "place virtually no constraints on the possible contents of hydrous minerals" in the martian surface [*Arvidson et al.*, 1989].

2.1.4 Focus of this Study

The purpose of this chapter is to show that even with all the uncertainties, the 2% result obtained by the Viking landers is reasonable for the water content of the martian soil. We demonstrate that the strong 3 μm absorption feature in the spacecraft reflectance spectra can be reproduced with plausible mineral mixtures containing less than 4% water by weight. Furthermore, we show that it is difficult to "hide" larger quantities of water in the martian surface layer while maintaining reflectance spectra consistent with those collected from spacecraft.

2.1.5 Past Work

Houck et al. [1973] collected 3 μm spectra from an aircraft instrument similar in depth to the ISM results, then estimated and inferred scattering coefficients for the martian particulate surface, and thereby constrained the water content of the soil to be approximately 1% (within a factor of 3). We use experimental rather than theoretical arguments, and more recent and much higher fidelity reflection spectra of Mars (ISM data) to show that the observed 3 μm absorption feature is consistent with Viking *in situ* measurements. We use the ISM and IRS spectra for comparison to our laboratory data because of the absence of terrestrial atmospheric interference and the high spatial resolution.

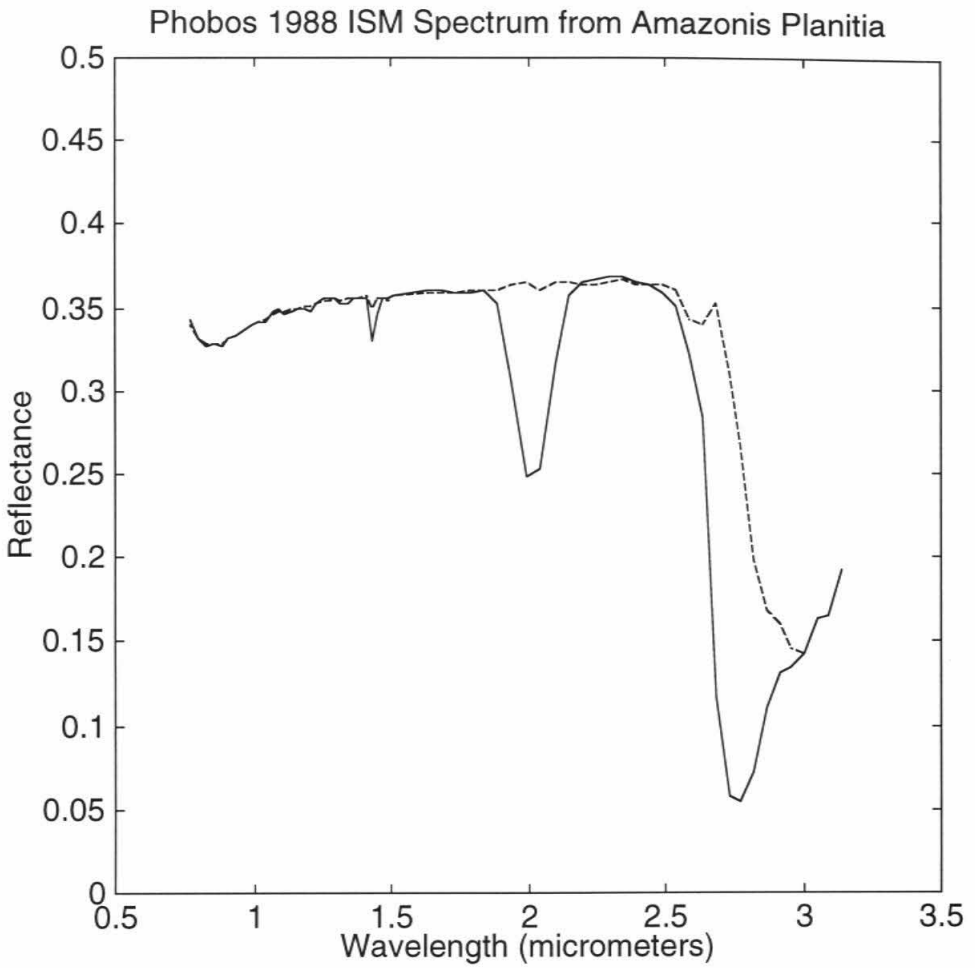

Figure 2.1: Reflectance spectrum of Amazonis Planitia collected by the infrared spectrometer onboard the Phobos '88 spacecraft. The dashed line represents the contribution from the martian surface after an atmospheric correction algorithm is applied. The strong absorption centered at 3 μm has been attributed to hydrated surface materials. Data from S. Erard.

2.2 Experiment Description

2.2.1 Overview

Mars-analog soil samples of varied water content were prepared and scanned using a Fourier transform infrared (FTIR) spectrometer. Thermal gravimetry (TG) was used to confirm the water content of the samples. The laboratory data were subsequently compared to published ISM and IRS spectra.

2.2.2 Sample Preparation

The water and OH-containing component of the particulate mixtures used in our experiments included palagonite, bentonite, goethite, and gypsum. The palagonite is the Pahala Ash from Hawaii (~2 miles west of Naalehu on Highway 11). Bentonite is a weathered volcanic ash consisting of mostly montmorillonite; our samples are from Clay Spur, WY (Clay Mineral Standard H-26). The goethite (α-FeOOH) sample is from Negaunee, Michigan, and the gypsum ($CaSO_4 \cdot 2H_2O$) is the selenite variety from Utah. The anhydrous portions of the mixtures included augite (clinopyroxene) from Ontario, Canada (near Syndenham), a fresh sample of Kilauea pahoehoe basalt, and near gem-quality plagioclase feldspar (~An70) from the Ponderosa Mine in Oregon. Basalts are largely plagioclase feldspar, but the transparent samples from Ponderosa Mine were used because they lack the highly absorbing dark-colored minerals such as magnetite. The objective of this study is not to test all possible martian surface constituents. Rather, samples were selected to be representative of the major categories of suspected mineral phases. Indeed, the results described below will show that the data depend primarily on water content and are relatively insensitive to the sample composition.

All of the samples were ground by hand using a mortar and pestle and dry sieved to exclude particles greater than 300 μm in diameter. Prior to making mixtures for FTIR analysis, the anhydrous components were baked at 850°C under air for 50 hours to minimize the adsorbed water. Neither the x-ray diffraction patterns nor the mid-infrared characteristics (with the exception of the removal of the 3 μm absorption) of the samples were altered by baking. The visual appearance of the basalt and the augite, however, changed from their initial gray and greenish colors to a more reddish-brown hue from thermal oxidation, which better resembles the visible color of Mars.

2.2.3 Particle Size Considerations

Martian soils are estimated to range from approximately 2 μm to 300 μm in particle size. Dust particles suspended in the martian atmosphere have typical sizes on the order of 2.5 μm [*Pollack et al.*, 1979]. Particles that are most easily saltated by surface winds have diameters of approximately 100 μm [*Greeley et al.*, 1992]. An average particle size of 100 μm is also consistent with observations of the drifts of fine grained sand in the vicinity of the Viking Landers [*Sharp and Malin*, 1984]. Thermal inertia studies of aeolian deposits suggest an average particle size of 300 μm [*Palluconi and Kieffer*, 1981]. Because we wish to show the plausibility of duplicating the ISM spectra using reasonable choices for particle size, sample material, and water content, we use particle mixtures that are no larger than 300 μm.

The approximate size distribution of our samples is listed in Table I. Sizes down to 35 μm were determined by sieving, the fraction smaller than 10 μm was

estimated by microscopic examination. The ISM instrument had a spatial resolution of approximately 25 km and undoubtedly sampled rocks, boulders, and other surfaces with length scales on the order of meters and larger. However, the roughness scale of most geologic surfaces combined with the sizes of aeolian material known to be on Mars indicate that surface spectra will be dominated by diffuse reflectance in the wavelength range studied here. This assumption facilitates a direct comparison between laboratory and spacecraft data.

Table I: Approximate Particle Size Distribution for Laboratory Samples

Particle Size Range	Percentage of Mixture
< 300 μm	100%
< 150 μm	65%
< 75 μm	40%
< 35 μm	20%
< 10 μm	10%

2.2.4 Sample Characterization

Each of the samples used in this study was analyzed with x-ray diffraction (XRD) to verify the composition. All powder patterns are as expected: Goethite, gypsum, augite, and plagioclase clearly match the database patterns. Bentonite and palagonite samples are dominated by montmorillonite. The low signal level in the palagonite sample indicates that this weathering product of basaltic glass is poorly ordered and almost amorphous. The diffraction patterns obtained for the basalt samples are dominated by plagioclase feldspars.

2.2.5 Thermal Analysis of Water Content

Dry basalt, feldspar, and pyroxene were mixed with hydrated mineral phases for comparison with the ISM spectra. Values for the water content of goethite and gypsum were initially estimated from stochiometry: 10.1% and 20.9% water by weight, respectively. After mixtures containing 2%, 4%, 6%, and 8% water by weight were made and scanned in the FTIR as described below, portions of the sample were extracted for thermal analysis using a Mettler TA2000C Thermoanalyzer (see figure 2.2) to confirm the water content. An example of a thermal gravimetry curve is shown in figure 2.3a. The intended amount of water from gypsum in this particular example is 2.0% by weight. An 82.3 mg sample of the mixture was heated to 1000°C at 10°C per minute, and the weight loss was measured as a function of temperature. The 1.64 mg of water lost as shown in the figure corresponds to 2.0 percent of the total mass, confirming the accuracy of our sample preparation.

Palagonite and bentonite are well known to adsorb large quantities of water (due to high surface area and interlayer sites in the clays, primarily montmorillonite). Because the actual stochiometry is unknown and unreliable for determining the quantity of water in these hydrated phases, initial estimates of water content were obtained from the thermal analysis curves. Small (< 50 mg) quantities heated to 1000°C at 10°C per minute show that the palagonite and bentonite samples used in this study contain approximately 18.5% and 11.6% water by weight, respectively (see figures 2.3b and 2.3c). Even though these samples are stored in sealed containers, exposure to variable humidity air during the sample preparation process affects the actual level of hydration. Thus,

analysis of the water content by these same thermal techniques immediately after collecting the infrared reflectance data was necessary to confirm that the desired water content was achieved.

2.2.6 Infrared Spectroscopy

After the powdered mixtures of baked basalt plus a hydrated phase were made (under air) and placed in sample cups, biconical diffuse reflectance spectra were obtained using a Nicolet 60SX Fourier transform infrared (FTIR) spectrometer (see figure 2.4). The purge gas flowing into the analysis chamber of the instrument was air which had been pressure cycled through zeolite to remove water vapor and carbon dioxide. A reflectance standard manufactured by Labsphere (Infragold) was used as the reference; manufacturer's data indicates that 94% to 97% of the incident flux in the applicable wavelength range is reflected from the surface. The infrared beam from the interferometer is focused to a spot size of approximately 3 millimeters by an off-axis paraboloid mirror (see figure 2.5). This focal spot is significantly larger than the particle size of the samples and the ~50 μm feature size of the Infragold standard, which allows collection of the diffuse portion of the reflectance. Scans of the reference target immediately precede scans of the soil mixtures, and a ratio between the two data sets were computed to eliminate the spectral contribution of the optical path through the instrument. The resulting data represent the reflectance spectra of the sample from 2 μm to 5 μm.

2.2.7 Conversion to Absorbance

Quantitative analysis using only reflectance spectra poses several challenges. First, the effects of wavelength dependent scattering alter the relative depths of the absorption features for samples with the same bulk water content but different particle sizes and packing densities. Furthermore, because reflectance values relative to a suitable standard range between zero and one, doubling the water content will not double the size of the absorption band. A number of techniques have been described in the literature for converting reflectance to absorbance in an effort to account for scattering processes and to relieve the effects of logarithmic compression, see *Hapke* [1993] for a review. None of these techniques is ideally suited for our particular problem, but one of the less unsatisfactory approaches for linearizing the reflectance data from the laboratory (as well as the spacecraft) measurements is to use the "apparent absorbance" (-ln(R)) [*Kortum,* 1969; *Clark and Roush*, 1984].

Reflectance band depths vary considerably as particle sizes and packing densities of the samples are varied in the laboratory. Our experiments show that variations as large 50% are achievable from changes in particle size and packing density while water content of the samples are constant. Conversion of these reflectances to apparent absorbance, however, yielded much smaller differences between samples (less than 10%). For example, figures 2.6a and 2.6b show reflectance and absorbance, respectively, for mixtures of palagonite and basalt of different particle sizes. While the reflectance band depths are different for the same quantity of water, the absorbance curves are nearly identical. Similar results have been demonstrated with packing density variations. Thus, conversion to apparent absorbance is robust to changes in packing density and particle size and

direct comparisons between curves of different quantities of water can be made after the conversion to absorbance is applied.

2.2.8 Results

Ten "families" of four curves shown in figures 2.7a through 2.7j were produced from these experiments. One set of curves was generated for each combination of dry (basalt, feldspar, pyroxene) and hydrated mineral phases (palagonite, bentonite, gypsum), and the tenth plot was produced from a mixture of basalt and goethite. The four curves in each plot represent 2, 4, 6, and 8 percent water by weight. To simplify comparison across the data sets, the curves were reduced to apparent absorbance heights after an approximate continuum baseline was subtracted from the absorbance spectra. Plots of apparent absorbance versus water content for the various mixtures are shown in figure 2.8a. The representative error bars shown on the figure were estimated from FTIR and thermal analysis of multiple mixtures with the same target water content and by bounding the range of absorbance values for different choices for baseline corrections. In the bentonite curves, where the absorbance peak is at 2.76 μm, the second highest peak (~2.9 μm) was used to determine the band size. This region of the curve is more appropriate for a direct comparison to the ISM results since the spacecraft data in the wavelength range of the largest peak are highly uncertain due to interference from atmospheric CO_2 (see discussion below).

Figure 2.2: Photograph of the Mettler TA2000C Thermoanalyzer used to determine the evolvable water content of the samples.

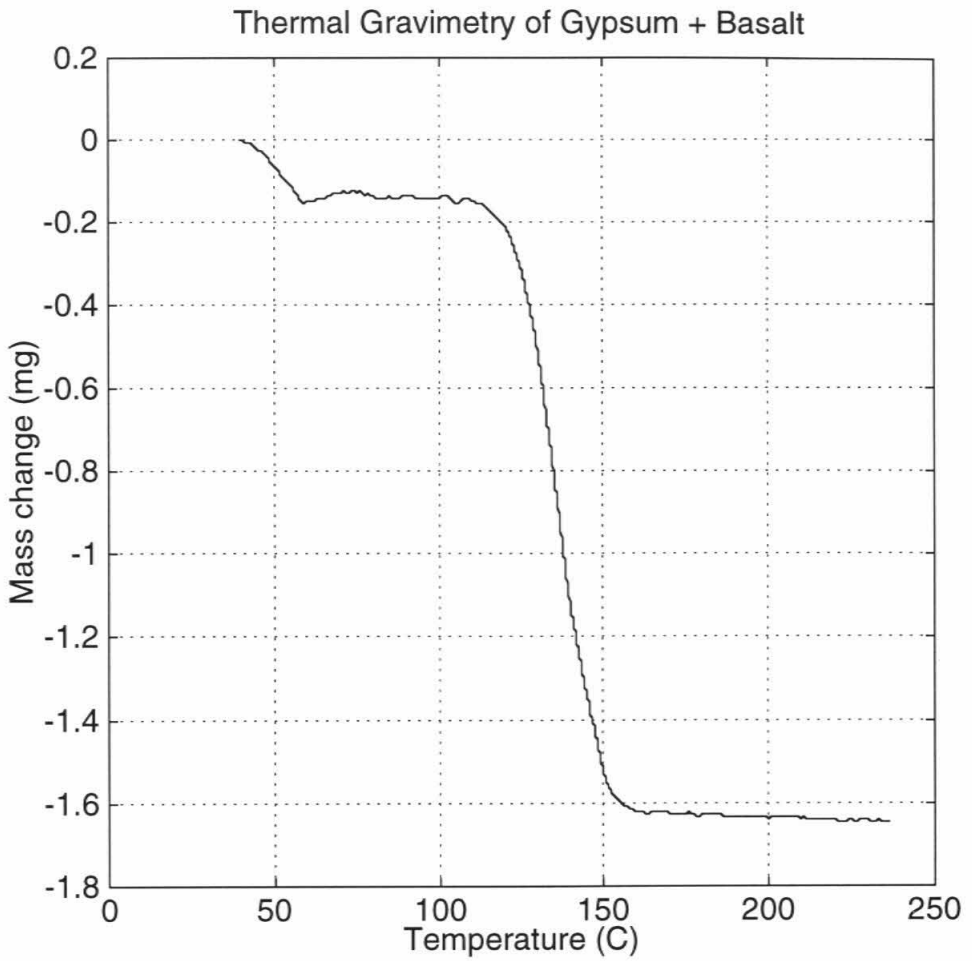

Figure 2.3a: Thermal gravimetry profile for a mixture of gypsum and basalt. The desired water content of this mixture was 2.0% by weight, which was confirmed experimentally with the loss of 1.64 mg from an 82.3 mg sample.

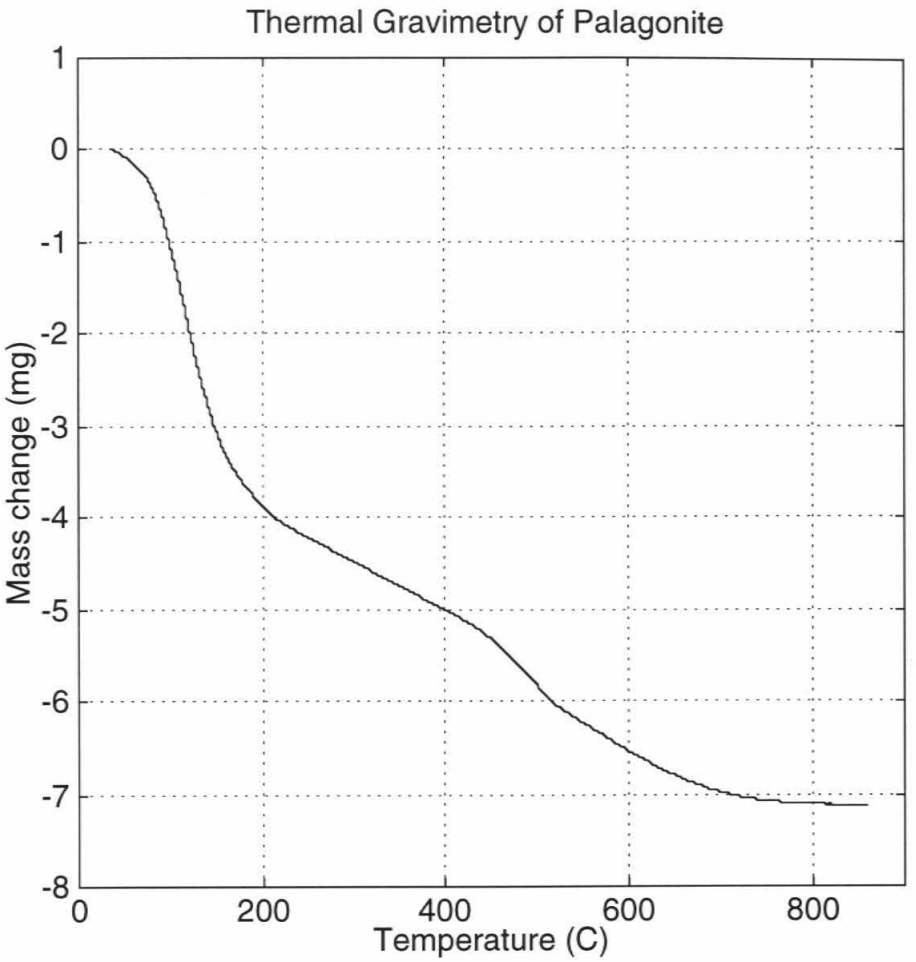

Figure 2.3b: Thermal gravimetry profile for Pahala Ash. A 7.1 mg mass loss from an initial sample of 38.4 mg indicates approximately 18.5% water by weight under the temperature and humidity conditions on the day of this thermal analysis.

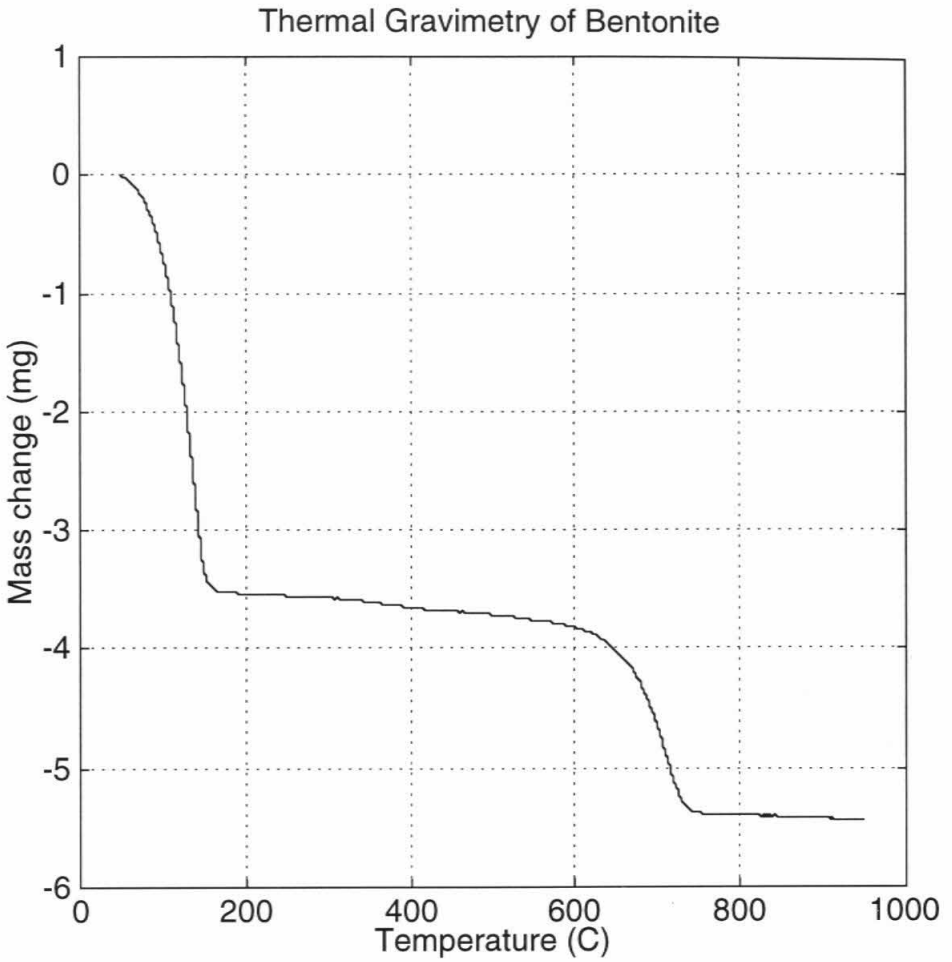

Figure 2.3c: Bentonite from Clay Spur, WY. A 5.4 mg change in mass from a 46.4 mg sample corresponds to an initial water content of 11.6 weight percent of the day of this experiment. Interlayer water is lost below 200°C while structurally bound OH is lost from the montmorillonite near 700°C.

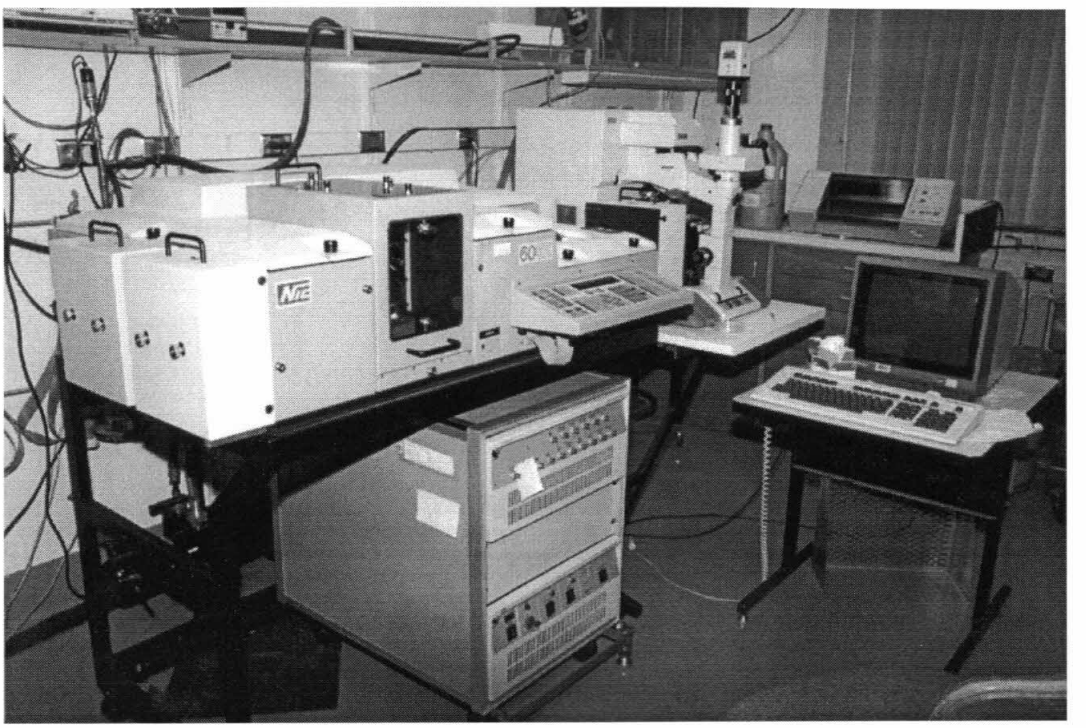

Figure 2.4: Photograph of the Nicolet 60SX Fourier transform infrared (FTIR) spectrometer used to collect the spectra shown in this chapter.

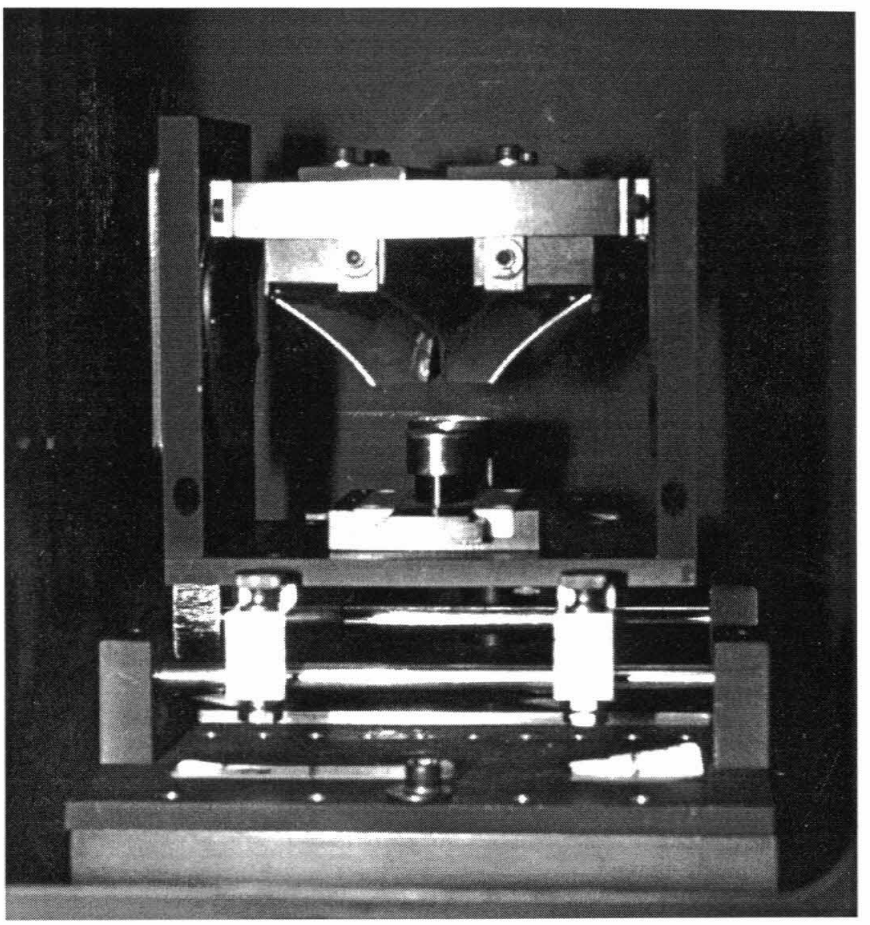

Figure 2.5: Photograph of the fixture used to collect reflectance spectra from particulate samples.

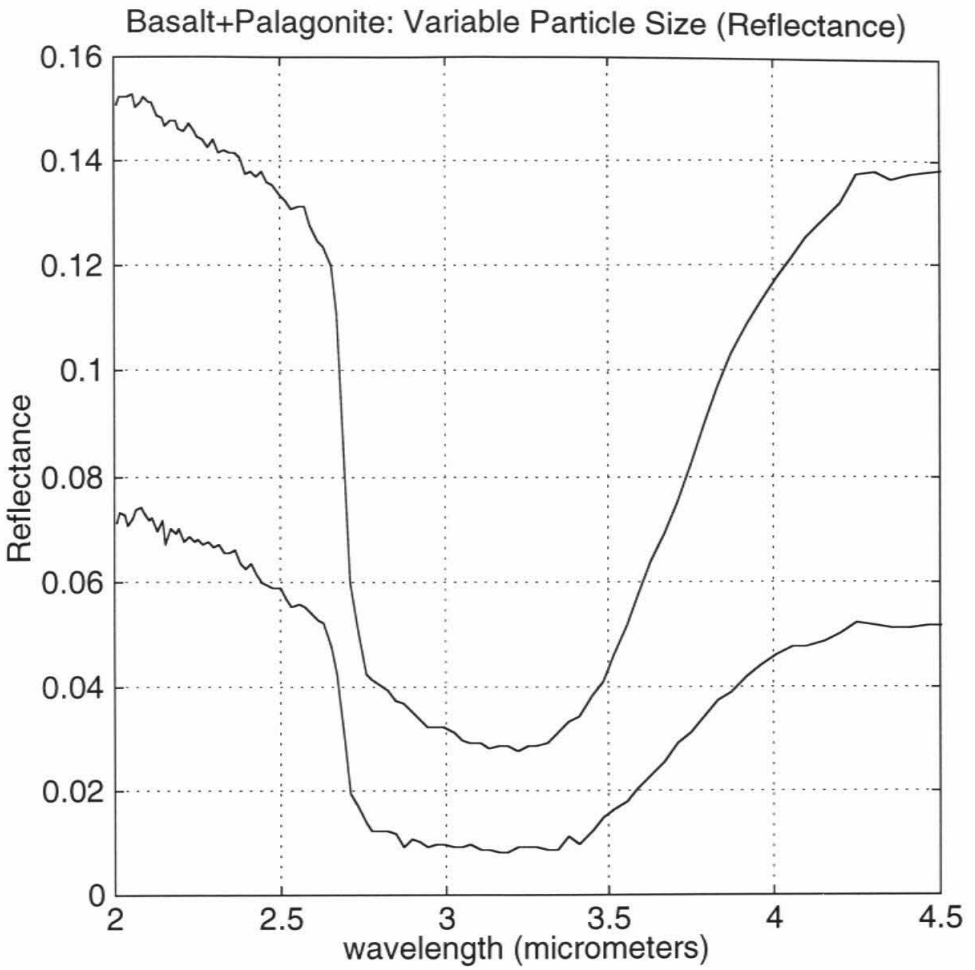

Figure 2.6a: Reflectance measurements for mixtures of palagonite and basalt. Upper curve represents particles less than 38 μm in size, while the lower curve is for particles between 75 and 150 μm (mixtures were made after sieving individual components).

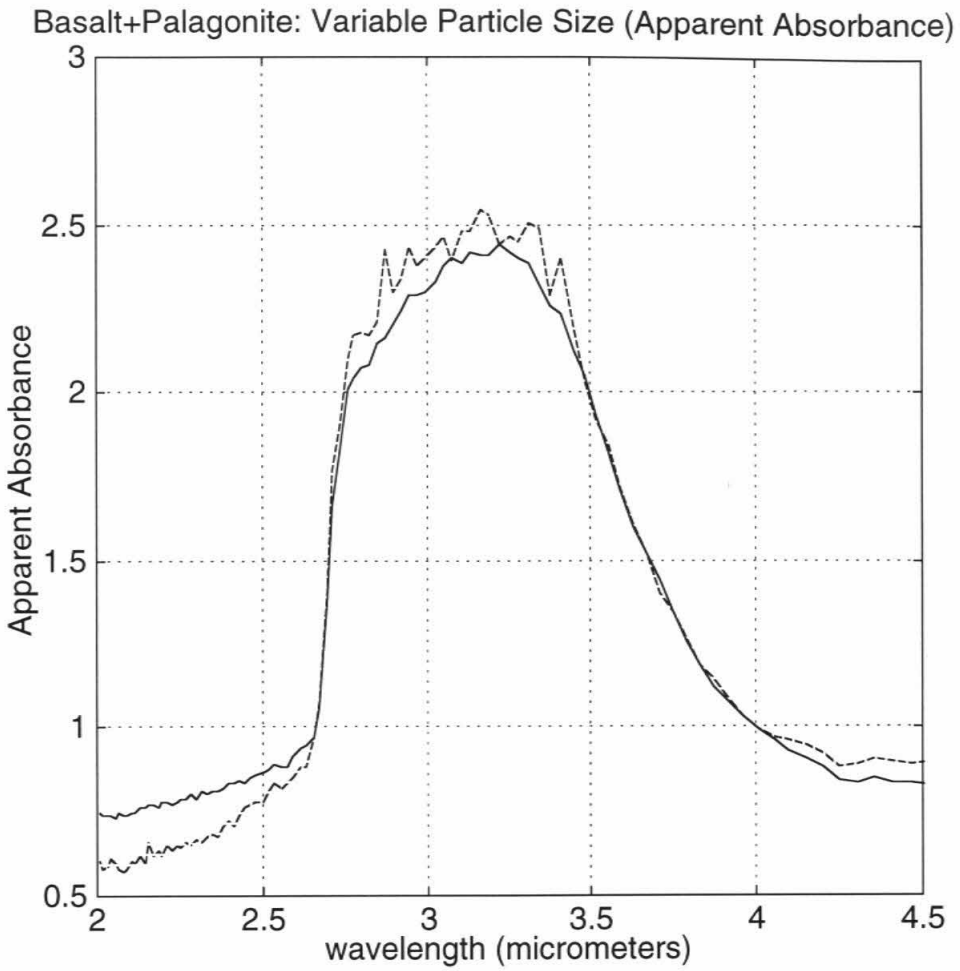

Figure 2.6b: Conversion of the curves in (2a) to apparent absorbance (-ln(R)) and superimposed for comparison. Absorbance is reproducible for constant water content and varying particle size, while reflectance band depths change with particle size.

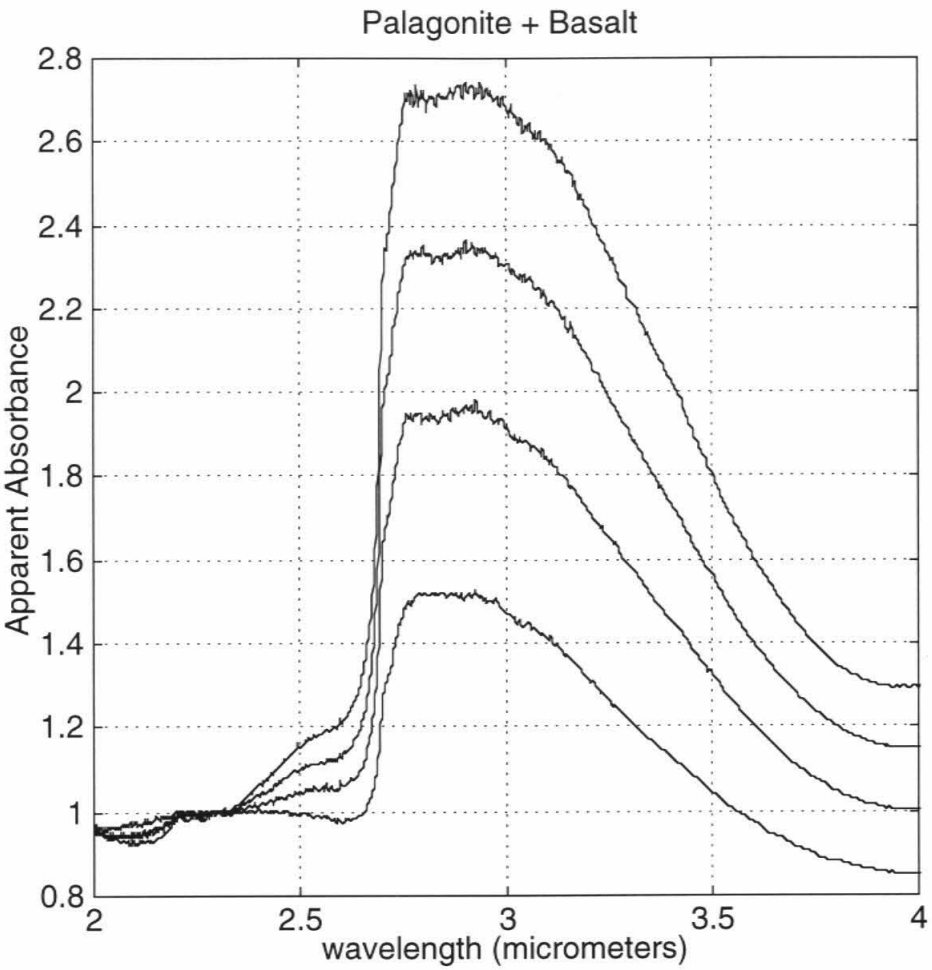

Figure 2.7a: Example of increasing absorbance with larger water content for mixtures of palagonite and basalt (each component dry sieved to diameters less than 300 μm). Reflectance spectra are converted to apparent absorbance. Vertical axis is offset to align curves. Water content varies from 2% (lowest curve) to 8% (highest peak); intermediate curves represent 4% and 6% water.

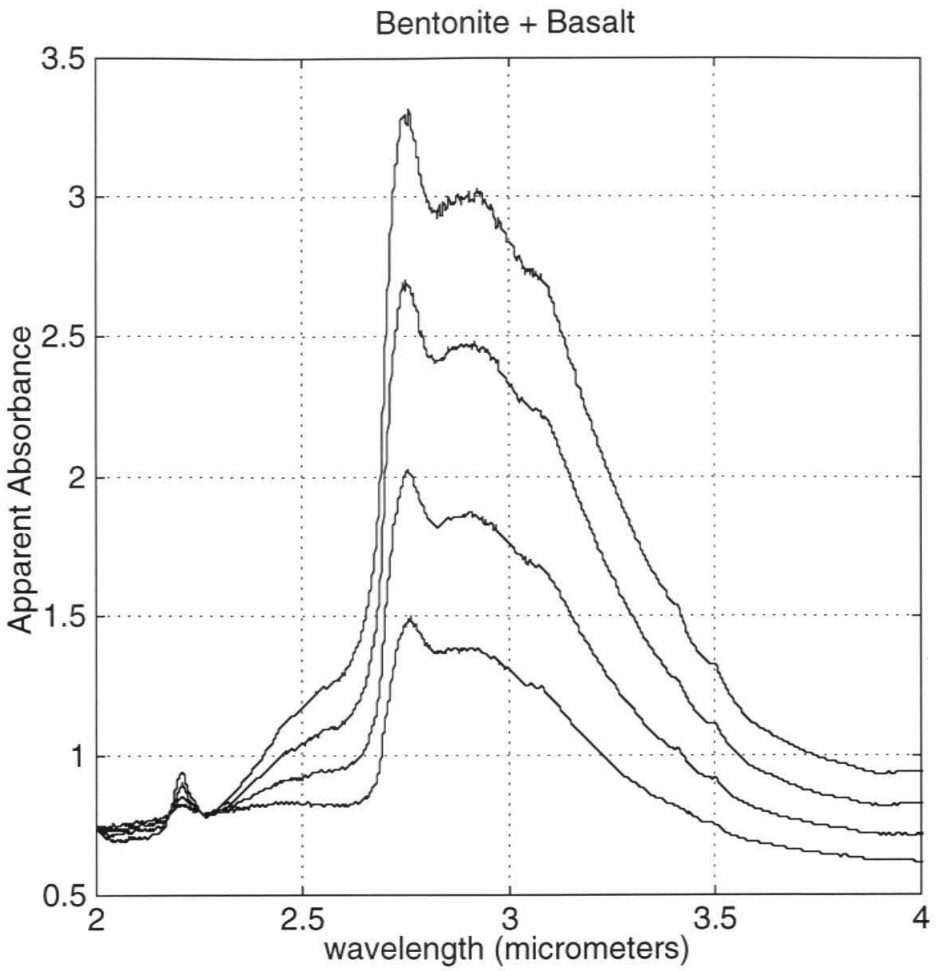

Figure 2.7b: Same as figure 2.7a for mixtures of bentonite and basalt. The small peak near 2.2 μm results from the combination of OH stretch and the Al^{3+}-OH lattice modes.

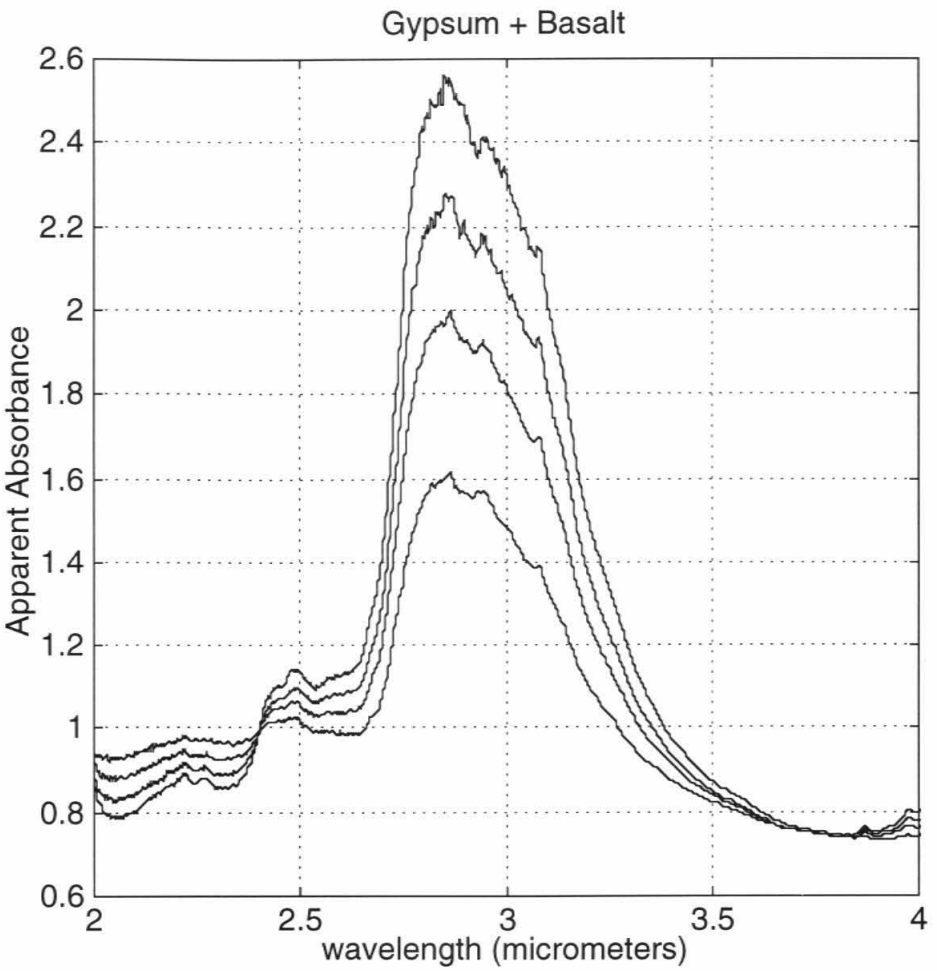

Figure 2.7c: Same as figure 2.7a for gypsum and basalt.

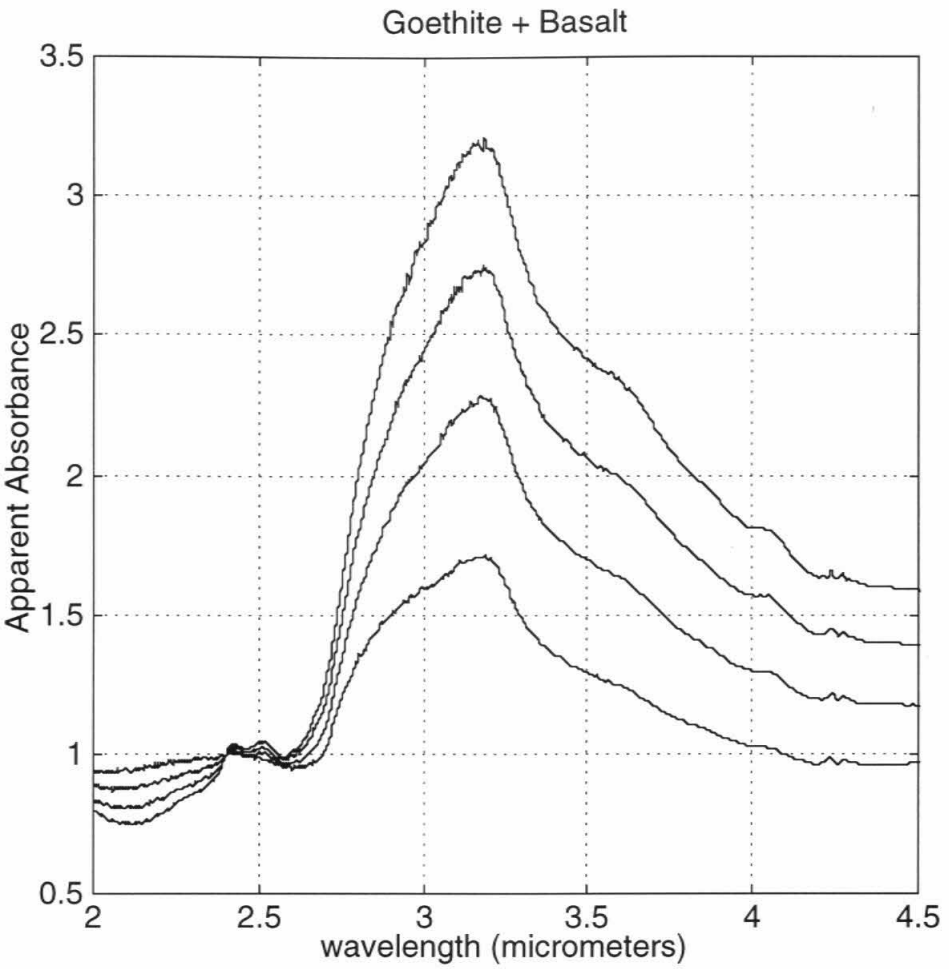

Figure 2.7d: Same as figure 2.7a for goethite and basalt.

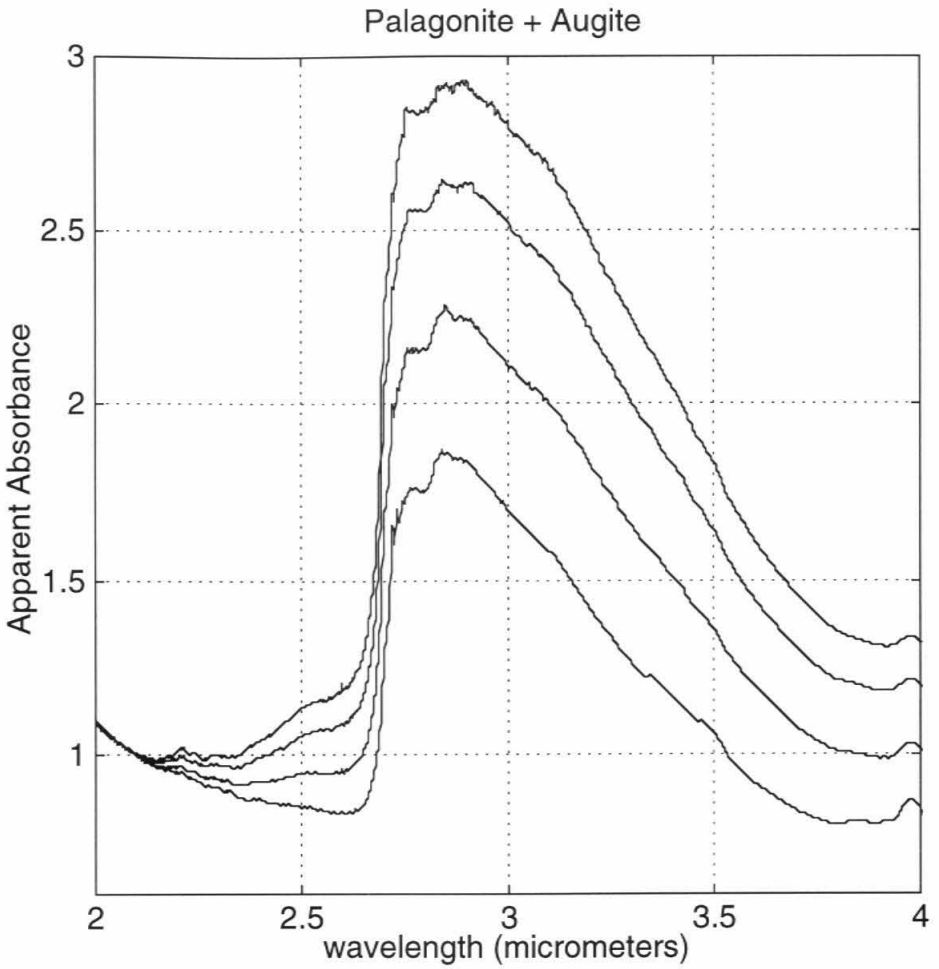

Figure 2.7e: Same as figure 2.7a for palagonite and augite.

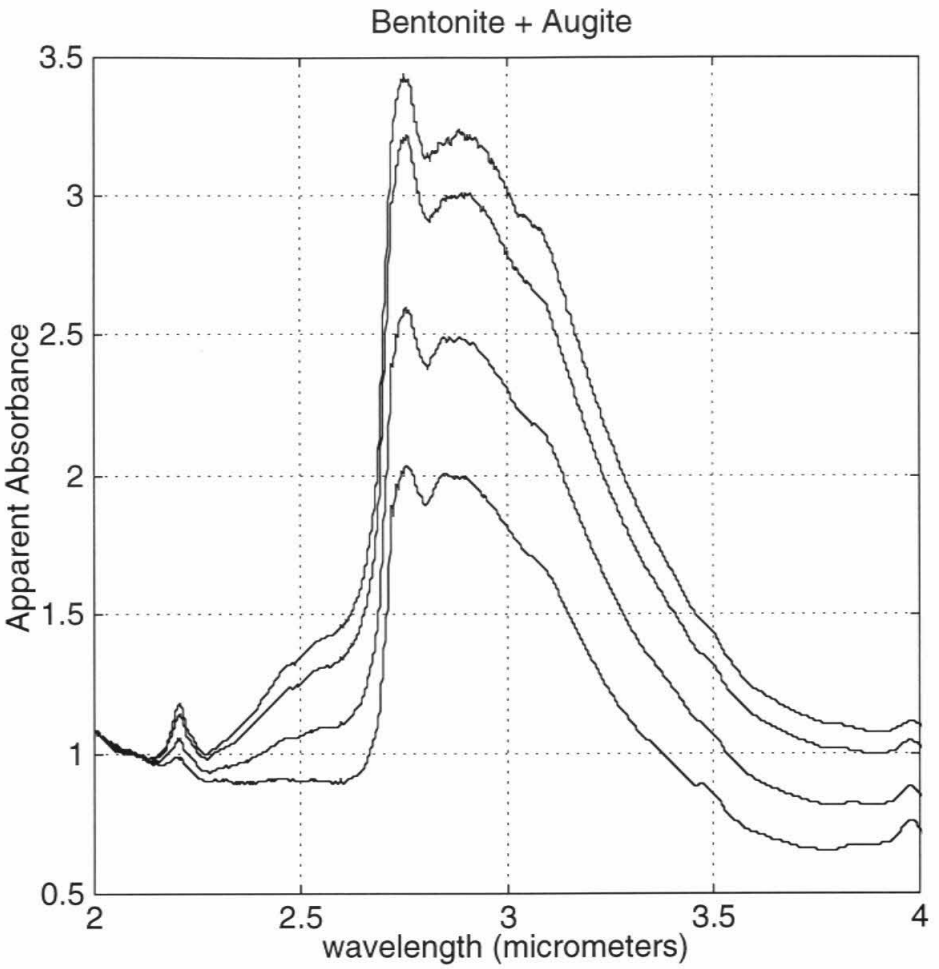

Figure 2.7f: Same as figure 2.7a for bentonite and augite.

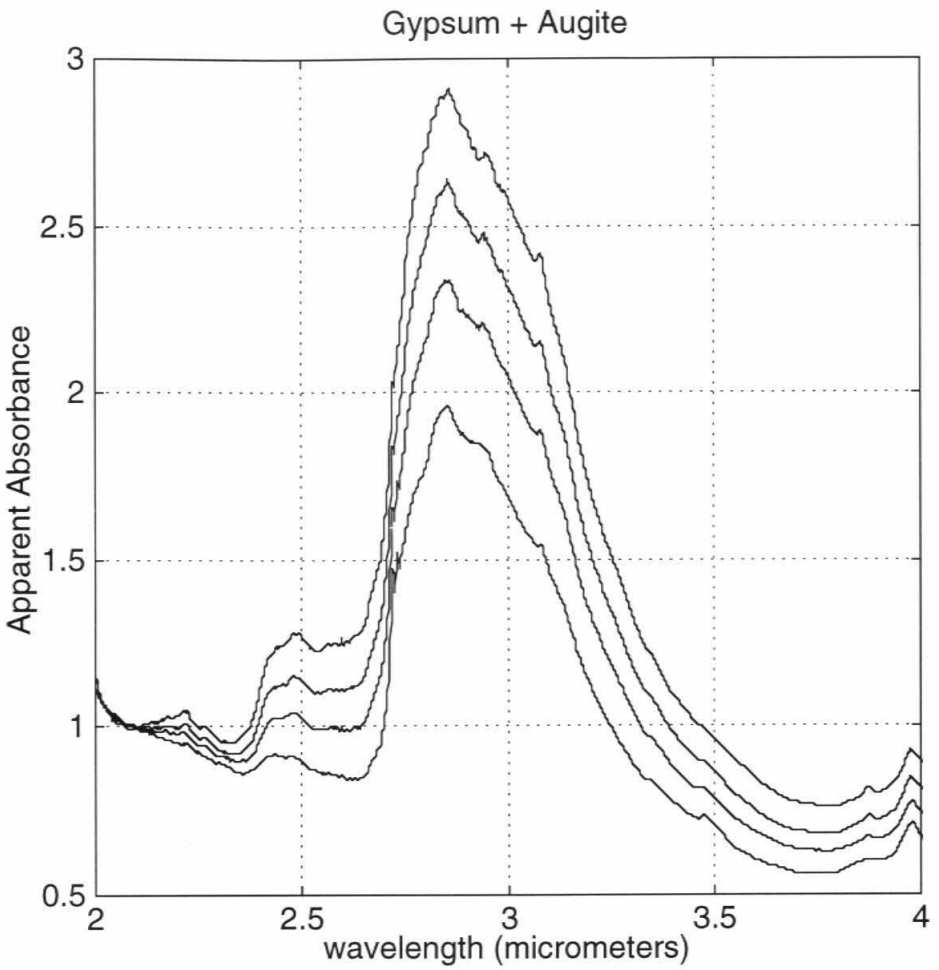

Figure 2.7g: Same as figure 2.7a for gypsum and augite.

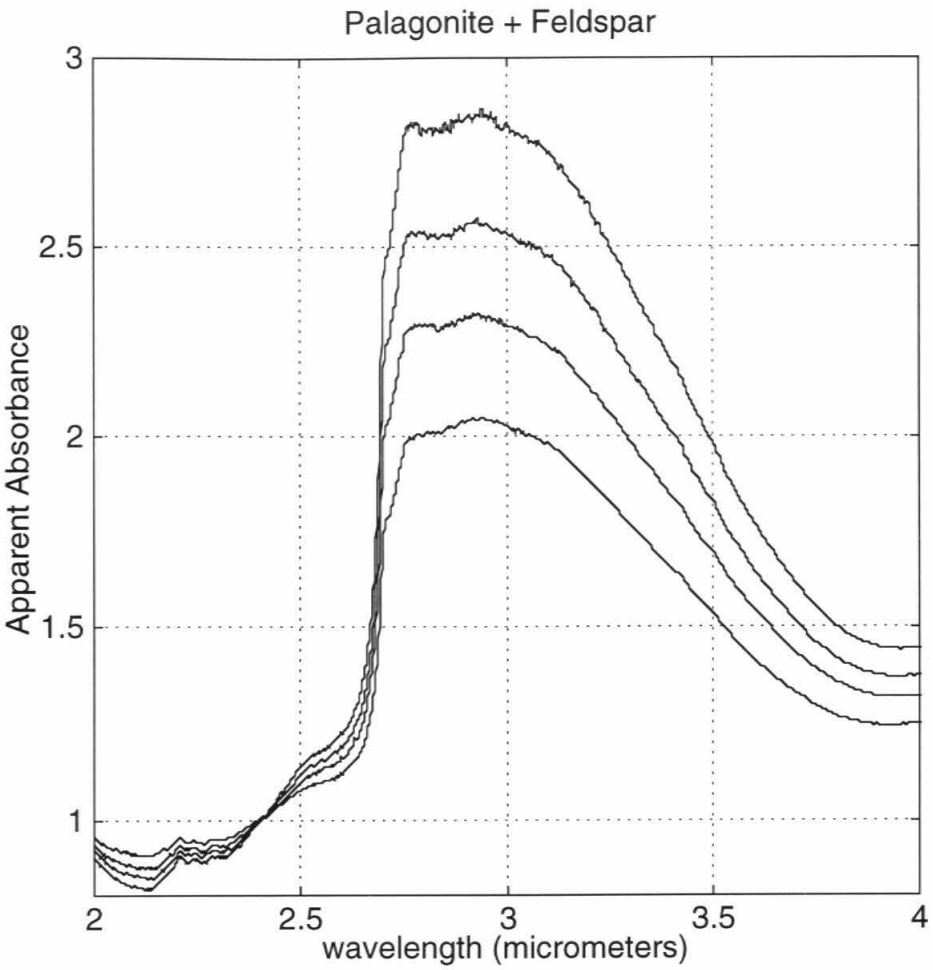

Figure 2.7h: Same as figure 2.7a for palagonite and plagioclase feldspar.

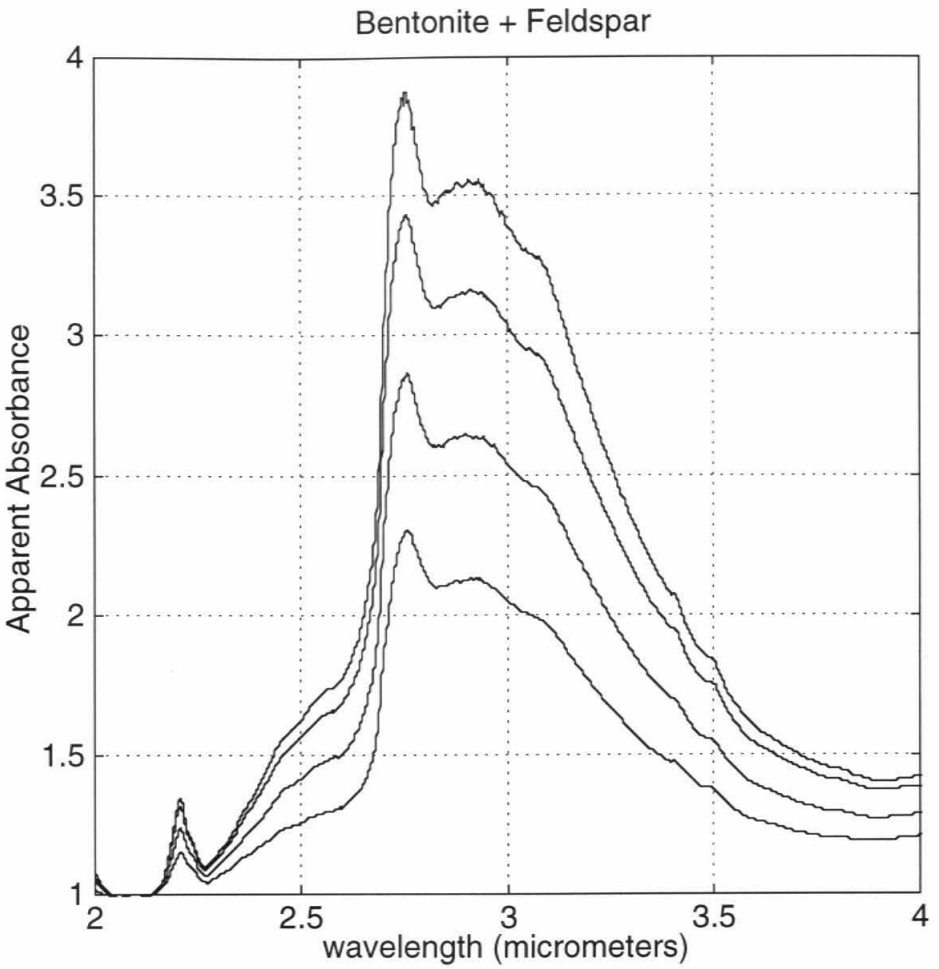

Figure 2.7i: Same as figure 2.7a for bentonite and plagioclase feldspar.

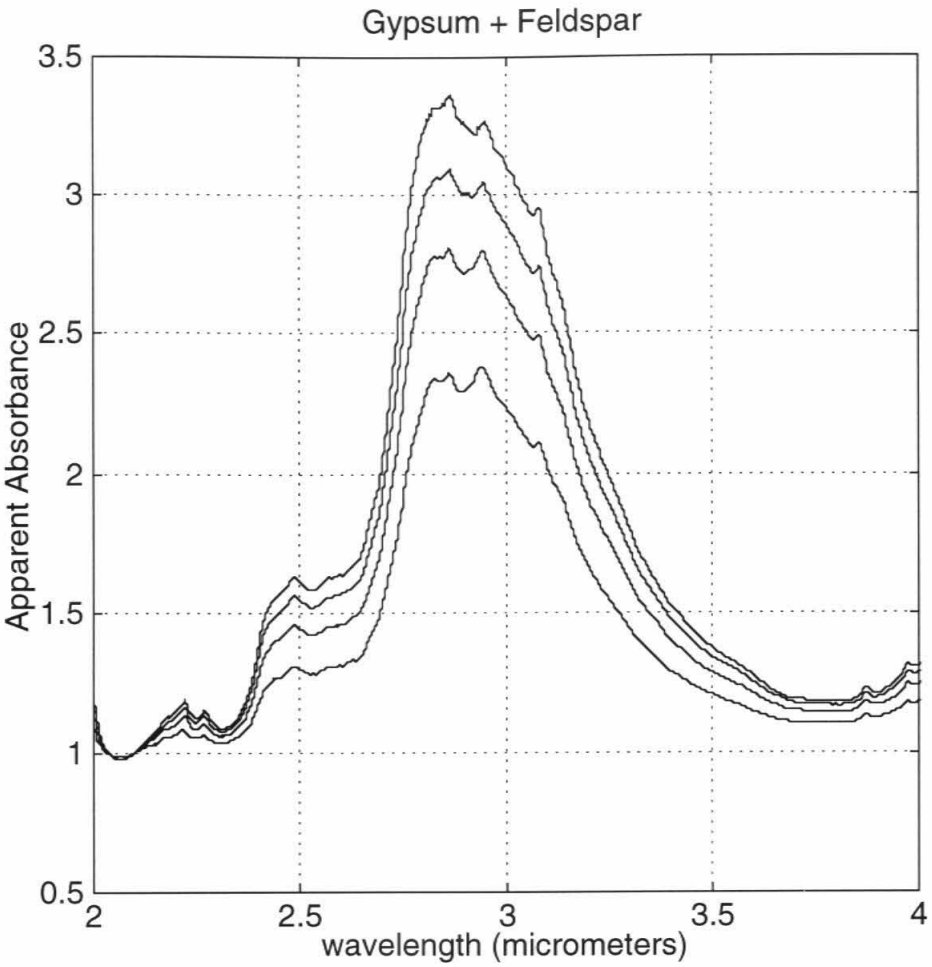

Figure 2.7j: Same as figure 2.7a for gypsum and plagioclase feldspar.

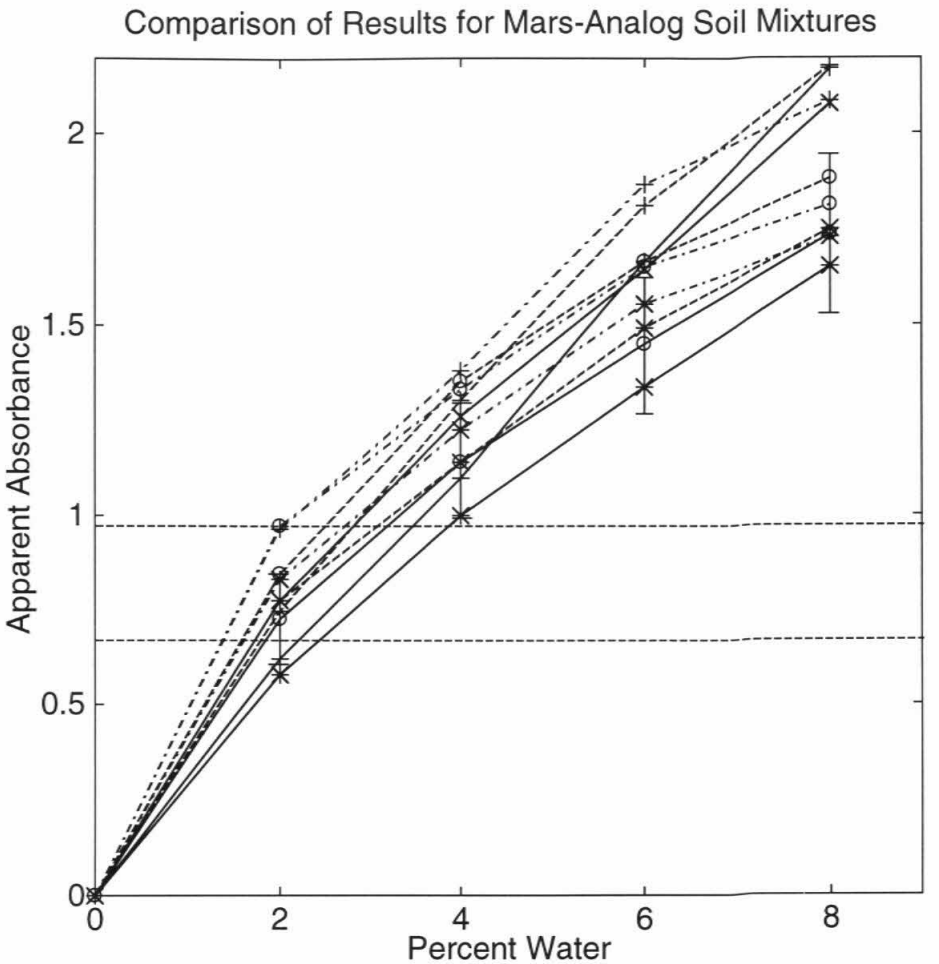

Figure 2.8a: Plot of apparent absorbances extracted from curves shown in figure 2.7a through 2.7j. Solid lines represent basalt, dashed lines are feldspar, and dash-dot lines are augite. Palagonite='*', bentonite='+', gypsum='o', and goethite='x.' Horizontal lines at 0.67 and 0.97 represent the range of absorbances for the martian surface calculated from ISM data (see text). Representative error bars are shown on the gypsum/basalt mixture.

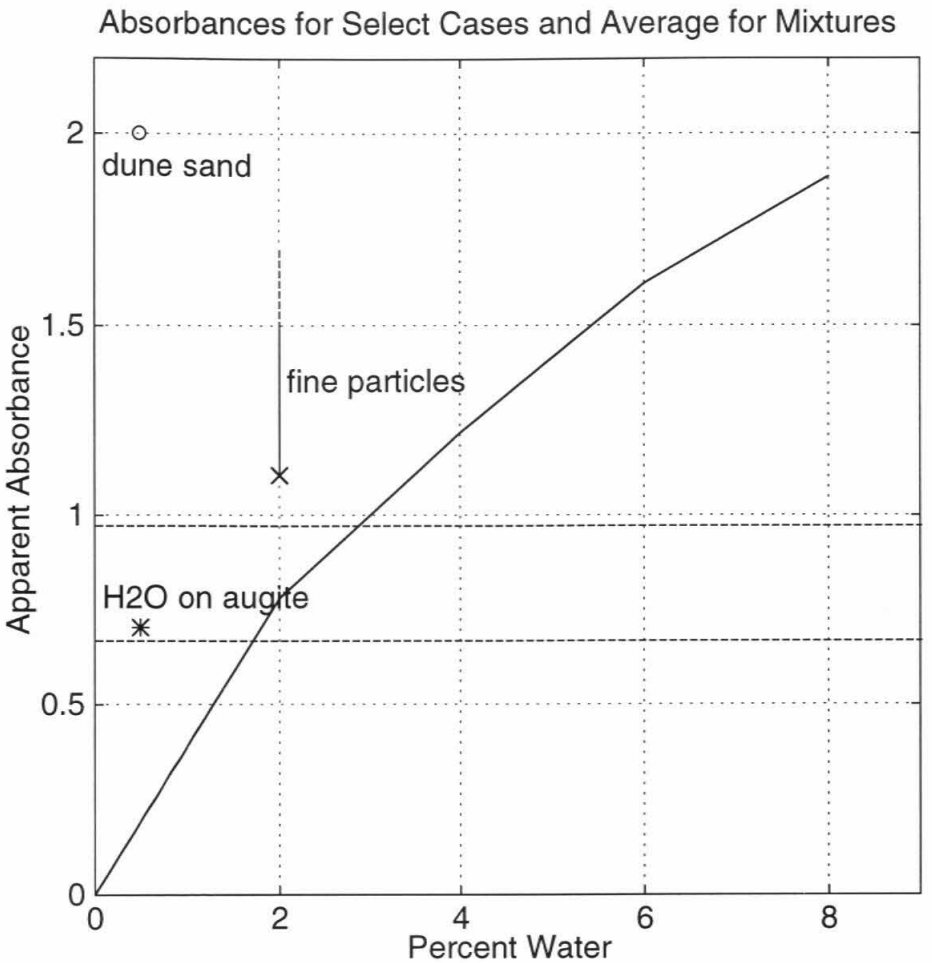

Figure 2.8b: Average apparent absorbance versus water content based on the curves from figure 2.8a. Data points for adsorbed water on augite, reduced particle sizes for the hydrated phases in the mixtures, and the Kelso dune sands are shown for comparison.

2.3 Discussion

2.3.1 Comparison with Spacecraft Data

The instruments which provide the best data for comparison against the laboratory spectra are the Infrared Spectrometers (IRS) onboard Mariners 6 and 7 and the imaging spectrometer (ISM) from the Soviet Phobos 2 spacecraft. An apparent advantage of the latter data set is that a number of authors have published ISM spectra covering the 3 μm absorption feature that have been "corrected" for the martian atmosphere (e.g., *Bibring et al.*, [1990]; *Erard et al.*, [1991]; *Murchie et al.*, [1993]; *Mustard et al.*, [1994]). This removal of the atmospheric signature from the surface reflectance, however, is not a straightforward task and can be misleading about the spectral content of the martian surface. The contribution of atmospheric water vapor to the surface signature is difficult to establish because an extremely weak feature at 2.544 μm provides the only constraint [*Erard et al.*, 1991]. The primary difficulty with the atmospheric correction, however, is due to a strong CO_2 absorption (centered ~2.75 μm) which overlaps the short wavelength range of the surface hydration feature. Because this band never exceeds 85% due to saturation attributed to stray light and atmospheric scattering [*Bibring et al.*, 1990; *Erard et al.*, 1994; *Erard and Calvin*, 1997], complete removal of the CO_2 contribution is nearly impossible to achieve.

The challenges associated with atmospheric correction are apparent from published surface spectra which are not consistent across various papers. For example, one "corrected" curve for Isidis Planitia [*Mustard et al.*, 1993] has a band depth approximately 40% larger than previously published reductions of ISM spectra for the same region of Mars [*Erard et al.*, 1991]. In a personal

communication, J. Mustard indicated that absolute calibration of the 3 μm region of the spectra was not a primary goal of his paper, and that due to saturation of the 2.7 μm CO_2 band, the processed data are correlated with altitude (which indicates an inaccurate removal). Mustard is confident in the relative accuracy of his plots, but suggested that curves from *Erard et al.* [1991] should be used for direct comparisons with laboratory data. The *Erard et al.* [1991] work, however, is a "first results" paper which had not incorporated more sophisticated atmospheric removal algorithms [*Erard*, personal communication]. Which calibration, then, should be used to compare against the laboratory data?

Recent work by *Murchie et al.* [in review] provides scatter plots of 3 μm band depths for the entire ISM data set. The absolute calibration of wavelengths larger than 2.6 μm in this work are tied to ISM observations of Phobos which is nearly featureless in this range. These authors determined band depths by comparing the continuum level at 2.5 μm to an average of the signal strengths at 2.95, 3.00, and 3.05 μm, which specifically excludes the regions of the strongest CO_2 absorptions. The results range from approximately 0.49 to 0.62 with a large concentration of points ~0.59. This range for the 3 μm band depths corresponds to apparent absorbance values between 0.67 and 0.97 (with a large fraction of the points ~0.89) for the ISM data set. These absorbance values are consistent with the ones we calculated from individual, corrected spectra that we obtained directly from S. Erard: Amazonis Planitia (0.94), Eos Chasmata (0.74), Lunae Planum (0.97), and Syrtis Major (0.69). This range of apparent absorbance (0.67 to 0.97) will be used for comparison to the laboratory results and is shown on figure 2.8.

2.3.2 Upper Limit for Water Content

Figure 2.8a shows a roughly linear increase in apparent absorbance as a function of water content. Departures from true linearity are likely due to incomplete modeling of scattering and diffuse reflectance by a simple logarithmic function. Regardless of the non-linearity, these curves establish a reproducible relationship between the size of the absorbance and the water content for plausible mixtures of martian surface materials and provide a reasonable data set for comparison against the spacecraft data. Since the magnitude and shape of the curves for the ten different mineral mixtures are roughly the same (close to the uncertainties of the experiment), the apparent absorbance does not appear to have a strong dependence on the choice of the Mars-analog minerals in the mixture. Based on the average curve through the data (figure 2.8b), I estimate the upper limit for the water content of the martian soil to be 4% by weight.

This value, which is based on the maximum absorbance in the ISM data is judged to be conservative for two reasons. First, the particle size distributions of the hydrated and the dry components of the mixtures that we used are approximately the same. In a natural environment, the smallest particles will likely be dominated by phyllosilicates since the weakly bound layers are easy to disrupt by physical weathering processes. Experiments using the minerals described above but with the hydrated phase limited to particles less than 35 μm resulted in apparent absorbances larger than 1.1 with only 2% water (see figure 2.8b for comparison with nominal results). Small hydrated particles covering the surfaces of anhydrous scattering centers provide even greater opportunities for incident photons to be absorbed at 3 μm. In the limit where the hydrated phase is a fine coating rather than individual particles observable with an optical microscope, large absorbances can be achieved with minimal quantities of water.

For example, an analysis of sands from the Kelso Dunes in the Mojave Desert, California shows an apparent absorbance of greater than 2.0 for only 0.5% water (see figures 2.9 and 2.8b). These 250 to 500 μm diameter sand particles consist of quartz, feldspar, and amphibole [*Sharp*, 1966] along with fine grained clay minerals which enhance the 3 μm absorption. Hydrated coatings or "rinds" around surface particles are thought to be consistent with models of martian soils (e.g., *Murchie et al.* [1993]).

Secondly, we found it difficult to "hide" quantities of water larger than 4% in the laboratory samples while maintaining the use of *plausible* mineral and size mixtures. It is, of course, possible to use fine particles of highly absorbing, but uncommon, materials to cover larger grains of hydrated phases to conceal large quantities of water. For example, experiments show that 1 μm particles of graphite covering 100 μm gypsum grains will yield an apparent absorbance of less than 0.4 for ~15% water by weight. The absolute reflectivities of Mars, however, are not consistent with an abundance of highly absorbing mineral phases. Our experiments with basalt and augite are already on the "dark" end of realistic visible albedoes with values between 10% and 15%. Experiments using these dark, but plausible, particles covering larger hydrated sulfate grains was insufficient to mask the strong OH signature. Thus, the particle size distributions and minerals used in our experiments allow us to conclude that the water content of the martian soil is likely to be less than 4% by weight.

2.3.3 Spectral Shapes

In addition to providing constraints on the water content, the 3 μm surface absorption feature contains information about the composition of the hydrated

phases in the martian soil. For example, montmorillonite has a characteristic peak at approximately 2.76 μm [*van der Marel and Beutelspacher*, 1976]. Palagonite lacks this peak and exhibits a much more abrupt entrance into the short wavelength end of the absorption feature when compared with gypsum. Unfortunately, these diagnostic compositional characteristics of candidate martian minerals are concentrated in the short wavelength end of the 3 μm absorption feature. The difficulties with atmospheric correction result in the greatest uncertainties occurring in this part of the spectrum and prevent the determination of surface composition from the 3 μm spectral shape.

One statement about spectral shape, however, can be made with relative confidence on the basis of our laboratory data: We can exclude goethite as the dominant hydrated mineral phase in the soil because its spectral peak for OH is at 3.18 μm (see figure 2.7d), while the peak of the Mars absorption is unlikely to be at wavelengths longer than 3.0 μm (e.g., *Erard and Calvin*, [1997]). This constraint on the peak location in the Mars data is independent of the atmospheric correction, because it relies primarily on data outside the CO_2 absorption.

2.3.4 Liquid, Frozen, and Adsorbed Water

One could argue that the origin of the feature in the ISM data is not necessarily associated with water bound in a hydrated mineral, but rather, could be due to liquid, frozen, or adsorbed water at the surface. Each of these options, however, is unlikely to be responsible for the entire absorption feature. Due to the low water vapor pressure in the atmosphere (on the order of a microbar), liquid water with or without brines is not stable at the martian surface. In the season (Ls ~10°) and latitude (L~10°N) of these Phobos 2 daylight observations (local time

0900 to 1600), frost is not likely to be at the surface (e.g., *Ingersoll* [1970], *Jakosky* [1985]). Furthermore, the peak location (~3.07 μm) of the water ice absorption feature is at a longer wavelength than the peak in the spacecraft data.

Some amount of adsorbed water in equilibrium with the atmosphere, however, should be present on the soil grains at the martian surface. We conducted experiments to determine absorption depths from water adsorbed on anhydrous particles. Only the smallest grains (less than 35 μm) were used so surface area could be maximized, and the samples were exposed to high humidity immediately prior to obtaining the infrared spectra. Augite samples yielded apparent absorbances of approximately 0.7, and a thermal analysis of these samples showed that they contained ~0.5 weight percent water (see figure 2.8b for comparison with other laboratory results). This apparent absorbance is at the low end of the absorbance values derived from the ISM data set. This indicates that at saturation in room temperature, a collection of angular (rough) anhydrous grains substantially smaller than the mean particle size of the martian soil still has insufficient surface area to hold a quantity of adsorbed water that could completely reproduce the ISM spectra. Under martian conditions, a recent model indicates that palagonite with a specific surface area of 17 m^2/g (consistent with an estimate by *Ballou et al.* [1978] for the Mars soil) would hold less than 0.04% adsorbed water [*Zent and Quinn,* 1997]. This quantity of water would have a much smaller absorbance than evident from the spacecraft data and is further evidence that adsorbed water cannot be responsible for the entire 3 μm feature. In addition, the GC-MS evolved much of its water at temperatures above 350°C [*Biemann et al.*, 1977]. Even for the rapid heating steps (< 30 seconds) utilized by the instrument, most of the adsorbed water should have been released at lower temperatures.

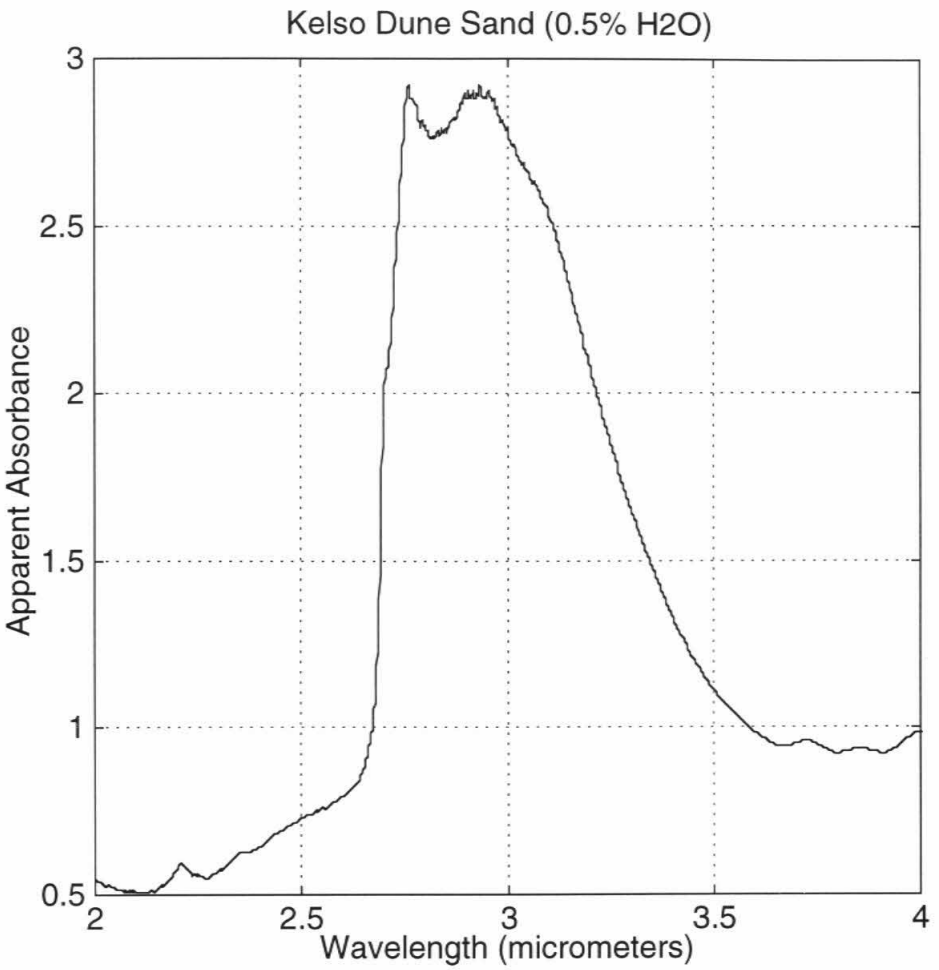

Figure 2.9: Apparent absorbance spectrum from Kelso Dunes sands. Thermal analyses indicate approximately 0.5% water by weight in these samples. This figure shows that absorbance values substantially larger than the range evident in the ISM data can be obtained with very small quantities of water when small particles of hydrous minerals cover the surfaces of larger anhydrous grains.

2.4 Conclusions

- On the basis of laboratory simulations of the 3 μm absorption feature, we believe that the surface of Mars contains a maximum of 4% water adsorbed and/or bound in the surface minerals. These results are consistent with the *in situ* measurements of evolved water performed by the gas chromatograph-mass spectrometer instrument on the Viking Landers and indicate a drier, more dehydrated soil than implied by much modeling of early Mars conditions.

- The shape of the short wavelength portion of the 3 μm absorption feature is highly uncertain in Mars spectra due to complexities in removal of the atmospheric CO_2 and water vapor. Goethite, however, can be excluded as a major component of the soil because its peak location is at longer wavelengths than the spacecraft data suggests and is in a region of the spectrum that is not affected by the atmosphere. Small amounts of dehydrated palagonite, hydrated sulfates such as gypsum, and poorly crystalline clays cannot be excluded on the basis of the existing 3 μm reflection spectra of Mars.

- Large apparent absorbances (greater than 0.7) can be achieved with relatively small quantities of water (~0.5%) physically adsorbed on the surfaces of anhydrous mineral grains. The evolution of water between 350°C and 500°C in the Viking Lander GC-MS indicates that adsorbed water is not the only form of hydration in the soil.

Chapter III: Ultraviolet Radiation-Induced Desorption of Water

3.1 Introduction

In chapter II, I conclude that the water content of the martian soil is consistent with the 2 weight percent value obtained by the Viking Landers. This figure appears inconsistent with the chemical weathering models that suggest the ubiquitous formation of hydrated mineral phases during aqueous episodes in Mars' history. In this chapter, I investigate the possibility that an initially abundant supply of hydrated minerals at the martian surface became desiccated by exposure to ultraviolet radiation over geologic time periods. These experiments show that ultraviolet radiation is capable of desorbing water from the surfaces of mineral grains but that the removal of bound water by UV stimulation is a negligible process on Mars. These results are consistent with the possibility that abundant quantities of hydrated minerals never formed at the martian surface. The presence of liquid water on Mars may have been too brief, too localized, or occurred at too low of a temperature to result in appreciable chemical weathering.

3.1.1 Ultraviolet Radiation at the Martian Surface

The composition and pressure of the martian atmosphere allows solar ultraviolet photons to reach to the surface. Models developed by *Kuhn and Atreya* [1979] indicate that under present climatic conditions, absorption by ozone centered at ~2550 Å allows 10^{-2} of incident solar photons to reach the surface (as

compared to 10^{-34} for Earth). They also indicate that wavelengths as short as 1900 Å to 2000 Å can penetrate the carbon dioxide atmosphere to the surface. Dust suspended in the atmosphere would receive even more UV radiation because of the shorter atmospheric path to these particles. In addition, during periods of low obliquity, the atmospheric pressure could be as low as 0.3 millibar [*Ward et al.,* 1974] and would result in a greater amount of ultraviolet flux at the surface. The UV radiation dose of material on Mars is clearly much higher than for mineral particles on the Earth.

3.1.2 Possible Effects of UV

What effects might this UV flux have on the martian surface materials? *Andersen and Huguenin* [1977] proposed that ultraviolet radiation is capable of dehydrating minerals. According to their abstract, photons with wavelengths shorter than 280 nm release H_2O (g) from goethite by ejecting OH^- groups which subsequently combine with H^+ from nearby sites. *Morris and Lauer* [1981], however, repeated the experiments and found no UV dehydration effects on goethite (α-FeOOH) or lepidocrocite (γ-FeOOH) in exposures equivalent to 10 to 100 years on the martian surface. They attributed the earlier findings to thermal dehydration rather than photocatalytic effects. On the other hand, recent work by *Muhkin et al.* [1996] demonstrate that ultraviolet photons are capable of decomposing carbonates and sulfates releasing CO_2 and SO_2, respectively. Furthermore, experiments applicable to interstellar and circumsolar grains have demonstrated that Lyman-α photons are capable of decomposing water ice [*Westley et al.*, 1995]. Thus, photo-induced alterations of solid surfaces is a relevant process in the planetary sciences, and the role of UV radiation in the dehydration of minerals on Mars warrants more detailed study.

3.1.3 New Experiments

We have developed a new series of experiments that offer 5 to 6 orders of magnitude greater sensitivity than the *Morris and Lauer* [1981] study of UV catalyzed dehydration of martian minerals. Our results show that ultraviolet radiation-induced desorption of water from the surfaces of mineral grains is observable on laboratory timescales. This finding has implications for the budget and the cycles for water at the martian surface. We do not, however, observe any effects of ultraviolet radiation on the OH in the crystal structure of iron oxyhydroxides. On the basis of our experiments, we calculate a minimum exposure time of 10^8 years for UV-induced dehydration of goethite or lepidocrocite at the martian surface. This minimum value is set by the sensitivity limits of our experiment and the actual required exposure times may be much longer. Thus, UV-stimulated desiccation of these minerals is not likely to be important on Mars and the relatively anhydrous current state may well be primary.

3.2 Experiment Description

3.2.1 Apparatus

A block diagram and photographs of our experimental setup are shown in figure 3.1. Samples are placed in a vacuum chamber which is maintained at pressures of approximately 10^{-10} torr using an ion-sputtering pump. An AMETEK Dycor quadrupole mass spectrometer with a Faraday cup and electron multiplier is used to monitor the gaseous species in the chamber. A mercury vapor lamp (peak flux at 254 nanometers) external to the vacuum chamber radiates the sample with ultraviolet photons through an Al_2O_3 window (there is no "line-of-sight" between the lamp and the quadrupole head). This lamp is controlled by a timer circuit which allows on/off cycling of power. The chamber can be baked at temperatures up to 200 °C using external strip heaters, and the sample itself can be precisely controlled to levels above ambient (up to 800°C) by a pyrolitic boron nitride heater mounted inside the vacuum chamber.

3.2.2 Samples

Recent results from the Mars Pathfinder camera [*Smith, et al.*, 1997] suggest that iron oxyhydroxides may be responsible for prominent 930 nanometer absorption in some soils. The magnetic properties experiments onboard Viking were interpreted to indicate the presence of 1% to 7% of a highly magnetic mineral phase, likely maghemite (γ-Fe_2O_3), in the martian soil [*Hargraves, et al.*, 1977]. These Viking results are supported by the recent Pathfinder data which suggest that most dust particles contain about 6% maghemite [*Hviid, et al.*, 1997]. Understanding the origin of this maghemite could significantly advance our understanding of the weathering processes at the martian surface. For example, one method of producing maghemite is through the dehydration of lepidocrocite

(γ-FeOOH). Here, we explore the possibility that ultraviolet radiation can catalyze the dehydration of γ-FeOOH. (Section 5.2 suggests yet another possible mechanism for forming maghemite on Mars.)

Thus, lepidocrocite is one of the primary hydrous mineral phases that we study in these experiments. Bentonite (a natural sample from Clay Spur, WY) and goethite (α-FeOOH) were also used because other iron oxyhydroxide phases [*Banin et al.*, 1993] as well as smectite clays [*Toulmin et al..,* 1977] have been suggested as significant components of the martian soil. Anhydrous control samples included hematite (α-Fe_2O_3) and maghemite (γ-Fe_2O_3). All of the iron oxides used in our work are synthetic, commercial products. The hematite and goethite samples were manufactured by Pfizer, while the lepidocrocite and maghemite were obtained from ISK Magnetics. X-ray powder diffraction analyses were conducted to verify the composition of the samples.

3.2.3 Procedure

To maximize the exposure of the minerals to ultraviolet radiation while minimizing contributions to the overall uncertainty by grain surfaces not exposed to UV, a great deal of effort was expended to minimize the thickness of each sample. We suspended small (~0.25 μm diameter) mineral grains in water using ultrasonic agitation and subsequently "airbrushed" the mixtures onto the surfaces of 0.5 inch diameter fused silica disks using pressurized nitrogen. The disks were maintained at 110°C during deposition to remove the water before large droplets could form. The total quantity of sample on each resulting disk was approximately 30 micrograms.

The upper portion of the vacuum chamber, which is separated from the ion sputtering pump by a gate valve, was opened in a glove bag under a positive-pressure flow of high-purity nitrogen when the prepared sample disks were introduced. Once the chamber was resealed using a new copper gasket, sorption pumps immersed in liquid nitrogen were used to rough the upper chamber. At a pressure of 1 to 2 μm as determined by a thermocouple gauge, the vac-sorbs were isolated, and the gate valve to the ion pump was re-opened to resume an ultra-high vacuum (UHV) chamber. The chamber walls and the sample were baked at ~150°C and 100°C, respectively, for 24 hours to minimize the quantity of adsorbed water in the system and in the sample. After baking, on/off cycles of the UV lamp (2 hour period) were initiated while the gas phase species in the chamber were monitored with the quadrupole mass spectrometer. Typical monitoring durations were approximately 150 hours with measurements collected every 30 seconds.

3.2.4 Results

Figure 3.2 illustrates a raw data profile for the water (AMU 18) in the chamber as a function of time as a lepidocrocite (γ-FeOOH) sample is periodically radiated with an UV lamp. The downward trend in the partial pressure of water is due to the gradual decrease in the total pressure as the ion pump continues to trap the free molecules in the chamber. Once the instrumental noise in the data is reduced by averaging and the DC bias is removed, the remaining AC signal (see figure 3.3) can be analyzed for frequency content correlated to the cycles of the UV lamp. The application of a fast-Fourier transform (FFT) to the data clearly shows that the power in the signal corresponds to a two hour period (figure 3.4). Similar results are obtained for goethite and for bentonite. Thus, the release of water from FeOOH and smectite clay samples is induced by the ultraviolet lamp.

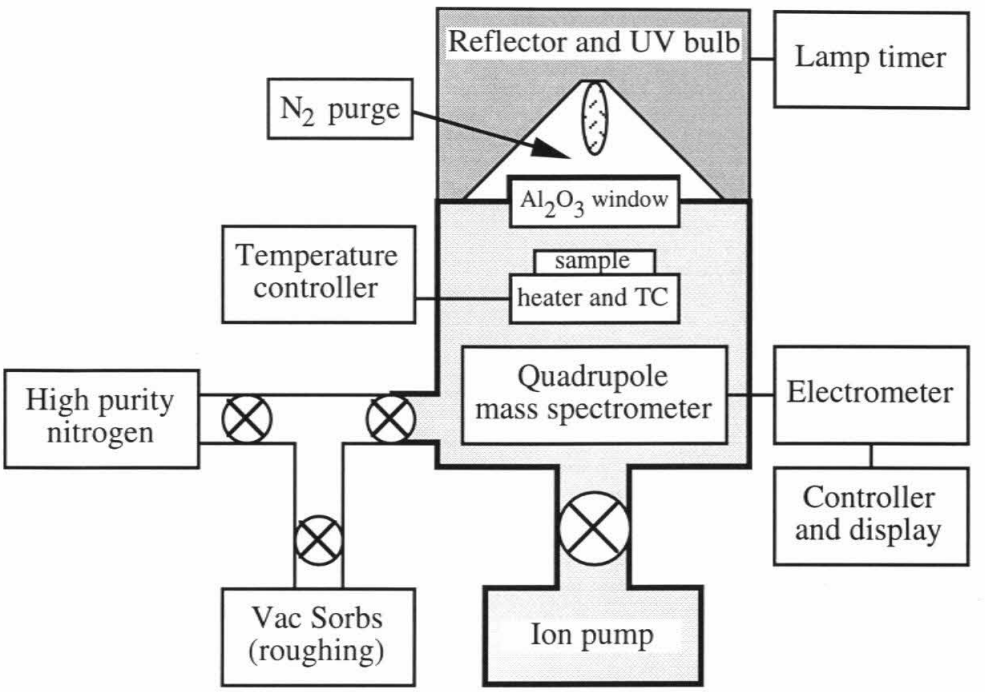

Figure 3.1a: Block diagram of experimental apparatus

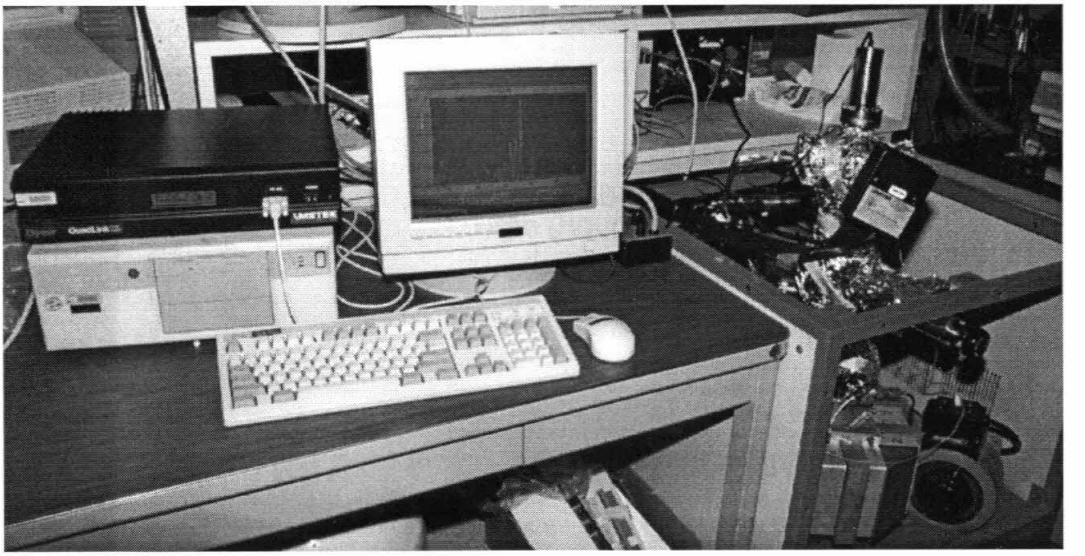

Figure 3.1b: Photographs of the experimental apparatus showing the vacuum chamber and associated data collection hardware.

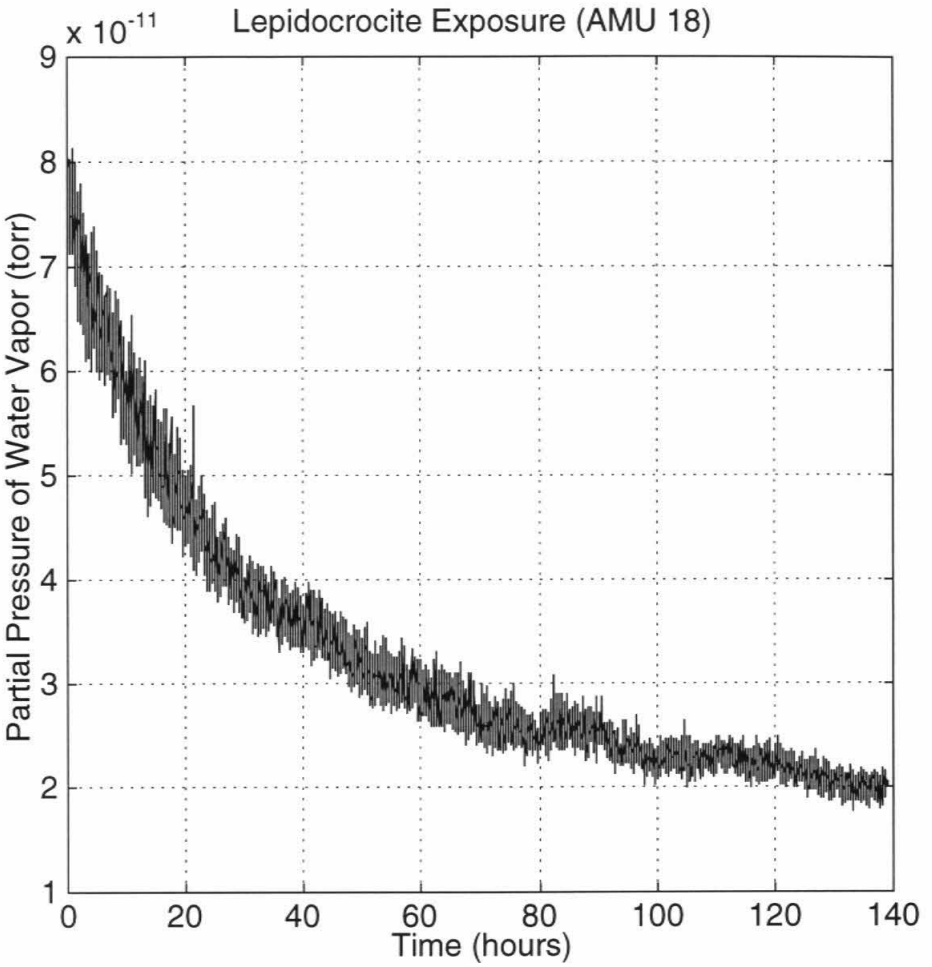

Figure 3.2: Raw mass spectrometer data from atomic mass unit 18 measured from lepidocrocite (γ-FeOOH) which was baked for 24 hours at 100°C. The ultraviolet lamp was cycled on/off (1 hour each) while these data were collected. Similar results were obtained for goethite (α-FeOOH).

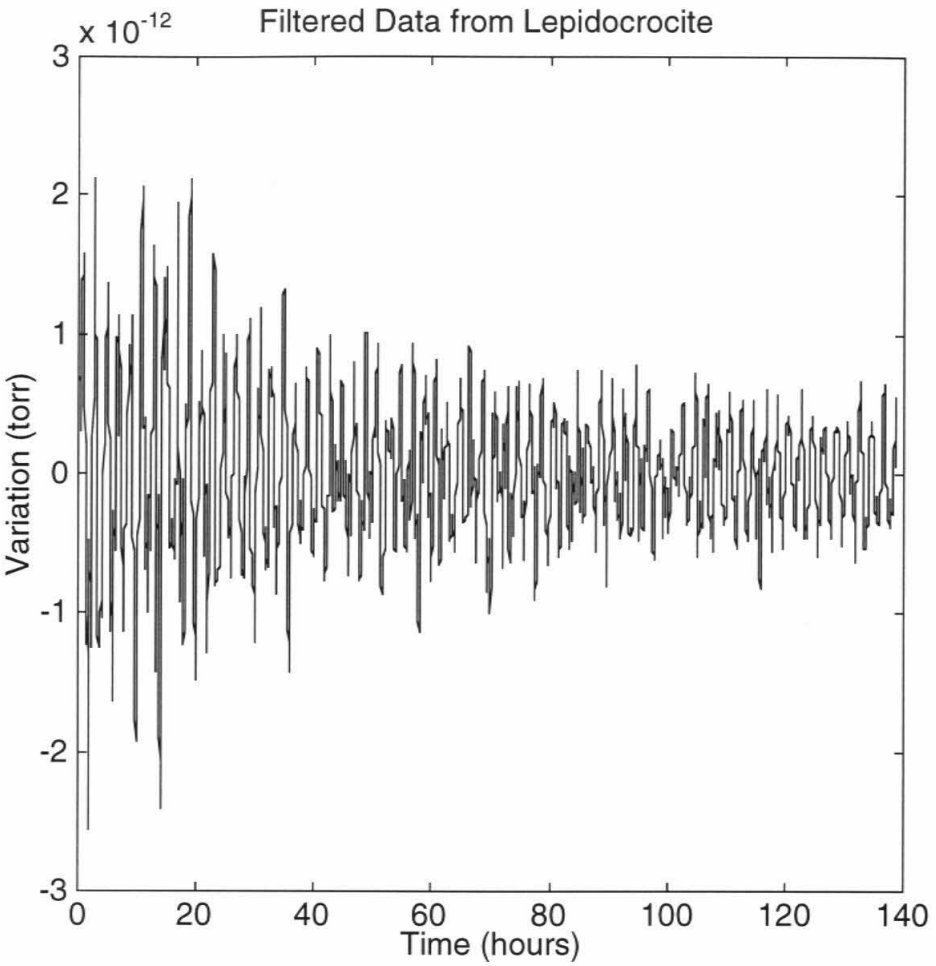

Figure 3.3: Filtered version of the signal shown in figure 3.2 with the trend removed.

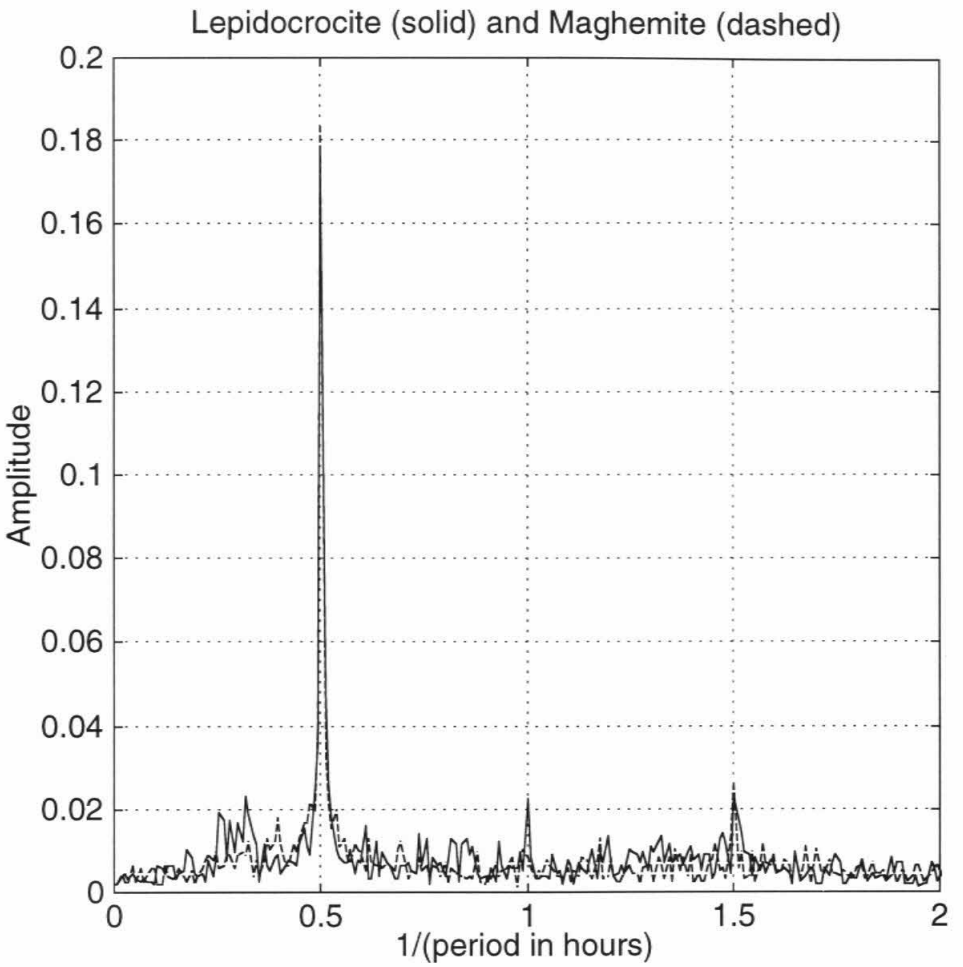

Figure 3.4: Fast Fourier Transform (FFT) of the data in figure 3.3 (lepidocrocite - solid line) and for a similar data set collected for maghemite (dashed line). Each curve is an average of 400 separate 4096 point FFTs. The spike at a period of 2 hours corresponds to water released from the samples while the lamp is on. The lack of a significant difference between the hydrated and anhydrous forms of this iron oxide indicate that adsorbed water which remained on the samples after baking at 100°C at pressures less than 10^{-8} torr was the source of the water signal.

3.3 Source of the Observed Water

There are three possible sources of the observed enhancement of water vapor concentrations in the vacuum chamber when the ultraviolet lamp is on: (1) The vacuum chamber itself, (2) OH from the crystal structure of the samples, and (3) molecules adsorbed onto the mineral surfaces. We address each of these possibilities in the following paragraphs.

3.3.1 Vacuum Chamber Contamination

The vacuum chamber itself could be the source of an erroneous AMU 18 signal correlated to the UV lamp. There have been reports of enhanced ionization efficiency by the Dycor head when exposed to UV photons [*Athey, personal communications*]. This interaction, as well as the possibility that the vacuum chamber walls are the source of the measured water, are, however, deemed unlikely. Cycles of the UV lamp using a blank fused silica disk as the sample, with all other aspects of the procedure identical to cases with coated disks, do not result in a water signal correlated to the illumination period. In addition, the mechanical design of the apparatus prevents photons from reaching the quadrupole head in less than 4 bounces inside the chamber. Thus, UV interactions with the instrumentation or the vacuum chamber cannot be responsible for the observed signal.

3.3.2 OH from the Crystal Structure

Lepidocrocite and goethite each contain hydrogen bound to oxygen in the octahedra of the crystal structure. We explore the possibility that the ultraviolet

photons catalyze the ejection of OH and H from these structures resulting in the enhanced water vapor concentration in the chamber when the ultraviolet source is energized. Thus, we compare the results from the two phases of FeOOH to the results obtained from their anhydrous counterparts: Maghemite (γ-Fe_2O_3) and hematite (α-Fe_2O_3). The process used in the preparation, baking, and data collection from the FeOOH polymorphs was carefully repeated for the Fe_2O_3 samples. An FFT result for the anhydrous gamma phase is plotted in comparison to the hydrated mineral in figure 3.4. These spectra indicate that there is no significant difference between the amount of water released from lepidocrocite as compared to maghemite. Similar results are obtained for the other polymorph: α-FeOOH (goethite) and α-Fe_2O_3 (hematite). As further evidence, we find that the visual colors of the lepidocrocite and the goethite samples are not altered by exposure to ultraviolet radiation. We, therefore, conclude that the water released by the incident UV photons in these experiments with iron oxides does not originate from the OH bound in the crystal structure.

3.3.3 Adsorbed Water

The thin-film samples used in these experiments are in equilibrium with the water vapor in the laboratory air prior to placing them into the vacuum chamber. Water molecules cling onto the surfaces of the mineral grains due to dipole molecular attraction. Subsequent monolayers are hydrogen bonded to the lower layers of H_2O. The original intent of this study was to determine the rate of removal of bound OH from the crystal structure, and adsorbed water was considered to be a noise source. Thus, we baked each of our samples for approximately 24 hours at 100°C inside the vacuum chamber with ambient pressures between 10^{-8} and 10^{-10} torr. It is nearly impossible, however, to

completely remove H_2O from a vacuum chamber. AMU 18 is typically the largest peak after hydrogen in a clean, baked, "empty" system. The large total surface area of the iron oxide samples makes it even more difficult to completely remove adsorbed water by baking. After numerous comparisons between results from the hydrated and the desiccated mineral phases in these experiments, we conclude that the water signal correlated with the UV lamp originates from H_2O molecules adsorbed on the surfaces of the mineral grains.

3.4 Mechanism

3.4.1 Thermal ?

Is it possible that the evolution of water from our samples is due to thermal desorption rather than an effect of the ultraviolet photons? *Morris and Lauer* [1981] attributed the earlier report of photodehydration by *Andersen and Huguenin* [1977] to heating by unfiltered visible and near-IR radiation. In our experiments, however, we use a mercury vapor line source rather than a broadband UV lamp. The power output from our source is primarily at 254 and 365 nm, and the bulb temperature is only a few degrees higher than the 100°C bakeout temperature that we used in our attempt to remove adsorbed water from the sample. Furthermore, experiments conducted with bakeout temperatures of 200°C and 300°C continue to yield water while the lamp is on (see figure 3.5). Thus, we feel confident that sample heating due to the ultraviolet source is not responsible for the observed water signal.

3.4.2 Electronic Interactions

Unlike infrared energy which couples directly to the vibrational modes in the irradiated materials, ultraviolet photons interact electronically. Absorption of a UV photon can result in one of the following: (1) Excitation of bound electrons and subsequent radiative emission (or chemical reaction), (2) thermalization of the excited state by dissipation of the energy in vibrational modes, (3) direct disruption of bonds between atoms, and (4) generation of charge carriers (electron-hole pairs) which can migrate, recombine, and deposit energy elsewhere in the sample. Pathways (1) and (2) would not result in the observed ejection of

water, while (3) and (4) could. We consider UV interactions with the substrate (mineral) and the surface water separately.

3.4.2.1 Substrate Interaction

The energy levels of the photons used in the laboratory as well as the ones incident on the martian surface and suspended dust have sufficient energy to break O-H and Fe-O bonds within the mineral lattice. A 1900Å photon incident on the martian surface or a suspended dust particle has an energy of 6.5 eV, while the 2537Å photons used in our experiments correspond to 4.9 eV. O-H and Fe-O bonds have strengths of approximately 4.5 and 4.1 eV, respectively. Our results, however, indicate that energy alone does not determine whether atoms can be released from the crystal structure. While some fraction of the incident photons will results in pathways (3) and (4), above, the fact that we do not observe the release of bound OH from the hydrated oxide phases leads us to conclude that the rate of annealing of the broken bonds in the crystal lattice is greater than the rate of disruption.

3.4.2.2 Effects at the Grain Surface

The interaction between the ultraviolet photons and the surface water, however, is different. The direct deposition of energy and/or the generation of electron-hole pairs in the substrate combining at the interface between the adsorbed water and the mineral grains is capable of counteracting the van der Waals forces that hold the water molecules onto the grain surfaces. We believe that these two electronic pathways are responsible for ejecting the water molecules that we observe while the UV lamp is on. In addition, these same

processes can likely sever the hydrogen bonds between H_2O molecules, but we do not expect this process to be applicable in our experiments because of our bakeout techniques. That is, we do not expect more than a monolayer of water to remain on our samples (hydrogen bonded to a lower layer) after baking at temperatures greater than 100°C under UHV conditions.

The demonstration of the photodesorption phenomena is not new. Photon stimulated desorption (PSD) of atoms, molecules, and ions has been studied in the field of surface science since the 1960's, see, for example, *Madey* [1994] for a review. Furthermore, commercial products can be purchased to introduce ultraviolet radiation into vacuum chambers to remove water adsorbed onto interior surfaces. Our results indicate that the efficiency of removing water from surfaces is greater using UV radiation as compared to thermal energy. That is, photodesorption can still remove water that remains after heating to temperatures as high as 300°C (see figure 3.5). This finding is consistent with the proposed advantages of UV products to clean chambers over less expensive thermal devices. We do, however, demonstrate the photodesorption of water from mineral surfaces which have much lower electron mobility when compared to the typical stainless steel vacuum chamber.

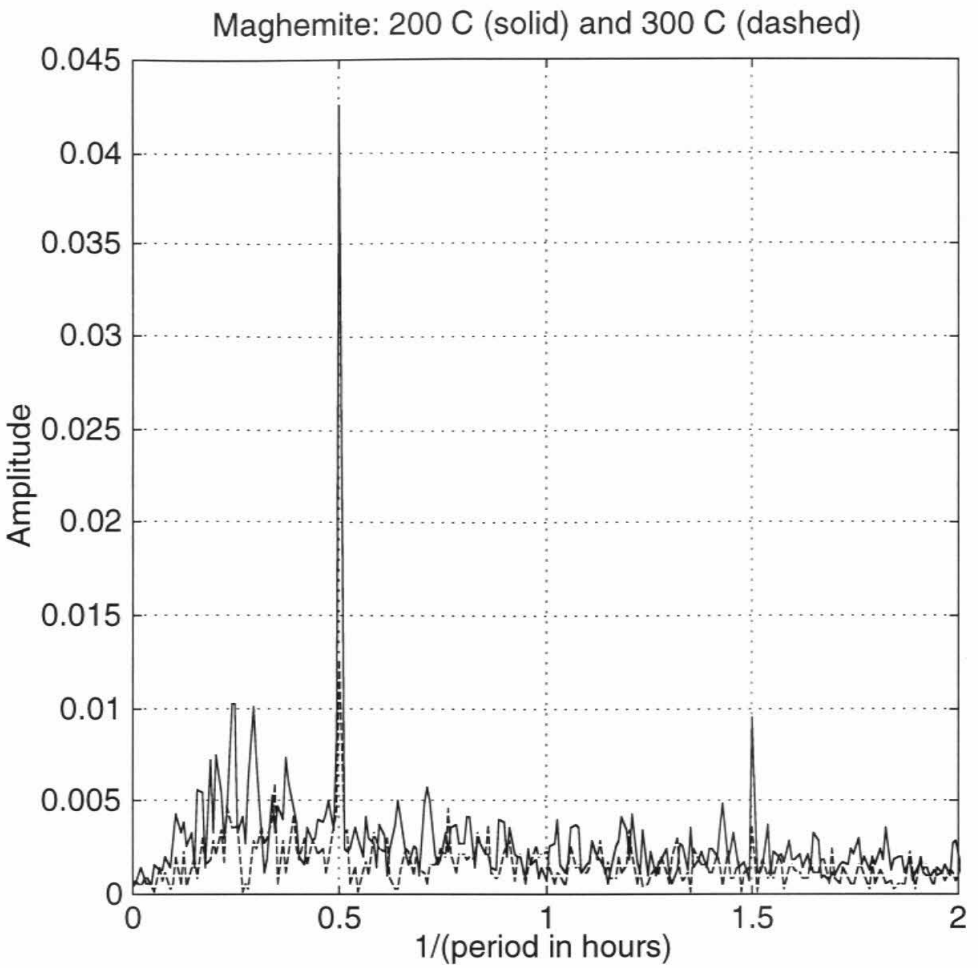

Figure 3.5: FFTs of the signals obtained from maghemite samples during exposures to cyclic UV radiation and after baking at 200°C (large peak) and 300°C (smaller peak) for 24 hours.

3.5 Application to Mars

3.5.1 Water on Soil Surfaces

In an "order of magnitude" estimate, the background pressure of water vapor in the chamber corresponds to ~10^{10} molecules, and the application of the UV source raises the pressure by a few percent while the ion pump continues to operate. An estimate of the sink rate for water in the system due to the ion pump indicates that ~10^9 molecules of water are released from the sample each hour during exposure to the UV photons. If each sample grain retained a tenth of a monolayer of water after heating to 100°C in the chamber (probably an overestimate) and had the surface area equivalent to a 0.5 μm diameter sphere (a certain underestimate), each sample exposed to UV radiation would contain approximately 10^{14} molecules of surface water. Even if all of these H_2O molecules on the mineral surfaces were accessible and permanently ejectable by photostimulation, it would take more than 10 years to accomplish. Thus, our laboratory experiments cannot realistically carry the surface dehydration to completion. This calculation is consistent with the relatively constant water signal during extended exposures (figure 3.6).

On Mars, geologic timescales are available for UV catalyzed desorption of water, but two factors will make the net rate of desiccation slower than what is observed in the laboratory: Total UV flux and diurnal cycles. The samples in these laboratory experiments, which are approximately 1 cm^2 in cross section, are exposed to roughly 5 milliwatts of radiation at a wavelength of 254 nanometers (4.9 eV). Assuming all photons from 2000 Å through 3500 Å are capable of ejecting water from martian dust and sand grains, a comparison of the incident power can be made. An integral of *Kuhn and Atreya's* [1979] model for solar

radiation incident on the martian surface yields an approximate average flux of 10^{-5} W cm^{-2}. Thus, these laboratory experiments provide a 500-fold enhancement of the ultraviolet flux as compared to the surface of Mars. If it takes 10 years to remove the adsorbed water from a sample in the vacuum chamber, it would take ~$5x10^3$ years for the same process to occur on Mars. This rough calculation does not account for the initial quantity of adsorbed water on the martian soil grains nor the diurnal cycles of UV radiation flux.

In the actual martian environment, we expect the soil particles at the immediate surface and the suspended dust particles to equilibrate with the surrounding atmospheric water vapor. In the daytime, however, temperature and pressure are not the only factors that need to be considered to determine the quantity of adsorbed water present. Ultraviolet radiation flux is important as well. The rates of evolution of adsorbed water calculated above are applicable to the initial quantities of water in the laboratory samples which are in equilibrium with an ultrahigh vacuum environment at 100°C and greater. A similar calculation using more realistic values for adsorbed water for martian soil [*Zent and Quinn*, 1997] would yield substantially larger exchange rates. Assuming a ten hour exposure to ultraviolet radiation, a square meter of the martian surface could evolve up to a milligram of water from UV stimulation alone. Thus, UV radiation could add a small source term to the models of diurnal water cycles [*Jakosky, et al.*, 1997; *Zent et al.*, 1993].

3.5.2 Interlayer Water

Clays, if present at the martian surface, provide large surface areas for retaining both adsorbed and interlayer water. Our experiments with a smectite

clay show that the strength of the evolved water signal due to UV illumination is larger (by approximately a factor of two) than that observed for the iron oxyhydroxides. Due to the lack of a suitable standard for comparison and uncertainties in the total surface area, we are unable to determine conclusively whether the origin of this observed water is from interlayer or surface adsorption sites. However, the possibility remains that the water desorbed by incident ultraviolet photons originated from the interlayer sites as well as from adsorbed molecules at the surface.

3.5.3 Bound OH

UV catalyzed removal of hydrogen bound in martian minerals would have significant implications for the evolution of the martian surface. The current state of desiccation [*Yen et al.*, in press] and weakness [*Murchie et al.*, 1993] or absence [*Dalton and Clark*, 1995; *McCord et al.*, 1982] of the cation-OH vibrational mode of phyllosilicates (~2.2 μm) in reflectance spectra could be the result of exposing an initially abundant supply of hydrated minerals to UV photons over geologic timescales. Furthermore, if dust particles suspended in the atmosphere are more susceptible to dehydration because of a larger UV dose, settling of these ubiquitous particles onto the surface could bias spectral observations. That is, radiation altered dust may mask underlying materials of mineralogical significance. In our experiments, however, we obtain no evidence for this photoinduced ejection of bound hydrogen. This finding is in contrast to the results published in *Muhkin et al.* [1996] where they found that carbonates and sulfates could be decomposed by incident UV. The efficiency of photodecomposition is apparently greater for carbonates and sulfates as compared

to iron oxyhydroxides. On the basis of our experiments we can set constraints on the rate of removal of water from these iron hydrates.

3.5.3.1 Surface Soil

The ~30 microgram samples that are used in these experiments contain roughly 10^{17} molecules of evolvable water from lattice sites. We observe no measurable differences between the quantity of water evolved from the hydrated as compared to the anhydrous samples used in the experiments for exposures of up to 250 hours of UV. The methods used here would allow us to detect UV stimulated dehydration from bound sites at rates as low as approximately 10^8 molecules per hour. We can therefore state on the basis of our experiments, that if all the bound OH sites in our sample were accessible by the UV photons or the migrating e^--h^+ pairs, each sample would take more than 10^5 years to dehydrate in our laboratory system. Extrapolating to Mars using the energy ratios as described above, an equivalent sample on the martian surface would take > $5x10^7$ years to completely dehydrate. This extrapolation assumes that the pressure and temperature effects on dehydration are not significant, which, of course, is not completely true.

The ~10^{-10} torr vacuum and room temperature environment for the lab experiments will shift the mineral into the stability regime of the desiccated phase and enhance the rates of dehydration relative to an equivalent sample on Mars. The low pressure in the experiment, however, isn't as large of a factor as intuition might suggest. *Pollack et al.* [1970] quoted a 1/e goethite dehydration timescale of 67 hours for a temperature of 225°C under air. This value is consistent with the observation that heating a sample to 200°C for 24 hours under UHV conditions

does not visibly convert the goethite to hematite. The interpretation is that the atoms inside the structure are not sensitive to the water vapor pressure at the surface of the grains.

Temperature, on the other hand, is a significant factor. For each 10°C increase in temperature, the rate of dehydration changes by a factor of 2 to 10 depending upon the activation energy of the process (between 15 and 40 kcal/mole, e.g., *Pollack et al.* [1970]). The temperatures to compare are the maximum surface temperature for Mars (~280°K) and the sample temperature while the lamp is on (~310°K). This 30° difference corresponds to a factor of 10 to 1000 change in the rates of dehydration. That is, if the minimum timescale for desiccation of a goethite or lepidocrocite grain is ~5×10^7 years on Mars (as extrapolated from a 310°K experiment), then the colder martian temperatures would change this estimate to a range of 10^8 to 10^{10} years. The timescale for overturning of mineral grains at the martian surface is likely to be shorter than the 100 million year minimum exposure time for desiccation. Furthermore, the effect of the ultraviolet radiation is an electronic interaction and will only be on the immediate surface (upper few nanometers) of each grain. Diffusion of hydrogen to the surface sites will also be necessary to completely dehydrate the grains. This leads us to conclude that ultraviolet radiation-induced dehydration of OH from the structure of iron oxyhydroxides at the martian surface is not a significant process.

3.5.3.2 Suspended Dust

The minimum timescale for the ultraviolet radiation induced dehydration of martian dust particles could be a factor of 10 shorter than the 100 million years

calculated above. Periodic storms continually inject small particles into the martian atmosphere where they experience a larger UV flux (due to the shorter atmospheric path length) than mineral grains at the surface. This 10^7 year timescale is a minimum value set by the sensitivity limits of our experiments. The actual required exposure time could be much longer and possibly irrelevant to the weathering processes on Mars.

3.5.3.3 Implications for the History of Water

An apparently desiccated surface of Mars (chapter II) and the inability to identify a mechanism to dehydrate minerals (this chapter) suggests that the martian surface may never have accumulated an abundant supply of hydrated mineral phases. The presence of liquid water at the surface may have been too brief, too localized, or occurred at too low of a temperature to result in appreciable chemical weathering. Further discussion of this speculative hypothesis can be found in section 5.1.

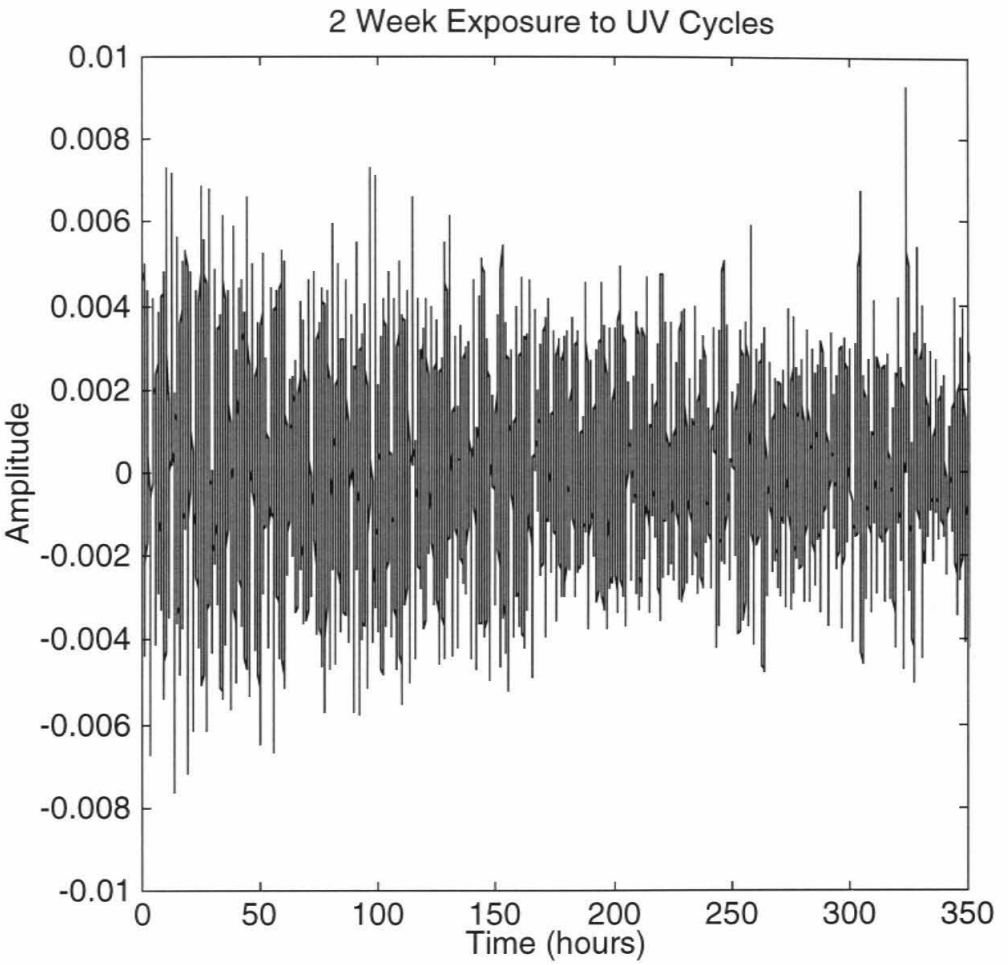

Figure 3.6: Extended duration exposure of a lepidocrocite sample to ultraviolet radiation cycles. The relatively small change in the amplitude over time is consistent with our estimate that complete removal of the adsorbed water would take ~100 years in the laboratory configuration.

3.6 Conclusions

- Laboratory experiments show that ultraviolet radiation incident upon samples of lepidocrocite, maghemite, goethite, hematite, and montmorillonite is capable of releasing adsorbed water from the mineral surfaces. Incident UV photons may also eject interlayer water. An extrapolation to martian conditions suggests that 1 milligram of water could be released per square meter of the surface during daytime exposures to ultraviolet radiation.

- Our experiments show no evidence that ultraviolet radiation is capable of liberating OH bound in the lattice of hydrated mineral phases. Based on the sensitivity limits of our experiments, we calculate a minimum required UV exposure time of 10^8 years for photodehydration of lepidocrocite or goethite at the martian surface. Because the actual value could be much higher and because the timescale of overturning for surface materials is likely to be shorter than this 10^8 year minimum, we conclude that UV radiation-induced removal of bound OH from hydrated minerals is not a significant process at the martian surface. One possible implication is that hydrated minerals never formed in abundance on Mars (see section 5.1).

- The applicability of photodehydration to martian dust particles is enhanced relative to soils at the surface. Suspension in the atmosphere, periodic dust storms, small particle sizes, and the greater UV flux at higher altitudes all increase the likelihood that ultraviolet radiation can induce the removal of bound OH from hydrated phases in the martian dust. While the sensitivity limits of our experiments set a shorter minimum exposure time for dehydration of suspended dust as compared to surface minerals (10^7 versus 10^8 years), the actual required time could be much longer, and we still have no evidence to support the occurrence of this physical process.

Chapter IV: Investigations of Ultraviolet Radiation-Stimulated Oxidation

4.1 Introduction

The results of chapter III suggest that aqueous chemical weathering may not have been a widespread process on Mars. Here, I extend the conclusions from the previous chapter and assess the possibility that ultraviolet radiation-induced oxidation is important to the production of the ferric iron components in the martian soil. The results indicate that the chemical alteration of minerals by this process is negligible but that efficient oxidation of *metallic* iron occurs by UV stimulation. Meteoritic metallic iron oxidized under environmental conditions similar to the current Mars could, in fact, be the source of some of the ferric iron in the soil and be mainly responsible for the color of Mars.

4.1.1 Weathering Processes on Mars

Recent data from the Thermal Emission Spectrometer (TES) onboard Mars Global Surveyor indicate the presence of unweathered pyroxenes and plagioclase feldspars in low-albedo regions of the martian surface [*Christensen et al.*, 1998]. The relatively bright dust and soils, on the other hand, exhibit weak reflectance in the blue and near-ultraviolet regions of the spectrum indicative of Fe^{3+} - O^{2-} charge transfer absorptions. These ferric assemblages are characteristic of highly weathered materials. What processes control the weathering of primary minerals on Mars? Are these processes active today, or

were all of the secondary minerals formed early in the martian geologic history? Useful constraints on climate change and the volatile inventory of the planet could potentially be established from knowledge of the weathering mechanisms.

Burns [1993] suggested that chemical weathering of martian minerals occurred by dissolution of basalts in acidic ground water, aqueous oxidation by dissolved oxygen, and subsequent precipitation of Fe^{3+} oxhydroxides, hydroxysulfates, and oxides. The eruption of volcanic lavas into ice-rich crustal layers has also been suggested as a possible formation mechanism for the oxidized soils [*Soderblom and Wenner*, 1978; *Allen et al.*, 1981]. In addition, hydrothermal alteration of impact melt could be responsible for the formation of martian soils [*Newsom,* 1980]. All of these proposed processes imply that much of the mineral weathering occurred in the martian past when (a) liquid water was present at or near the surface and/or (b) volcanoes were active and/or (c) the impact rate was high.

Contemporaneous mechanisms for chemical weathering have also been proposed. Gas-solid reaction models using the present day martian atmosphere suggest that 0.1 to 4.5 cm thick layers of basaltic glasses can be weathered into clay minerals in 10^9 years [*Gooding et al.*, 1992]. In addition, based on observations in the Antarctic, *Allen and Conca* [1991] conclude that the formation of etch pits and iron-rich clay minerals can occur in cold, arid climates from thin films of water which periodically form on rock surfaces during the melting of frosts. Identification of the past and present processes which contribute to the formation of the oxidized soils would greatly improve our understanding of the evolution of the martian surface.

4.1.2 Ultraviolet Radiation Weathering

Another possible mechanism for ongoing oxidative weathering of minerals on Mars was proposed by *Huguenin* [1973a and 1973b]. He obtained experimental evidence that magnetite ($Fe^{3+}(Fe^{2+}Fe^{3+})O_4$) could be weathered to hematite (α-Fe_2O_3) and possibly some maghemite (γ-Fe_2O_3) in the presence of ultraviolet radiation in an atmosphere containing O_2. This result is especially interesting given the conclusions of the Mars Pathfinder magnetic properties experiment indicating that martian dust particles contain about 6% maghemite [*Hviid et al.*, 1997]. *Huguenin* [1974] further applied the photo-stimulated oxidation idea to suggest that basalts could be altered to produce a global layer of clays, goethite, and metal oxides 1 to 1000 meters thick.

Photo-stimulated oxidation of basalts or magnetite, however, was never successfully duplicated by other experimentalists. *Booth and Kieffer* [1978] did not detect reddening of iron-rich basaltic powders exposed to ultraviolet radiation. *Morris and Lauer* [1980] measured the saturation magnetization of magnetite samples before and after exposure to filtered radiation from a xenon arc lamp and were unable to detect changes resulting from ultraviolet photons alone. When longer wavelength, infrared energy from the arc lamp was allowed to irradiate the samples, however, temperatures over 500°C were reached, and some of the magnetite was converted to hematite. The implication of *Morris and Lauer's* work is that Huguenin's experiments thermally oxidized the samples and that UV-induced weathering of minerals on Mars, while possible as a theory, has yet to be demonstrated in laboratory experiments.

4.1.3 New Experiments

Part of the difficulty in observing weathering processes that might only be significant on timescales comparable to the age of the solar system is the sensitivity limit of laboratory techniques. Furthermore, the interactions between ultraviolet photons and soil grains occur only as a surface phenomena. Bulk analysis tools are not well suited for establishing the existence of photo-stimulated weathering. With my colleagues, I have developed a surface analytical process which has the ability to measure the oxidation of materials at levels smaller than a single atomic monolayer. These measurements are several orders of magnitude more sensitive than previous studies. We apply this technique to investigate the possibility of ultraviolet radiation-induced oxidation of materials at the martian surface.

4.2 Experiment Description

4.2.1 Thin-film Sensors

Thin-film chemical sensors are devices which exhibit a measurable change in some physical property when exposed to an environment which reacts with that film. The applications of such sensors are extremely broad and include the monitoring of gas and solid phase species (e.g., ozone, oxygen, carbon dioxide, nitrogen dioxide, organic molecules, and many others) by electrical, optical, or acoustic transducers. The goal of the Mars Oxidant Experiment (MOx), which was launched onboard the Russian Mars '96 spacecraft, was to investigate the oxidative properties of the martian soil using metal and organic thin-films up to several hundred nanometers in thickness [*Grunthaner et al.,* 1995; *Manning et al.,* 1997]. MOx would have used optical techniques to sense reflectivity changes in the films as they reacted with the martian soil, but the failure of the launch vehicle brought the mission to a premature end. The work described here is based on the MOx development, but resistance measurements rather than "micromirrors" are used to detect oxidative changes. The "chemiresistors" used in this study are conductors as a pure film and insulators as an oxide. The thickness of each film is a few 10's of atomic monolayers, and the oxidation of a fraction of a monolayer results in a large change in conductivity. Thus, a simple measurement of resistance is a very sensitive way to detect the growth of an oxide layer.

4.2.2 Apparatus

We used an electron-beam deposition system to prepare the films used in this study. This apparatus is the same one that supported the development of

MOx and is located in room 147 of JPL's Microdevices Laboratory (see figure 4.1). Electrons from a 10 kilovolt source were electromagnetically steered into pockets containing bulk film material. The impingement of electrons induces the evaporation of the material into the vacuum chamber. The deposition rate was controlled by a closed-loop quartz crystal microbalance system which sensed the thickness of the film and adjusted the electron beam power level to achieve the desired rate of deposition (typically ~1 Å/sec). The sample substrates were located a large distance (60 cm) from the source material to achieve optimal uniformity across the film. The pressures inside the stainless steel bell jar were maintained at pressures of $\sim 10^{-7}$ torr using a cryopump.

Resistances of the films were monitored by a digital multimeter connected to the sample substrate across electrical feedthroughs into the vacuum chamber. Data were relayed to a computer for storage across a RS232 connection. For greater sensitivity to small changes in resistance, a wheatstone bridge was used to monitor voltage changes as the film resistance varied. A mercury vapor ultraviolet lamp was mounted inside the chamber (on top of a shutter mechanism) and could be activated with an external timer circuit connected to the bulb using vacuum feedthroughs. The chamber environment could be maintained under ultrahigh vacuum conditions or backfilled with ultrahigh purity nitrogen at pressures up to atmospheric. In order to minimize the adsorbed contaminants inside the chamber, laboratory air was never introduced. All samples were handled using polyethylene glove bags through a stainless steel transfer glove box.

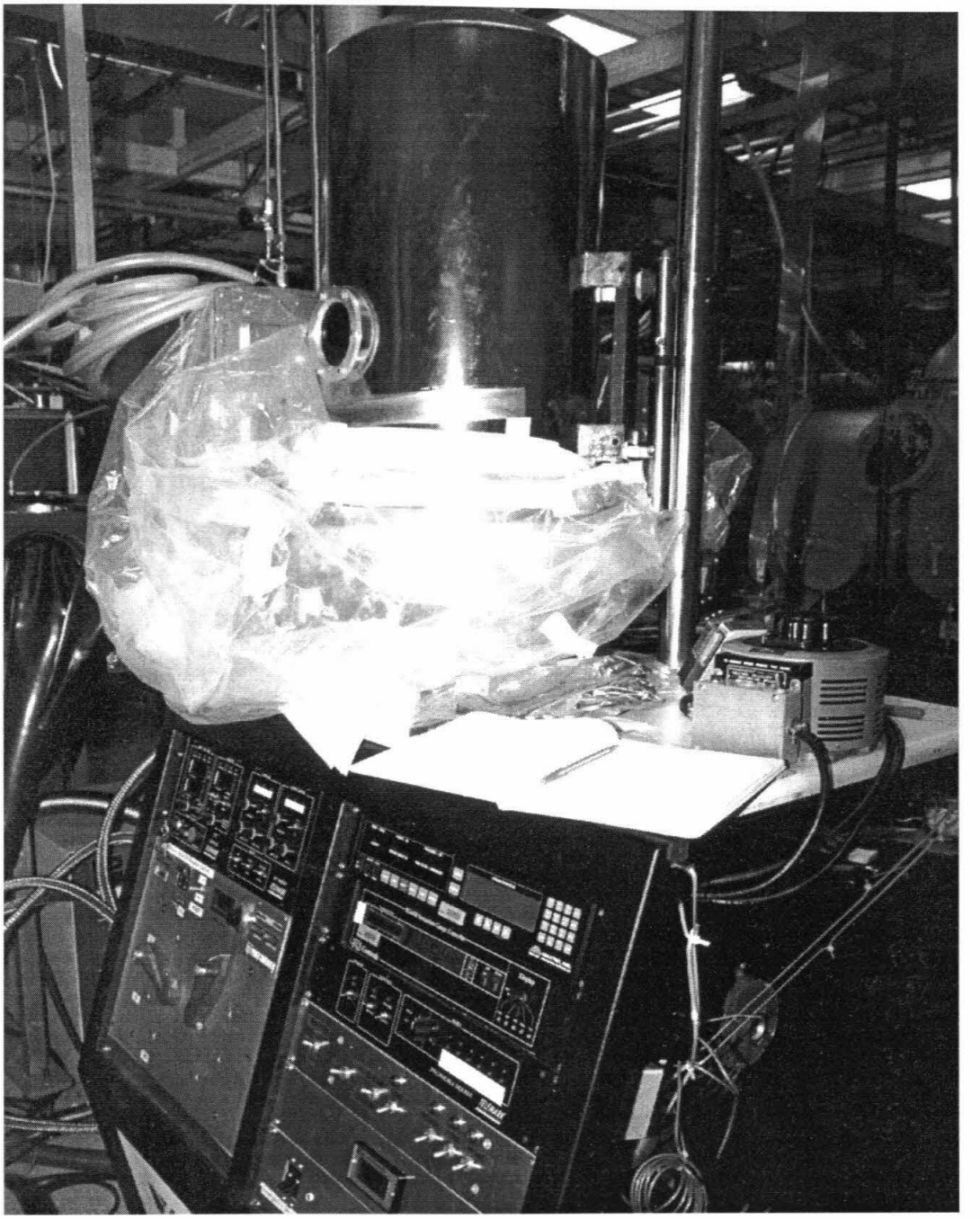

Figure 4.1: Photograph of the electron-beam evaporator system used for this study. It is located in room 147 of JPL's Microdevices Laboratory. The stainless steel bell jar houses the electron gun, the pockets of material for deposition, the samples, and the ultraviolet lamp. Associated power supplies, controllers, and vacuum hardware are located beneath the chamber.

4.2.3 Samples

The most direct method for establishing and quantifying photo-induced oxidation on Mars would involve the use of actual minerals. For example, observing the conversion of ferrous to ferric iron resulting from a true UV stimulus, such as in the conversion from magnetite to hematite, would provide a convincing argument for the applicability of this process. A difficulty, however, is that minerals are insulators and the limited mobility of electrons would severely constrain the ability to measure any UV-induced effect. As a result, we chose to observe the effects of highly reactive metal surfaces in exposure to ultraviolet radiation. If this phenomena is not observable for metals in our experimental setup, then either (a) photo-stimulated oxidation is not likely to be an active process minerals on Mars, or (b) the interaction between UV photons and surfaces is substantially different from the mechanism that we describe in section 4.3. We concentrate our study on thin films of metallic iron, from which chemiresistors can be easily fabricated. Furthermore, it is a cosmochemically significant material which has been delivered to the martian surface by meteoritic infall.

4.2.4 Procedure

The experimental procedure consists of several steps: (1) Deposition of electrical contacts on the substrate, (2) deposition of the chemiresistor, and (3) monitoring resistance changes of the film under a variety of environmental conditions.

Fused silica microscope slides (1" x 3") were used as the substrates for the chemiresistors. The electron beam system described above was used to deposit the conductive contacts (see figure 4.2) for the measurement electrodes. Stainless

steel shims were cut and spot welded to create a shadow mask to limit the deposition to the desired portions of the substrate. These contacts consisted of a 100 Å layer of chromium and a 2500 Å thick layer of gold. The chromium film was necessary to improve the adhesion of the gold onto the substrate.

After the deposition of the contact films, the chamber was filled with high purity nitrogen, and through the use of glove bags, the shadow mask was removed. Wire leads connected to the vacuum feedthroughs were attached to the samples using spring clips. The resistance between the contacts could then be monitored using meters outside the chamber. Before the iron film is deposited, the resistance is infinite, and as material is sputtered onto the area between the contacts, the resistance drops to measurable levels. Figure 4.3a shows the drop in resistance with time during the deposition of ~70 Å of iron. The change in slope resulting from the transition between electron "hopping" across small islands of metallic iron and conduction through a continuous film of material begins after ~70 seconds in figure 4.3a. Another deposition of iron, this one conducted using a chamber at Sandia National Laboratories, was carried to a greater thickness, and the transition between "hopping" and bulk conduction is more pronounced (figure 4.3b). In order to increase the sensitivity to the formation of small amounts of oxide, the depositions in the work at JPL were terminated soon after the bulk conduction phase was initiated. That is, the film was thick enough to start at a resistance of a few tens of ohms and thin enough such that small changes in the conductive cross section would still be observable.

4.2.5 Results

An increase in the resistance of the films is observed upon the introduction of ultra-high purity nitrogen into the vacuum chamber; see figures 4.4a and b. This purge gas is plumbed into the Microdevices Laboratory from the boiloff of liquid nitrogen. The gas stream is filtered through polymers which removes impurities, and the resulting concentration of contaminants is less than a few parts-per-million and is typically reduced to parts-per-billion. These results showing the effects of introducing the purge gas are consistent with the data we obtained during proof-of-concept studies performed at Sandia National Laboratories. In the work at Sandia, films of chromium and iron were thermally deposited and monitored over time. At Sandia, we had the advantage of opening the chamber to air without fear of contaminating the apparatus. Some of the results are shown in figures 4.5 and 4.6. The similarity of the results obtained from different hardware and deposition techniques gives us confidence in the data and the performance of the chemiresistors

The apparatus at Sandia was not configured to allow exposure to ultraviolet radiation. Experiments relevant to photo-stimulated oxidation were conducted in the chamber at JPL. The films were radiated with the UV lamp while under vacuum and while under high purity nitrogen. These results are shown in figures 4.7, 4.8, and 4.9.

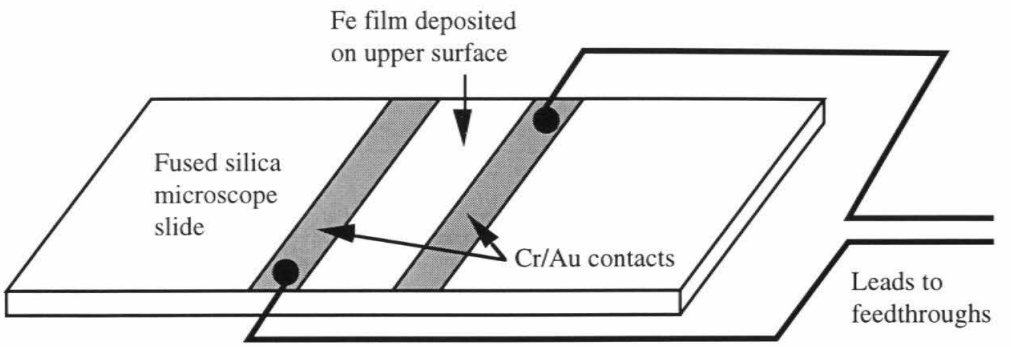

Figure 4.2: Sketch of the geometry for the Fe films and the Cr/Au contacts in the experiments conducted at JPL. The electron-beam deposited contacts are separated by a distance of approximately 1 cm. After deposition of the contacts, electrodes are connected, and the chemiresistor film is sputtered onto the slide.

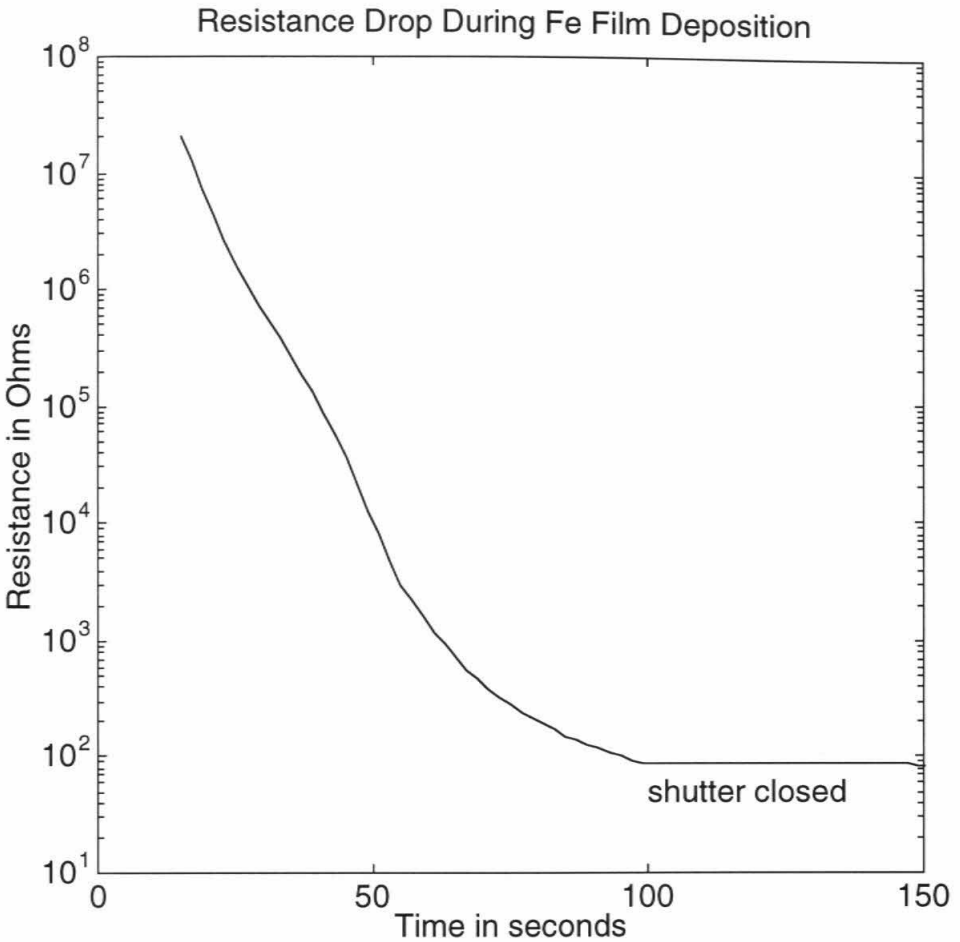

Figure 4.3a: Drop in resistance with time as a 70 Å film of iron is deposited onto the fused silica substrate with Cr/Au contacts. The deposition rate is approximately 0.7 Å/sec. Once the shutter is closed, no further deposition or change in resistance occurs.

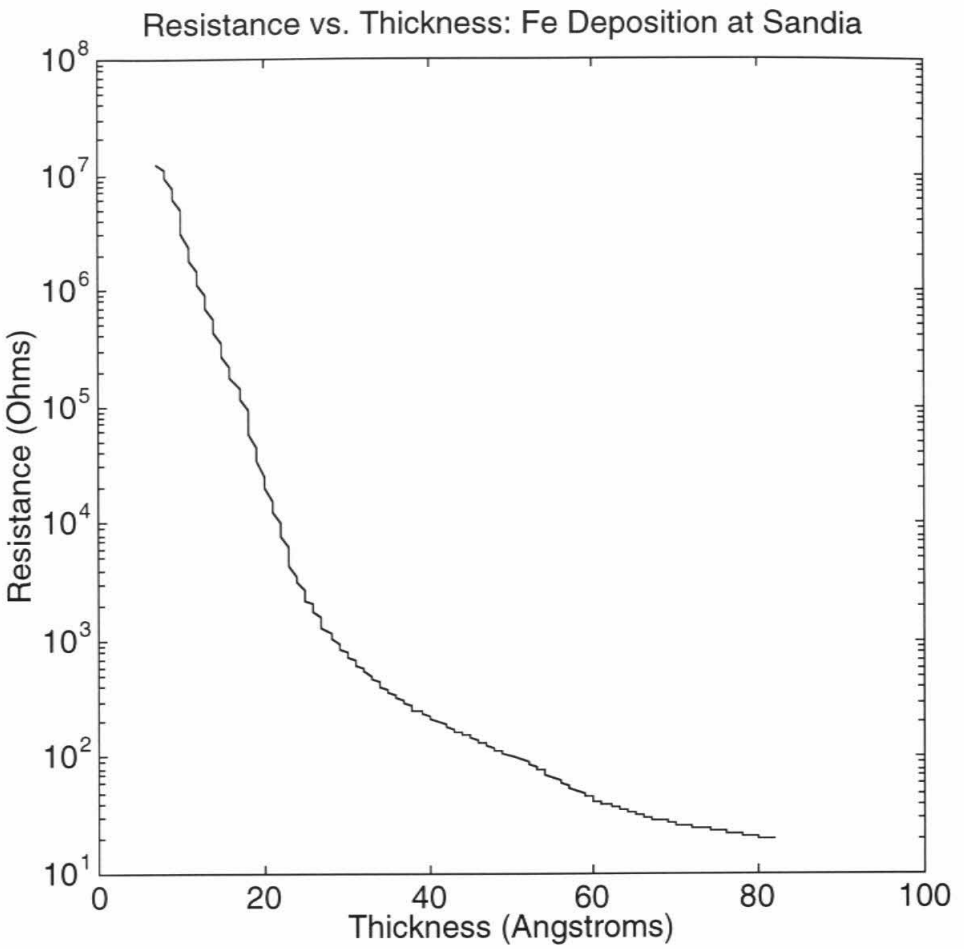

Figure 4.3b: Resistance versus thickness for a iron film deposited using a thermal deposition apparatus at Sandia National Laboratories. The geometry of the contacts on the substrate is different than in the work conducted at JPL. The change in slope at a thickness of 25 to 30 Å in this plot illustrates the transition from charge hopping between islands of metal to bulk conduction through a nearly continuous film.

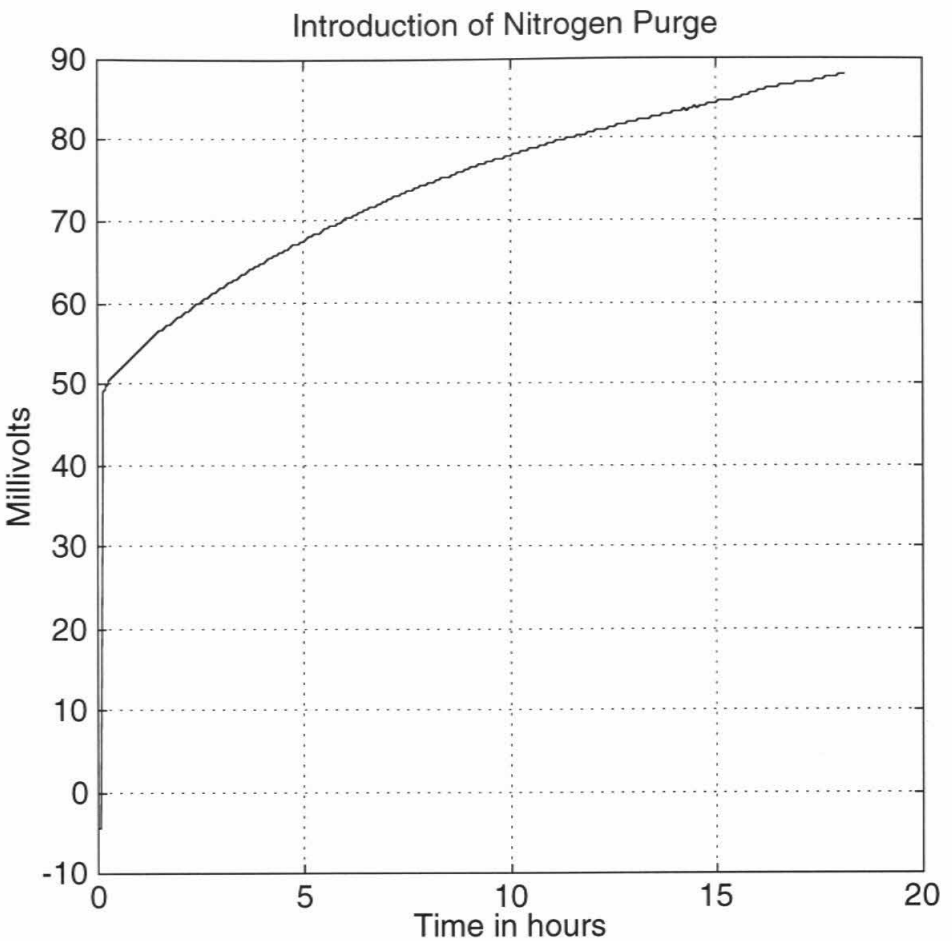

Figure 4.4a: Voltage increase in the bridge circuit corresponding to an increase in resistance of an iron film upon the introduction of ultra-high purity nitrogen into the vacuum chamber. A 1 ohm resistance change corresponds to approximately 5.3 millivolts in this plot.

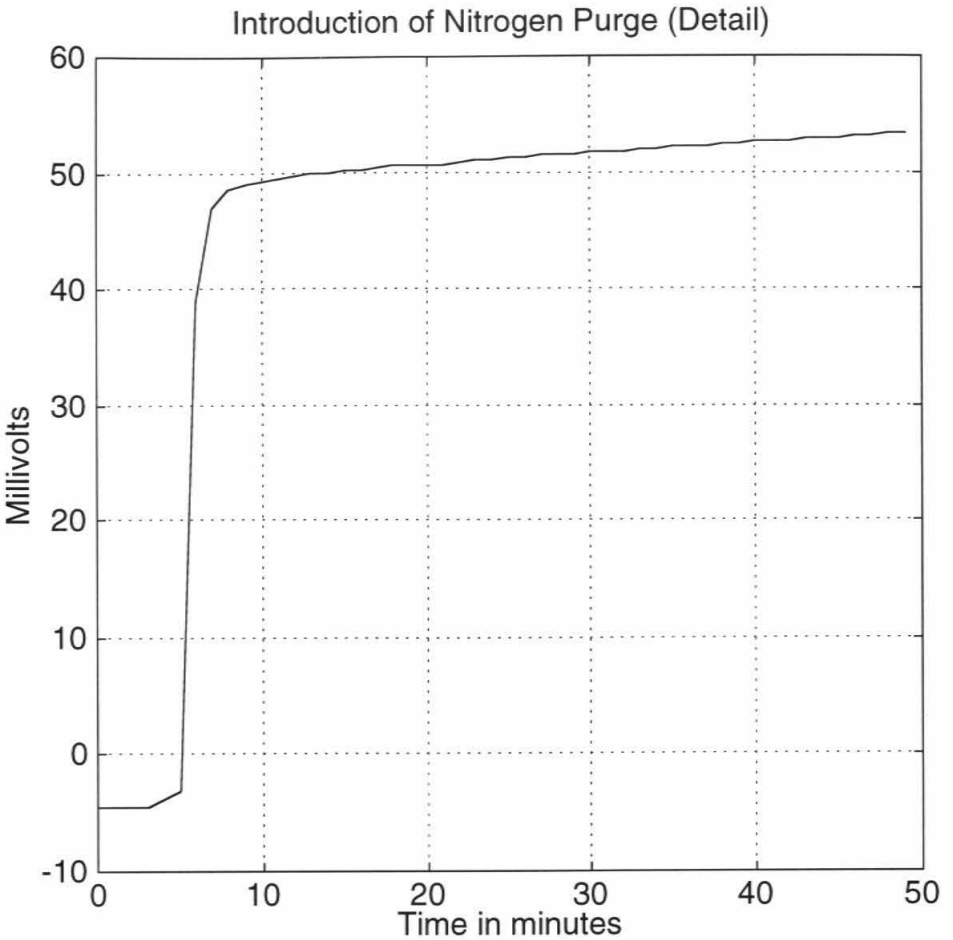

Figure 4.4b: Detailed plot of figure 4.4a showing the immediate voltage change upon exposure to the purge gas. A noticeable increase in the resistance occurs within 30 seconds of opening the nitrogen valve.

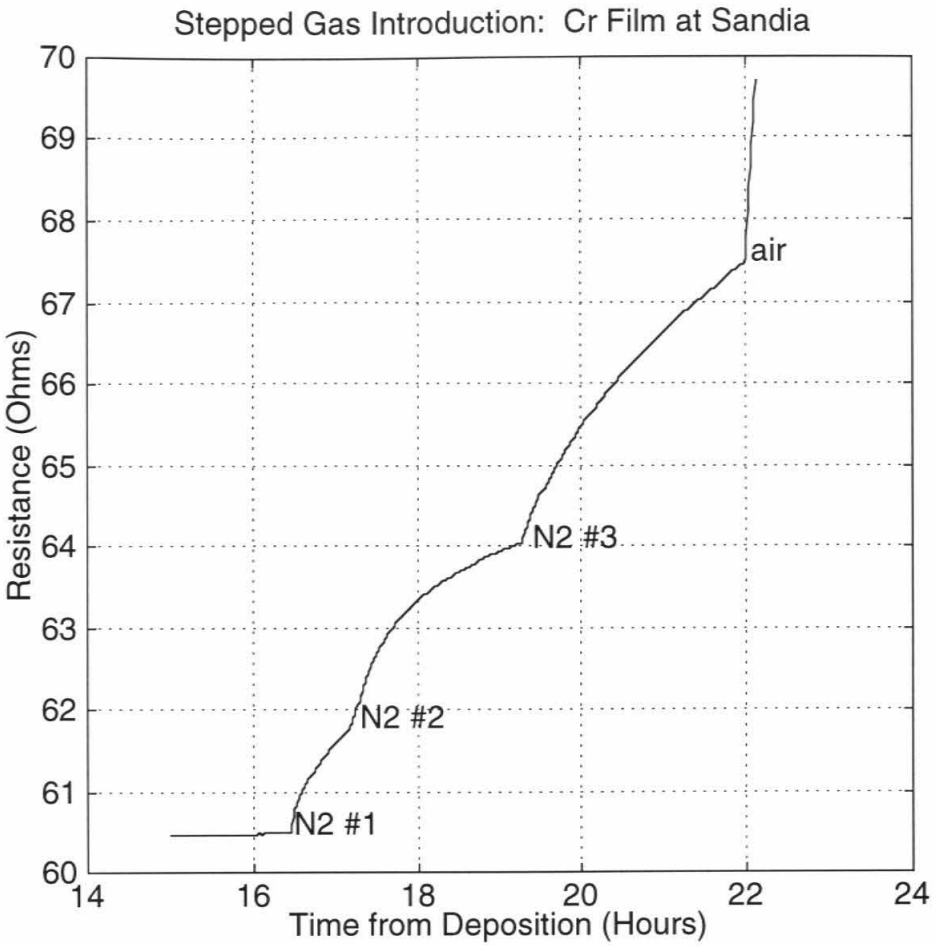

Figure 4.5: Data collected from experiments conducted at Sandia: Resistance versus time for an 80 Å thick film of chromium. Maintaining the sensor under high vacuum results in minimal changes over 16 hours. As nitrogen gas and associated impurities are introduced at successively higher pressures (450 torr for "N2 #1" and atmospheric pressure for "N2 #3"), the metal surface oxidizes and the resistance increases measurably. Opening the chamber to air 22 hours after deposition increases resistance rapidly. These resistance changes in the Sandia data cannot be directly compared to the results obtained at JPL, because the configuration (spacing) of the electrodes is different.

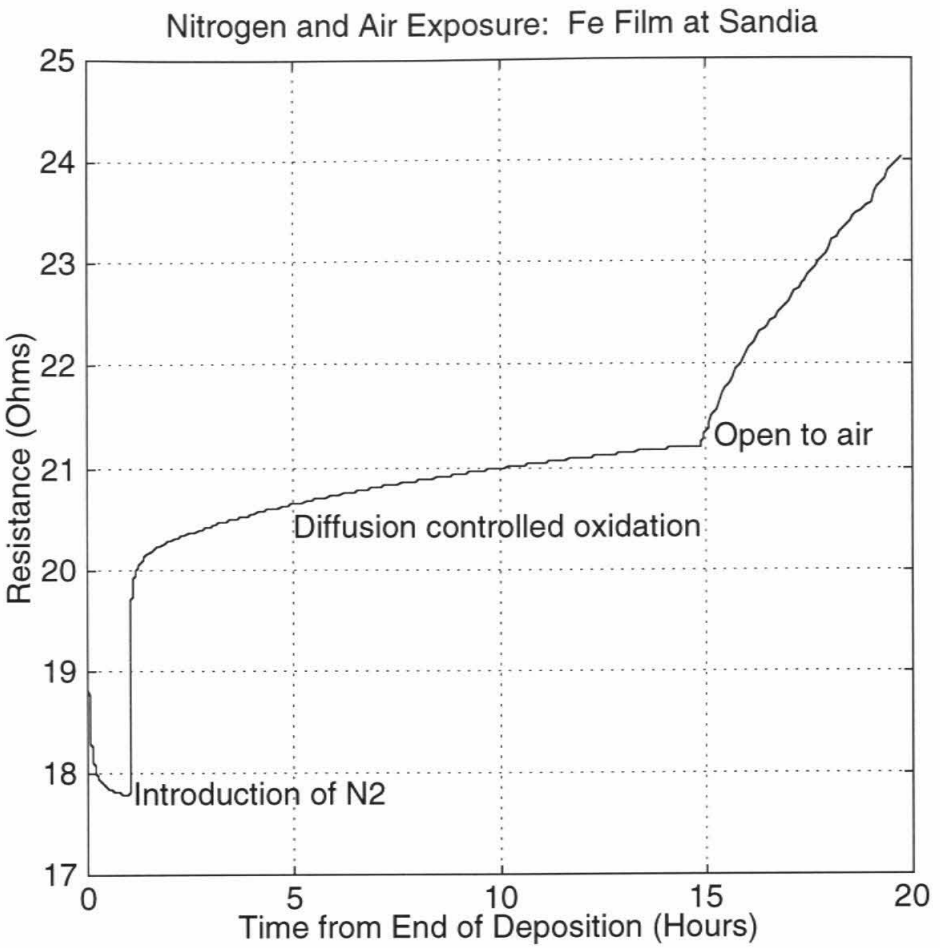

Figure 4.6: More data collected at Sandia: Resistance versus time for an 82 Å thick film of iron. Resistance drops during the first hour after deposition as the film cools under high vacuum. As nitrogen gas and associated oxygen containing impurities are introduced, the iron film initially oxidizes quickly. Further oxidation requires diffusion across the oxide layer and is significantly slower. Exposure to air oxidizes the film further.

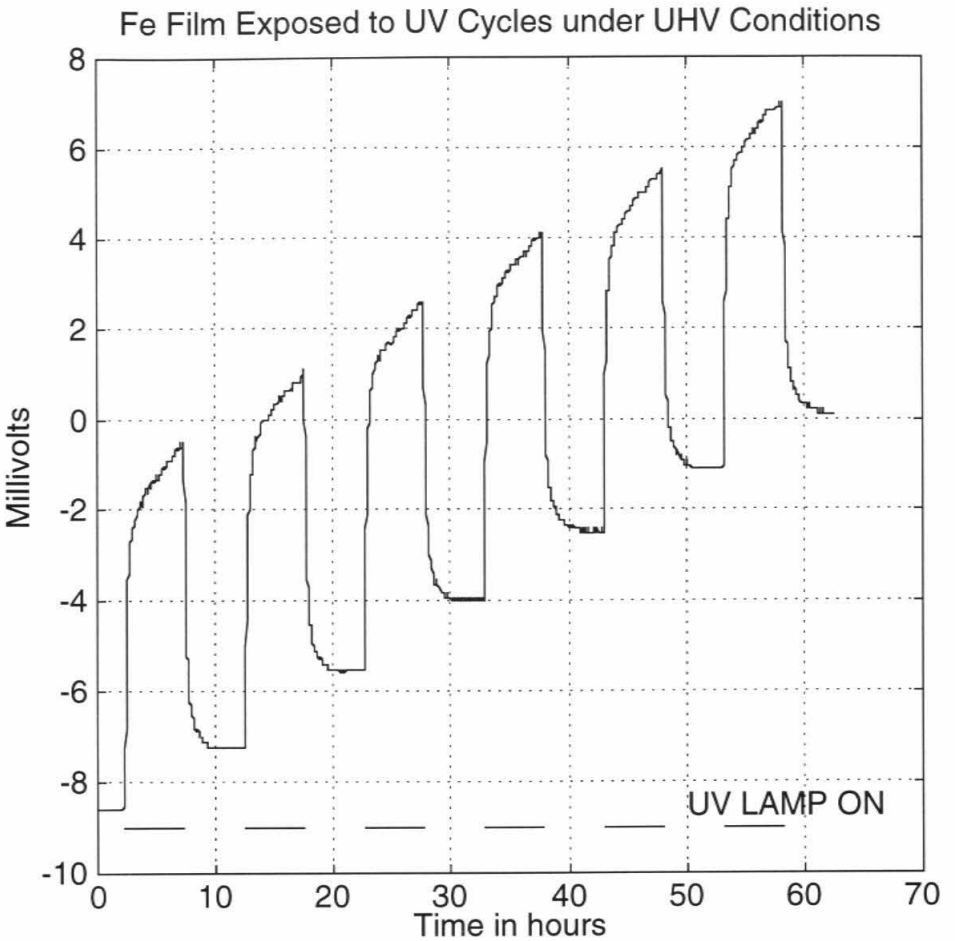

Figure 4.7: Iron film under vacuum (~10^{-7} torr) with periodic UV illumination (as indicated on the figure). Resistance changes in the film are monitored with a Wheatstone bridge circuit to increase the measurement sensitivity; 0.0 millivolts in this plot corresponds to 90.9 ohms. The large changes in voltage are probably due to film heating of approximately 3°C when the lamp is illuminated. However, a larger rate of resistance change is evident at the peaks of the cycles (when the lamp is "ON" as compared to the relatively flat valleys (lamp "OFF"). This behavior is not easily explained as a purely thermal phenomena. See text for discussion.

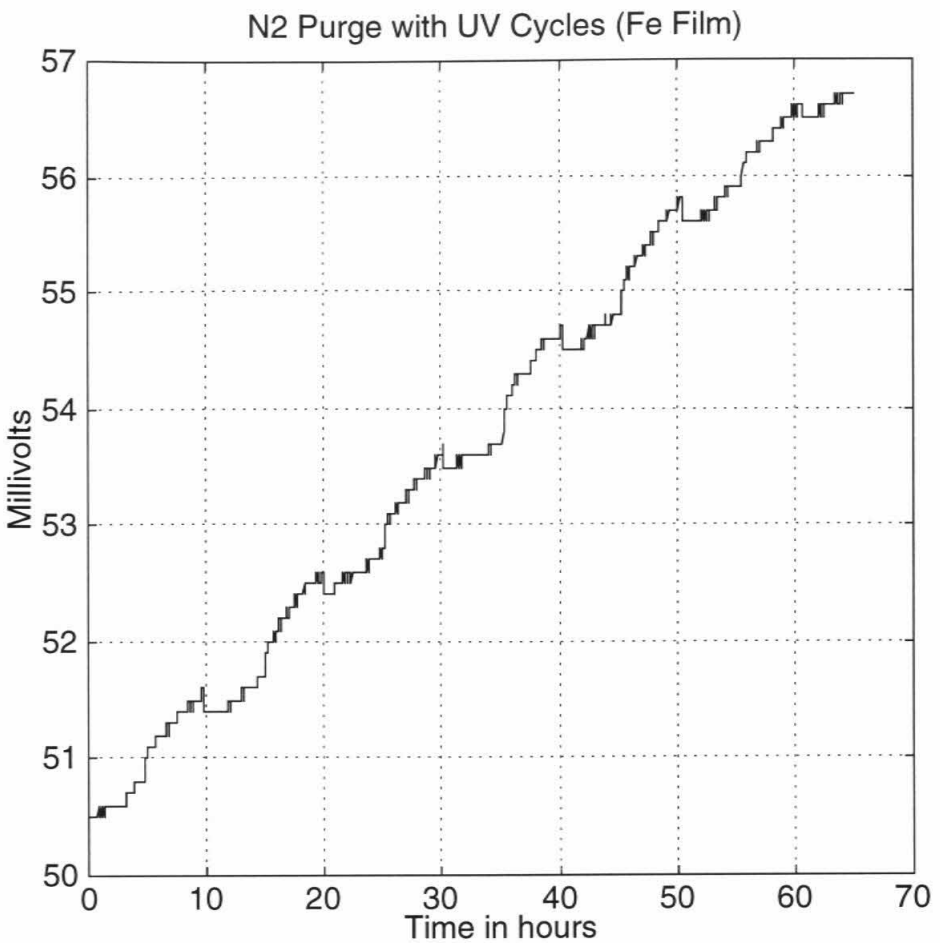

Figure 4.8: Iron film under dry nitrogen with periodic stimulation by the ultraviolet lamp in the chamber (the lamp is "ON" from hours 5 to 10, 15 to 20, 25 to 30, etc. and "OFF" all other times). The rate of oxidation of the film is larger under UV illumination. When the lamp is turned off, the measured voltage drops by less than 0.3 millivolts. This corresponds to a temperature drop of <0.1°C (see text).

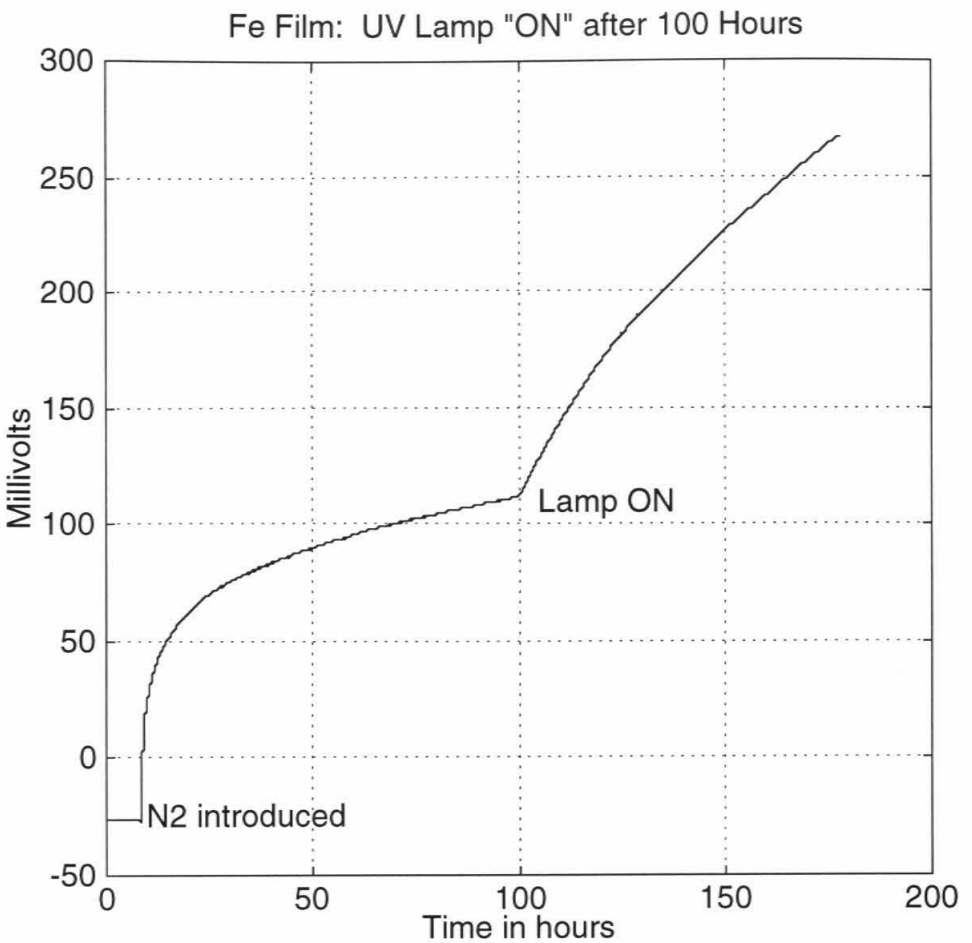

Figure 4.9: Iron film under vacuum for initial 8 hours of plot and under nitrogen after that time. Ultraviolet lamp turned "ON" at 100 hours. 0.0 millivolts corresponds to a film resistance of 101.4 ohms, and 1.0 ohm is approximately equivalent to 3 mV. The rate of oxidation increases by more than a factor of 6 once the ultraviolet lamp is turned "ON."

4.3 Interpretation

Three classes of results are evident from the data shown in figures 4.4 through 4.9. First, film resistances increase upon exposure to purge gases and air. Second, the application of ultraviolet radiation under high vacuum conditions results in a measured resistance which is higher, and the removal of the UV flux causes the measured resistance to drop. Third, exposure to ultraviolet photons while under the purge gas results in a higher rate of resistance increase as compared to the unexposed condition.

4.3.1 Purge Gases

The most likely explanation for the resistive changes upon exposure to the purge gases is a reaction between the clean metal surface and the oxidizing impurities in the gas stream to form a partial layer of oxide. The formation of this metal oxide, which is a poor conductor, leaves less of the metallic film available to conduct electrons across the circuit. As a consequence, the resistances of the films increase. In figure 4.5, increasing the pressures of the purge gas results in larger partial pressures of water vapor, oxygen, and other oxidizing species. Noticeable changes in the oxidation rate are observed with each successive addition of more gas. The final introduction of laboratory air into the chamber greatly enhances the oxidizing potential of the gases in contact with the metal surface and dramatically increases the rate of oxidation. It is also interesting to note that longer duration exposures to oxidizing gases results in resistance changes in two steps. The first is a rapid rise in resistance as exposed surfaces of the metal film are quickly (within minutes) converted to oxide. Once the initial phase is over, further oxidation of the film occurs at a much lower rate (see

figures 4.4a and 4.6). This is likely because the uppermost monolayer of metal is almost fully converted to oxide, and further oxidation is limited by diffusion. Electrons, or adsorbed electron receptors, need to migrate across the existing oxide layer to further increase the resistivity of the film. This process is slower than the initial rate of oxidation of a clean film, and this slower rate is represented in the data. These proof-of-concept experiments give us confidence in the usability of chemiresistors as a sensitive transducer for the state of oxidation on a surface.

4.3.2 Ultraviolet Lamp in a Vacuum

The application of these chemiresistors to the question of photo-stimulated oxidation on Mars is pursued by adding an ultraviolet lamp to the chamber. The mercury vapor lamp, which has a peak flux at 254 nm, can be activated without breaking the vacuum. At pressures of ~10^{-7} torr, periodic activation of the UV lamp (5 hours "ON" followed by 5 hours "OFF") results in the cyclic voltage pattern shown in figure 4.7. Voltage changes across the bridge circuit correspond to resistance variations: For this particular data set, 1 ohm is equivalent to approximately 4 millivolts. The interpretation of the rapid rise in resistance upon stimulation by ultraviolet radiation was initially attributed to the photoelectric effect. Photons incident on a clean metal surface in a vacuum will eject electrons if the radiation is at a sufficiently high energy level. We postulated that this effect removed enough electrons from the film to affect the apparent drift velocity and corresponding resistance. Upon further consideration, however, it appears more likely that the thermal stimulus from the lamp is responsible for the bulk of the resistance variations.

When the lamp is turned off or on, the time constant of the resistance change is on the order of tens of minutes which is suggestive of a thermal phenomenon. A quantum effect would most likely have a tighter temporal correlation with the stimulus (on the order of a second or less). A rough calculation using known physical properties of iron is also consistent with a thermal process. The ~6.5 millivolt drop in the signal when the lamp is turned "OFF" (see figure 4.7) is equivalent to a 1.6 ohm decrease in resistance (the absolute value is approximately 90 ohms). The temperature resistance coefficient of iron between 0° and 100°C is 0.0065/°C [Weast and Astle, 1981]. This means that the temperature of the film has to drop by less than 3°C to fully account for the apparent change in resistance. Given the bulb surface temperature (~90°C), the geometry of the apparatus (bulb to sample distance < 10 cm), and the mounting of the sample (minimal conductive heat paths), a 3°C drop in sample temperature when the lamp is deactivated does not seem unreasonable. Thus, the large changes in the signal correlated to the ultraviolet lamp "ON" times are most likely due to heating of the sample by the lamp and the temperature dependence of the film resistance.

Another aspect of the signal shown in figure 4.7, however, may or may not be a thermal effect. After the large rise in resistance after the lamp is initially turned "ON," the resistance of the film continues to climb while illuminated. The behavior of these parts of the signal is in contrast to the regions of the curve when the lamp is "OFF," where the resistance of the film remains constant (after the film cools to its equilibrium temperature). This rate of change of resistance, ~80 milliohms/hour, appears to be "permanent" and is not reversed when the photons are removed; it adds to the overall resistance of the film. Oxidation of the iron is the most likely cause of this observed increase in resistance. Whether the

oxidation is stimulated thermally or by the ultraviolet photons cannot be determined from the available data.

Some thoughts on the likelihood of the possible mechanisms can, however, be discussed. Chemical processes such as oxidation are typically exponentially dependent upon temperature. Using a reasonable range of activation energies, a 3°C increase in temperature, as calculated above, is unlikely to alter the reaction rate from near zero to 80 milliohms per hour. This is at least suggestive that a process other than one which is directly dependent upon temperature is responsible for the slope change. Photo-stimulated oxidation, however, is not the only possible explanation which can be postulated. Secondary thermal effects could also be possible. For example, the oxidation that occurs when the lamp is "ON" may eliminate the surfaces that are available for oxide formation at lower temperatures, and the 5 hours between the UV stimulus is insufficient to establish a "baseline" rate of oxidation under vacuum. This would result in a more dramatic difference in apparent oxidation rate than is truly occurring. Further experiments to isolate the effects of a slightly higher temperature when the lamp is "ON" need to be conducted.

4.3.3 Ultraviolet Lamp under "Dry" Nitrogen

With the addition of one atmosphere of ultra-high purity nitrogen, convective transport alters the thermal environment of the sample. Based on the measurements under vacuum, which show that the chemiresistor is very sensitive to temperature variations, some thermal constraints can be derived from the data in figure 4.8. Under nitrogen, the apparent resistance drops by less than 0.08 ohms (0.3 millivolts) when the lamp is turned off. Using the thermal resistance

coefficient for iron described above, the corresponding temperature change in the film is approximately 0.1°C. This value is consistent with the mounting geometry of the sample: It is not directly above the lamp, but offset approximately 10 cm, and convective eddies could rise unobstructed to the top of the chamber and dissipate.

Figure 4.9 shows the change in resistance when the lamp is turned on approximately 4 days after allowing the nitrogen purge gas to fill the chamber. Upon exposure to the UV photons, the slope of the curve changes by more than a factor of 6 (from 0.42 to 2.7 millivolts/hr, or from ~0.14 to ~0.9 ohms/hr). It is unlikely that this change in slope, which I interpret as a greater rate of oxidation of the iron film, is completely due to the inferred temperature change of 0.1°C. I, therefore, suggest that ultraviolet radiation-induced oxidation of this film could be occurring. The rate of oxidation when the lamp is "ON" is roughly a factor of 10 larger than the rate of oxidation when the lamp is "ON" with the sample under vacuum. This difference in rate is consistent with the larger quantity of oxidizing gas species that are available when the nitrogen purge is introduced to the chamber. This suggests that the process is not limited by the number of photons, but rather by the number of electron acceptors available at the surface of the sample. Further work, however, is necessary to confirm that the photochemical generation of gas phase reactive species is not responsible for the increased rate of oxidation when the lamp is "ON."

4.4 Postulated Mechanism

One possible pathway for photo-oxidation, if it is occurring, could be as follows: (a) The ultraviolet photons interact electronically with the metal film and mobilize charge carriers. (b) Some electrons migrate to the surface or are ejected photoelectrically and are captured by adsorbed oxidizing species residing on the surface of the film. (c) The electrostatic potential between a negatively charged ion at the surface and the net positive charge of the metal film draws the atoms together to form a bound oxide. This somewhat speculative process, thus, requires the presence of ultraviolet photons *and* adsorbed oxidants (see figure 4.10). The laboratory data presented here are not adequate to prove this conjecture, but they are consistent with it. In any case, a pure thermal process does not appear able to explain the observed behavior of these chemiresistors.

The first step of this postulated oxidation mechanism has supporting evidence. For example, it has been known for quite some time in the terrestrial sewage treatment industry that organic materials mixed with titanium dioxide can be decomposed upon exposure to ultraviolet photons. TiO_2 increases the capture cross section of the UV photons and liberates an electron-hole pair which starts a series of reactions resulting in the breakdown of complex organic molecules into inorganic compounds. See, for example, *Formenti et al.*, [1972]. *Chun et al.* [1978] have extended this oxidation process to Mars in an effort to explain the lack of organic molecules above the parts-per-million to parts-per-billion sensitivity limits of the Viking Lander gas chromatograph-mass spectrometer (GC-MS) [*Biemann et al.*, 1977]. *Stoker and Bullock* [1997] conducted experiments to show that ultraviolet photons could decompose organics under martian conditions without the presence of titanium dioxide. Thus, the

stimulation of chemical processes by UV photons at solid surfaces is not a new phenomena and might indeed have applicability to the weathering of material at the martian surface.

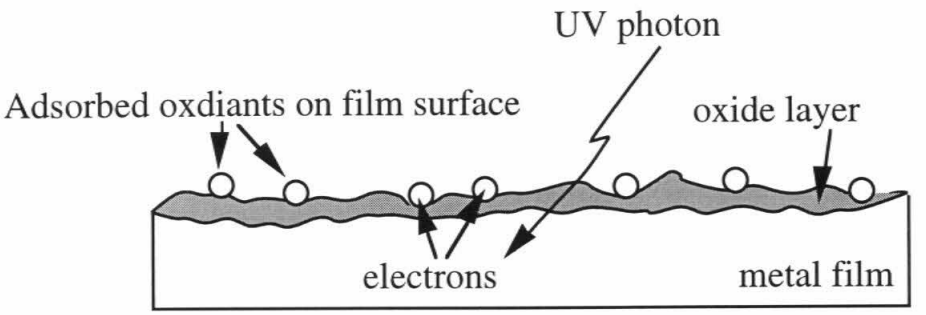

Figure 4.10: Conceptual sketch showing ultraviolet photons mobilizing electrons in the metal film which are subsequently captured by adsorbed oxidants on the surface to form a stable oxide.

4.5 Application to Mars

Models indicate that ultraviolet photons as short as 200 nm can penetrate to the martian surface at levels of approximately 10^{13} photons/cm^2/day/Å [*Kuhn and Atreya*, 1979]. Obliquity variations periodically cause the surface atmospheric pressures to drop as low as 0.3 mbar [*Ward et al.*, 1974]. This shortens the atmospheric path length available to absorb incoming UV photons and allows a greater radiation flux at the surface. *If* the observed resistance changes on the metal films in the laboratory are indeed the result of UV stimulation, what would it mean for the weathering of materials at the martian surface? Consider some "order of magnitude" estimates:

An approximation to figure 4.3a indicates that the resistance changes by a roughly a factor of 10 for every 10 Å in film thickness. Resistance of *thin* films are, by definition, not in the linear regime where resistance is proportional to length and cross sectional area. Conduction occurs across discrete islands of material rather than through a bulk continuous film. As thicknesses greater than several hundred angstroms are deposited, the gaps between the islands begin to be filled, and resistance changes proportional to cross section begins. The resistance change rates calculated above for a vacuum (80 milliohms/hour) and for nitrogen (900 milliohms/hour) correspond to approximately 10 nm/year and 100 nm/year, respectively. These values apply to the laboratory experiments where the UV energy incident per unit area is roughly 100 times larger than on Mars.

4.5.1 UV Weathering of Minerals

The biggest difference between the laboratory experiments and the surface of Mars, however, is that metallic iron is not the dominant constituent of the martian soil. Most minerals are excellent electrical insulators and the yield in generating charge carriers within the crystal which can migrate further than a local charge transfer between neighboring cations is low. For this order of magnitude estimate, we assume that the oxidation rate is dependent upon the ability to mobilize electrons which we further assume is directly related to the resistivity of the radiated material. Laboratory studies of iron-titanium oxides indicate electrical resistivities of 10^6 to 10^{10} ohm-cm at 200°C [*Lastovickova and Kropacek*, 1983]. Assuming a constant activation energy and extrapolating these results to lower temperatures using the Arrhenius' relation suggests resistivities larger than 10^{12} ohm-cm at 0°C. This value is approximately 17 orders of magnitude larger than the resistivity of metallic iron. Using the laboratory results for the iron film under nitrogen and these estimates for the UV flux and conductivity of materials at the martian surface, we obtain a rate of oxidation of 1 nm per 10^{17} years. This is clearly an irrelevant timescale for martian weathering.

We have taken a great number of liberties in the computation of this order-of-magnitude estimate. Non-linear effects which have not been considered may substantially change the result. Because eight or more orders of magnitude would have to be accounted for, this calculation suggest that photo-stimulated oxidation is not an applicable weathering process on Mars. This statement is consistent with the unweathered pyroxenes and feldspars observed by the Thermal Emission Spectrometer (TES) onboard Mars Global Surveyor [*Christensen et al.*, 1998]. The following three statements, however, add some uncertainties to this conclusion:

(1) TES data is obtained at wavelengths of ~6 to 50 μm, and consequently, the signal originates from and samples depths larger than the tens of nanometer scale that is relevant to surface oxidation. Ferric oxide coatings could form on these primary minerals without being observed by TES, and they could be eroded by aeolian processes to form local soils and to expose additional pristine material for further weathering.

(2) The laboratory experiments indicate that the rate of oxidation is greater under nitrogen than it is under vacuum. This indicates that the process is not photon limited, but rather more likely constrained by the availability of electron acceptors. If the process were photon limited, we would expect a similar or slightly greater rate of oxidation under vacuum. The martian soils evolve O_2 when humidified, and this characteristic has been attributed to the presence of superoxides in the surface materials [*Oyama and Berdahl*, 1977]. The availability of these species in the soil could greatly enhance the rate of oxidation relative to the calculations here which are based on the concentration of oxidants in ultra-high purity nitrogen.

(3) The bulk conductivity of minerals may not necessarily be the figure of merit in calculating rates of oxidation. Defects in the crystal structure which can trap charge carriers may increase the local residence time of holes and make the material more susceptible to charge assisted diffusion.

Thus, extrapolations from laboratory data suggest that photo-stimulated oxidation is not likely to be an effective weathering process for minerals on Mars, but additional work is necessary to firmly establish this conclusion (see chapter VI).

4.5.2 Weathering of Meteoritic Iron

The UV-stimulated oxidation of metallic iron, which I observed in these laboratory experiments, however, may be directly applicable to Mars. The ability to oxidize metallic iron in the absence of liquid water allows speculation about the source of the ferric iron component of the martian soil. Oxidation of impact fragments from metallic iron-containing meteorites in the presence of UV rather than aqueous chemical weathering could, in fact, be responsible for the fine particle sizes in the martian dust (~2.5 μm [*Pollack et al.,* 1979]). Furthermore, analyses of the oxidation rinds of nickel-iron meteorites indicate that maghemite is the primary weathering product [*Golden et al.,* 1995]. Thus, the UV-stimulated oxidation of metallic iron could be partially responsible for the maghemite detected in the martian soils by the Pathfinder magnetic properties experiment [*Hviid et al.,* 1997]. Additional discussion of this speculative idea can be found in section 5.2.

4.6 Conclusions

- New experiments establish thin-film chemiresistors as sensitive transducers for measuring the formation of oxide layers on metal films.

- These experiments show that the rate of oxidation increases when the metal films are exposed to stimulus from an ultraviolet lamp. The postulated mechanism for oxide formation involves the enhanced mobility of photo-stimulated electrons, the capture of electrons by adsorbed species on the film surface, and the bonding of iron and oxygen ions to form a layer of electrically resistive oxide. Theoretical calculations suggest that temperature changes of the film cannot fully account for the increased rate of oxidation. Further experimental studies, however, are necessary to confirm that thermal effects are, in fact, negligible.

- Based on the greater rate of oxidation under the nitrogen purge gas as compared to under vacuum, it is not believed that the process active in these experiments is limited by photons. Rather, the availability of oxidants appears to be the limiting factor. Additional experiments, however, are necessary to confirm that the photochemical generation of gas phase reactive species is not responsible for the increased rate of oxidation when the lamp is "ON."

- An "order of magnitude" calculation suggests that photo-stimulated oxidation would only account for the formation of 1 nanometer of ferric iron oxide in 10^{17} years on Mars. There are a large number of uncertainties in this estimate,

but if true, ultraviolet radiation-induced weathering of minerals on Mars is a negligible process.

- Ultraviolet radiation-stimulated oxidation of meteoritic iron could be responsible for the ferric iron component of the martian soils. Thus, the fine dust particles on Mars may not, in fact, be the product of aqueous chemical weathering of local minerals but rather derived from an exogenic source of iron.

Chapter V: Synthesis and Ideas

The conclusions from each set of experiments are discussed individually in chapters II, III, and IV. In this chapter, I extrapolate further from the experimental results and speculate about the implications for the nature and evolution of Mars' surface. These thoughts are guided largely by scientific intuition but are based on and consistent with the laboratory data. The conceptual models discussed below establish testable hypotheses and set the framework for future laboratory and spacecraft research.

The conventional view of martian soil as described in chapter I predicts abundant hydrated and oxidized minerals in the martian soil which formed as a result of interactions between liquid water and igneous rocks during past aqueous epochs. Contrary to this view, the research and analysis presented in this thesis suggests that chemical weathering under aqueous environments probably was never a significant process on the martian surface and that hydrated minerals did not form in abundance. Furthermore, the reddish-brown color, which is characteristic of Mars, is not necessarily the signature of Earth-like oxidation of minerals, but instead may result from UV-weathering of exogenic metallic iron.

5.1 Water on Mars

Chapter II concludes that the upper limit for the water content of the martian soil is 4% by weight. The 2% value suggested by the Viking Lander, or even much smaller quantities of evolvable water in the surface soils, could easily

be responsible for the broad, deep 3 μm features observed in reflectance spectra. Either Mars' surface has been dehydrated by its environment or abundant hydrous minerals never formed. The results of chapter III indicate that ultraviolet radiation is not capable of ejecting bound water from minerals on Mars over geologic timescales. Dry surface soils and the inability to determine a plausible mechanism for desiccating minerals, therefore, suggests that hydrated minerals never formed in large quantities on Mars. The Thermal/Evolved Gas Analysis (TEGA) instrument on the Mars Surveyor Lander will directly test the hypothesis that the soil minerals are relatively anhydrous (see chapter VI).

The presence of liquid water at the martian surface may have been too brief, too localized, or occurred at too low a temperature to result in appreciable weathering. The surface could have been episodically wet, but never globally warm enough for liquid water to be stable for long periods of time. This view of Mars is consistent with the new MGS TES results which indicate the presence of unweathered pyroxenes and feldspars on the surface [*Christensen et al.*, 1998] as well as with Mars Pathfinder images which show seemingly unweathered dark gray rocks that are mantled by a bright red dust [*Golombek et al.*, 1997] on a surface easily 2.5 billion years old. Catastrophic outflow channels, valley networks, and other fluvial features may have formed a protective ice cover soon after or during the major fluvial episodes which prevented atmospheric interaction and Earth-like chemical weathering. Furthermore, some atmospheric models indicate that there is no likely path from a warm (> 250°K mean global temperature) and wet (> 30 mbar surface pressure) martian past to present day conditions [*Haberle et al.*, 1994]. Thus, the frequently postulated 2 to 3 bars of CO_2 constituting an early, dense martian atmosphere with global temperatures high enough to sustain liquid water at the martian surface [*Pollack et al.*, 1987]

may, in fact, never have been present for the timescales required to form an abundance of hydrated mineral phases.

This possibility is also consistent with what is known about carbonate minerals. Liquid water exposures to a 2 to 3 bar carbon dioxide atmosphere would have resulted in the collapse of that atmosphere due to the formation of carbonates in less than 10^7 years [*Pollack et al.,* 1987]. The fact that TES has not yet found evidence of carbonates above the ~10% sensitivity limit of the instrument [*Christensen et al.*, 1998] also supports the idea that a thick CO_2 atmosphere (several bars) never interacted chemically with the surface to form significant carbonate deposits.

This hypothesis that Mars was never warm enough or wet enough to form large amounts of hydrated minerals at the surface can be pursued by determining the mineralogy of the martian soils. Knowledge of the mineralogy tightly constrains the formation environment for each particular sample. The TEGA instrument is designed to provide the necessary data (see chapter VI). Furthermore, subsurface analyses in regions that are believed to be ancient lake beds, such as areas of Valles Marineris that contain thick sequences of layered deposits [*Mckay and Nedell,* 1988], could help determine the true nature of the martian conditions at the time the postulated lakes were on Mars. Follow-on missions based on the DS2 penetrator could deliver the necessary instruments to the martian subsurface (see chapter VI).

5.2 The Color of Mars

Chapter IV concludes that the rate of oxidation of metallic iron increases upon exposure to ultraviolet radiation. Analyses of the oxidation rinds of nickel-iron meteorites indicate that maghemite is the primary weathering product [*Golden et al.,* 1995]. Metallic iron will also oxidize into maghemite under martian conditions [*Morris, personal communications*]. I suggest that the UV-stimulated oxidation of meteoritic iron in the presence of oxygen could be responsible for the maghemite component as well as the pigment of the martian soils.

The experiments indicate that a layer of iron 100 nanometers thick could be oxidized each year under laboratory conditions during exposure to ultraviolet radiation in the presence of an oxidant. The lower UV flux on Mars relative to the experiment could inhibit the oxidation rates by a factor of 100, but the higher concentration of oxidants could make up this difference. Martian soil is believed to have >1 PPM of a thermally labile and ~10 PPM of a thermally stable oxidant [*Zent and McKay*, 1994]. The purge gas used in the laboratory has sub-PPM levels of impurities, not all of which are oxidizing. Thus, the oxidation rate of metallic iron on Mars could, in fact, exceed what is observed in the laboratory. The limitations on Mars would then be the availability of iron surfaces exposed to UV. The vaporization and subsequent condensation and precipitation of impactors would provide a population of small particles with large total surface area for oxidation into maghemite. The moon has had a similar influx of metallic bodies and is also exposed to hard UV, but the absence of an oxidant on the moon is likely the reason for the color difference.

Based upon the experiments which indicate that iron films are effectively weathered to oxide upon exposure to ultraviolet photons, I postulate that exogenic metallic iron is converted to maghemite on Mars. This mechanism may help explain the 6% γ-Fe_2O_3 found in the martian soils by the Pathfinder magnetic properties experiment [*Hviid et al.*, 1997]. Furthermore, small quantities of a powerful pigmenting agent such as γ-Fe_2O_3 could be responsible for the color of Mars. This uniquely martian weathering process seems more plausible than hypothetical, global, aqueous formation of ferric minerals from martian rocks given the presence of unweathered pyroxenes and feldspars inferred from the TES data [*Christensen et al.*, 1998]. Further research should be conducted to confirm the likelihood of this idea (see chapter VI).

5.3 Summary

The experiments conducted in this thesis research indicate that the water content of the martian soil is a few percent by weight, that ultraviolet radiation can desorb water from the surfaces of mineral grains but cannot eject bound hydrogen, and that UV radiation in the presence of an oxidant can stimulate the oxidation of metallic iron but not minerals. Speculation about the nature of the martian surface based on these experimental results suggest that an abundant supply of hydrated minerals never formed at the martian surface and that aqueous episodes in Mars' history may have been under environmental conditions (temperature, duration, location, etc.) that prevented widespread chemical weathering. I also speculate that the formation of ferric oxides on Mars may have been derived from exogenic sources rather than local minerals. These ideas are in contrast with the conventional views of the martian soil published in the open literature. More experiments over the next decade such as the ones suggested in the next chapter will help assess the viability of these new ideas.

Chapter VI: Future Tests

The hypotheses proposed in the previous chapter have significant implications for our understanding of Mars' surface history. Much additional work is necessary to more firmly establish these somewhat speculative ideas, but they are indeed testable by a combination of laboratory experiments and new spacecraft data.

6.1 Laboratory Experiments

Some of the experiments described below are logical extensions of the existing experimental configurations. Others tests require different and possibly more sophisticated hardware. The goal of each of these experiments, however, is to further test and support the hypotheses described in chapter V.

6.1.1 Dehydration of Minerals

The story that I have presented on the history of water on Mars is based significantly on the inability to establish a plausible mechanism for dehydrating minerals under martian conditions. Neither the low vapor pressure of water in the atmosphere [*Pollack et al.,* 1970] nor ultraviolet photons (chapter III) is likely to convert a large initial supply of hydrated mineral phases to the current state of the martian soil. How firm are each of these two analyses? What other processes could possibly affect the retention of hydrogen by minerals? These questions

need to be addressed in future laboratory studies to increase confidence in the conclusions.

The work described in chapter III can be carried further in the laboratory to completely eliminate ultraviolet radiation as a possible desiccation mechanism. A shorter wavelength (higher energy) UV source should be used in the same experimental procedure. Photons at 190 to 200 nm can penetrate to the martian surface, but the current system uses a mercury vapor line source at 254 nm. The photodissociation threshold for water vapor occurs at 246 nm [*DeMore et al.*, 1994]; thus, shorter wavelengths might make a difference.

The removal of bound water by ultraviolet stimulation was only investigated for iron oxyhydroxides, and to some extent clay minerals. Other phases clearly need to be studied to have some confidence in the idea that abundant hydrated minerals never formed on Mars. Hydrated sulfates such as gypsum would be good candidates for further study. There is a high content of sulfur in the martian soils (~3%) [Clark et al., 1977] and initial suggestions of thermal emission spectra are consistent with sulfates [*Christensen, personal communications*]. The results of *Muhkin et al.*, [1996] which show photodecomposition of carbonates and sulfates to be an effective weathering process are in contrast with the experimental results of chapter III and clearly show that different minerals react differently to UV exposure. The use of other hydrated phases in this experiment is therefore necessary.

A number of other details should also be addressed in future experiments with the existing apparatus. The results of chapter III which indicate that water can be desorbed from the surfaces of mineral grains on Mars by incident

ultraviolet photons can be further pursued with improved techniques. A cold trap should be introduced to the chamber to verify that the observed water molecules evolved from the sample are not recycled. This would allow a more precise estimate of the quantity of water desorbed during UV illumination. Furthermore, given the results of chapter IV which indicate that small temperature changes in the sample can be generated by the lamp, the possibility of thermally induced desorption must be addressed (as suggested by an anonymous reviewer of the submitted manuscript). Varying the intensity of the lamp would help distinguish between a photon induced quantum process and a thermal one: Photo-desorption should scale linearly while a thermal process should vary almost exponentially with intensity.

One additional, useful test that might be performed with only small changes to the existing apparatus is to attempt to replicate the photodecomposition of carbonates demonstrated by *Muhkin et al.* [1996]. Why can UV apparently decompose carbonates with ease and yet have no observed effect on hydrates? Looking for CO_2 above calcite in a stainless steel chamber, however, could be a difficult experiment to do well. Regardless of the extent of baking, a seemingly endless supply of CO desorbs from the chamber walls when exposed to UV. Reactions between CO and other species in the chamber may easily enhance the mass 44 signal. Could it be possible that this is what Muhkin and coworkers observed?

6.1.2 Ultraviolet-Induced Oxidation

The experiments discussed in chapter IV suggest that the rate of oxidation of metallic iron increases upon exposure to ultraviolet radiation. Three aspects of

the work described in chapter IV, however, require further attention to establish greater confidence in the assertions made in chapter V: (1) Full characterization of the thermal effects on oxidation, (2) an understanding of the photochemical generation of oxidants in the chamber, and (3) a confirmation that the oxidation products of iron under martian conditions is, in fact, maghemite.

6.1.2.1 Thermal Effects

Temperature related uncertainties in the oxidation rates of iron under exposure to ultraviolet radiation can be alleviated relatively easily. A heater can be added in place of the ultraviolet lamp, and a thermocouple attached to the sample slide. Resistance trends could be collected at various heater power levels in an order to correlate resistivity variations with temperature. This experimental configuration would readily allow a comparison between thermally induced resistance trends and data from the ultraviolet lamp alone. A UV-stimulated phenomena could be isolated from thermal effects with this technique.

6.1.2.2 Photochemical Effects

Ultraviolet radiation has at least two possible effects in the context of the UV-stimulated oxidation experiments. It can induce oxidation through the mechanism described in section 4.4, or it can stimulate oxidation by photochemically generating short-lived reactive species. Further experiments should be performed to separate the two effects. The addition of a photon shield to prevent direct illumination of the sample could help determine if photochemistry is playing a significant role. If the rates of oxidation with and without the shield in place while the lamp is "ON" remains constant, then all of

the results discussed in section 4.3 result primarily from the photochemistry of trace gases in the chamber. These experiment can be further extended to include different gas phase compositions at different pressures including Mars-like conditions to test various photochemical ideas. The use of lamps of different wavelengths could also help increase the understanding of the chemical and physical processes occurring within the chamber.

6.1.2.3 Oxidation Products

The claim that metallic iron oxidizes to maghemite under martian conditions would be worthwhile to establish directly. Metallic iron films as well as iron-nickel films can be deposited using the electron-beam evaporator described in chapter IV. These samples can simulate the surfaces of iron-containing meteorites. The oxides that form on these metallic surfaces under exposure to different conditions could be analyzed by x-ray diffraction (XRD) techniques. The diffraction patterns for maghemite, hematite, and other iron oxides are distinct, and thus, the phase of the oxide could be determined. There is some concern, however, that a layer of oxide 10 Å thick may not provide enough of a signal to readily identify the mineral. XRD may only be the start of this analysis, other techniques, possibly Mossbauer spectroscopy, might be employed to fully characterize the resulting oxides.

6.2 Spacecraft Instruments

Much of what we know about the martian surface is based on data obtained from spacecraft missions. This will continue to be true in the years to

come. As the exploration of Mars evolves to include more landed science instruments, additional tests of the ideas related to the work presented in this thesis can be obtained.

6.2.1 Thermal Emission Spectrometer

The conclusion that abundant hydrated mineral phases will not be found at the martian surface can be initially addressed with an existing orbital instrument. The Thermal Emission Spectrometer (TES) onboard the Mars Global Surveyor spacecraft will continue to collect emission spectra and may be able to identify minerals other than the pyroxene and plagioclase which fit the data [*Christensen et al.*, 1998]. The direct, unambiguous detection of hydrated mineral phases using TES may remain elusive, but correlations between TES results and the Mars Orbiter Camera (MOC) images or the Mars Orbiter Laser Altimeter (MOLA) data could provide some insight into the history of water on Mars. If, for example, evaporite minerals such as gypsum were well contained in areas of high albedo, with suggestions of sedimentary layering, and in local topographic depressions, then convincing arguments for ancient lakes could be made. MGS can therefore provide a global perspective of the possible interactions between water and the surface, and can possibly help support the claim that liquid water was never stable at the martian surface for extended geologic time periods.

6.2.2 Thermal/Evolved Gas Analyzer (TEGA)

A more direct way to determine the mineralogy of the surface is to analyze samples in situ. The Thermal/Evolved Gas Analyzer (TEGA) onboard the Mars Surveyor lander that will be launched in January, 1999 will have the ability to

heat soils samples up to 1300°K and perform calorimetry and evolved gas analyses. The adsorbed and bound water content, as well as the mineral phases present, can be established by this instrument. Based on the experiments conducted in this thesis research, and upon our conclusion that UV radiation does not significantly impact the state of bound water in martian minerals, we expect minimal differences between the mineralogy at the immediate surface (top centimeter) as compared to samples obtained from depth (~50 cm). The quantity of ice and adsorbed water, however, could increase with depth. Furthermore, if the formation process for minerals at high latitudes is similar to those in the equatorial regions sampled by spacecraft-based reflectance spectrometers, then TEGA should find less than 4% water in hydrated minerals.

6.2.3 Deep Space 2

Imagers and spectrometers onboard orbiting spacecraft only obtain information about the uppermost materials of the martian surface (micrometers to millimeters). In contrast, the wheels of Pathfinder's rover were able to disturb some of the dust and sand to allow imaging of material beneath the immediate surface. The robotic arms of the Viking Landers were able to dig to a depth of approximately 20 centimeters. The arm associated with the TEGA instrument may be able to dig 50 cm beneath the surface. Understanding weathering and soil formation processes on Mars, however, requires access to greater depths, for both a knowledge of the intrinsic subsurface properties or of changes in characteristics from the surface to the subsurface.

It would be scientifically interesting to be able to send instruments to investigate, for example, the depths of the cryosphere at low and mid latitudes or

to the levels (kilometer depths) which might support liquid water. However, more realistic near-term goals would be to sample material from one to several meters beneath the surface. The New Millennium Deep Space 2 penetrators which will be flown as piggybacks onboard the January, 1999 launch of the Mars Surveyor lander will provide data from the subsurface (50 to 100 cm depth) related to the conclusions in this thesis. It will also demonstrate the technology for future penetrator missions.

The global inventory of water on Mars can be addressed by the evolved water analysis instrument on the DS2 spacecraft. This instrument actively collects a sample from outside the wall of the penetrator and heats it from ambient to at least 10°C and possibly to higher temperatures. Temperatures at the edge and center of the sample cup as well as spectroscopic data from the evolved gases will be collected to determine the quantity of ice in the sample. These penetrators will impact at a latitude of approximately 76° S, and thermal models suggest that ice is stable at depths less than 20 cm in these regions [*Paige and Keegan*, 1994]. The quantity of water on Mars, however, may not necessarily be sufficient to populate all regions in which ice is expected to be stable. The determination of the quantity of subsurface ice by the DS2 mission will further constrain the past and current inventories of water on Mars.

References

Allen, C. C. and J. L. Conca, Weathering of Basaltic Rocks Under Cold, Arid Conditions: Antarctica and Mars, *Proc. of Lunar and Plan. Sci. 21*, 711-717, 1991.

Allen, C. C., J. L. Gooding, M. Jercinovic, and K. Keil, Altered Basaltic Glass: A Terrestrial Analog to the Soil of Mars, *Icarus, 45*, 347-369, 1981.

Andersen, K. L. and R. H. Huguenin, Photodehydration of Martian Dust, *Bull. AAS, 9*, 449, 1977 (abstract).

Anderson, D.M. and A.R. Tice, The Analysis of Water in the Martian Regolith, *Journal of Molecular Evolution, 14,* 33-38, 1979.

Arvidson, R.E., J.L. Gooding, and H.J. Moore, The Martian Surface as Imaged, Sampled, and Analyzed by the Viking Landers, *Reviews of Geophysics, 27,* 39-60, 1989.

Athey, D. Personal Communications. AMETEK Corporation, Pittsburgh, PA. July, 1997.

Baird, A.K., A.J. Castro, B.C. Clark, P. Toulmin III, H. Rose Jr., K. Keil, and J.L. Gooding, The Viking X Ray Fluorescence Experiment: Sampling Strategies and Laboratory Simulations, *J. Geophys. Res.*, *82*, 4595-4624, 1977.

Ballou, E.V., P.C. Wood, T. Wydeven, M.E. Lehwalt, and R.E. Mack, Chemical Interpretation of Viking Lander 1 Life Detection Experiment, *Nature, 271*, 644-645, 1978.

Banin, A. and L. Margulies, Simulation of Viking Biology Experiments Suggests Smectites not Palagonites as Martian Soil Analogues, *Nature*, *305*, 523-526, 1983.

Banin, A., T. Ben-Shlomo, L. Margulies, D.F. Blake, R.L. Mancinelli, and A.U. Gehring, The Nanophase Iron Mineral(s) in Mars Soil, *J. Geophys. Res.*, *98*, 20,831-20,853, 1993.

Bell, J.F., III, R.V. Morris, and J.B. Adams, Thermally Altered Palagonitic Tephra: A Spectral and Process Analog to the Soil and Dust of Mars, *J. Geophys. Res.*, *98*, 3373-3385, 1993.

Bibring, J.P., M. Combes, Y. Langevin, C. Cara, P. Drossart, T. Encrenaz, S. Erard, O. Forni, B. Gondet, L. Ksanfomaliti, E. Lellouch, P. Masson, V. Moroz, F. Rocard, J. Rosenqvist, C. Sotin, and A. Soufflot, ISM Observations of Mars and Phobos: First Results, in *Proceedings of the 20th Lunar and Planetary Science Conference*, pp. 461-471, Lunar and Planetary Institute, Houston, 1990.

Biemann, K., J. Oro, P. Toulmin III, L. E. Orgel, A. O. Nier, D. M. Anderson, P. G. Simmonds, D. Flory, A. V. Diaz, D. R. Rushneck, J. E. Biller, and A. L.

Lafleur, The Search for Organic Substances and Inorganic Volatile Compounds in the Surface of Mars, *J. Geophys. Res., 82,* 4641-4658, 1977.

Bishop, J.L., C.M. Pieters, and R.G. Burns, Reflectance and Mossbauer Spectroscopy of Ferrihydrite-Montmorillonite Assemblages as Mars Soil Analog Materials, *Geochimica et Cosmoch. Acta, 57,* 4583-4595, 1993.

Blackburn, T. R., H. D. Holland, G. P. Ceasar, Viking Gas Exchange Reaction: Simulation on UV-Irradiated Manganese Dioxide Substrate, *J. Geophys. Res, 84,* 8391-8394, 1979.

Booth, M. C. and H. H. Kieffer, Carbonate Formation in Mars Like Environments, *J. Geophys. Res., 83,* 1809-1815, 1978.

Bullock, M. A., C. R. Stoker, C. P. McKay, and A. P. Zent, A Coupled Soil-Atmosphere Model of H2O2 on Mars, *Icarus, 107,* 142-154, 1994.

Burns, R. G., Rates and Mechanisms of Chemical Weathering of Ferromagnesian Silicate Minerals on Mars, *Geochimica et Cosmochimica Acta, 57,* 4555-4574, 1993.

Burns, R.G. and D.S. Fisher, Rates of Oxidative Weathering on the Surface of Mars, *J. Geophys. Res., 98,* 3365-3372, 1993.

Burns, R.G., Gossans on Mars, in *Proceedings of the 18th LPSC,* 713-721, Lunar and Planetary Institute, Houston, 1988.

Calvin, W.M., Variation of the 3-mm Absorption Feature on Mars: Observations over Eastern Valles Marineris by the Mariner 6 Infrared Spectrometer, *J. Geophys. Res., 102,* 9097-9107, 1997.

Carr, M.H., *Water on Mars,* 229 pp., Oxford University Press, New York, 1996.

Christensen, P. R. Personal communications. LPSC 1998.

Christensen, P. R., D. L. Anderson, S. C. Chase, R. T. Clancy, R. N. Clark, B. J. Conrath, H. H. Kieffer, R. O. Kuzmin, M. C. Malin, J. C. Pearl, T. L. Roush, and M. D. Smith, Results from the Mars Global Surveyor Thermal Emission Spectrometer, *Science, 279,* 1692-1698, 1998.

Chun, S. F. S., K. D. Pang, J. A. Cutts, J. M. Ajello, Photocatalytic Oxidation of Organic Compounds on Mars, *Nature, 274,* 875-876, 1978.

Clark, B. C. III, A. K. Baird, H. J. Rose, Jr., P. Toulmin III, R. P. Christian, W. C. Kelliher, A. J. Castro, C. D. Rowe, K. Kiel, and G. R. Huss, The Viking X-Ray Fluorescence Experiment: Analytical Methods and Early Results, *J. Geophys. Res., 82,* 4577-4594, 1977.

Clark, R.N. and T.L. Roush, Reflectance Spectroscopy: Quantitative Analysis Techniques for Remote Sensing Applications, *J. Geophys. Res., 89,* 6329-6340, 1984.

Craddock, R. A., and T. A. Maxwell, Geomorphic evolution of the Martian Highlands through Ancient Fluvial Processes, *J. Geophys. Res., 98,* 3453-3468, 1993.

Dalton, J. B. and R. N. Clark, Detection Limits of Martian Clays, *Bulletin AAS, 27,* 1090, 1995 (abstract).

De Bruyn, C.M.A. and H.W. van der Marel, Mineralogical Analysis of Soil Clays, *Geologie en Mijnbouw, 16,* 69-83, 1954.

DeMore, W. B., S. P. Sander, D. M. Bolden, R. F. Hampson, M. J. Kurylo, C. J. Howard, A. R. Ravishankara, C. E. Kolb, M. J. Molina, Chemical Kinetics and Photochemical Data for Use in Stratospheric Modelling, JPL Publication 94-26, 1994.

Erard, S. and W. Calvin, New Composite Spectra of Mars, 0.4 - 5.7 μm, *Icarus, 130,* 449-460, 1997.

Erard, S. Personal communications. Fall 1997.

Erard, S., J. Mustard, S. Murchie, J.P. Bibring, P. Cerroni, A. Coradini, Martian Aerosols: Near-Infrared Spectral Properties and Effects on the Observation of the Surface, *Icarus, 111,* 317-337, 1994.

Erard, S., J.P. Bibring, J. Mustard, O. Forni, J.W. Head, S. Hurtrez, Y. Langevin, C.M Pieters, J. Rosenqvist, and C. Sotin, Spatial Variations in Composition of the Valles Marineris and Isidis Planitia Regions of Mars Derived from ISM Data, in *Proceedings of Lunar and Planetary Science, Volume 21*, pp. 437-455, Lunar and Planetary Institute, Houston, 1991.

Formenti, M., F. Juillet, P. Meriaudeau, S. J. Teichner, and P. J. Vergnon, *J. Colloid Interface Sci., 39*, 79-89, 1972.

Golden, D. C., D. W. Ming, M. E. Zolensky, Chemistry and Mineralogy of Oxidation Products on the Surface of the Noba Nickel-iron Meteorite, *Meteoritics, 30,* 418-422, 1995.

Golombek, M. P., R. A. Cook, T. Economou, W. M. Folkner, A. F. C. Haldemann, P. H. Kallemeyn, J. M. Knudsen, R. M. Manning, H. J. Moore, T. J. Parker, R. Rieder, J. T. Schofield, P. H. Smith, and R. M. Vaughn, Overview of the Mars Pathfinder Mission and Assessment of Landing Site Predictions, *Science, 278,* 1743-1748, 1997.

Gooding, J. L., R. E. Arvidson, M. Y. Zolotov, Physical and Chemical Weathering, in *Mars*, edited by H. H. Kieffer, B. M. Jakosky, C. W. Snyder, and M. S. Matthews, pp. 626-651, Univ. of Ariz. Press, Tucson, 1992.

Gooding, J. L., Soil mineralogy and chemistry on Mars: Possible Clues from Salts and Clays in SNC Meteorites, *Icarus, 99,* 28-41, 1992.

Gooding, J.L. and K. Keil, Alteration of Glass as a Possible Source of Clay Minerals on Mars, *Geophys. Res. Letters, 5*, 727-730, 1978.

Greeley, R., N. Lancaster, S. Lee, and P. Thomas, Martian Aeolian Processes, Sediments, and Features, in *Mars*, edited by H.H. Kieffer, B.M. Jakosky, C.W. Snyder, and M.S. Matthews, pp. 730-766, Univ. of Ariz. Press, Tucson, 1992.

Grunthaner, F. J., A. J. Ricco, M. A. Butler, A. L. Lane, C. P. McKay, A. P. Zent, R. C. Quinn, B. Murray, H. P. Klein, G. V. Levin, R. W. Terhune, M. L. Homer, A. Ksendzov, P. Niedermann, Investigating the Surface Chemistry of Mars, *Analytical Chem., 67*, 605A-610A, 1995.

Haberle, R. M., D. Tyler, C. P. McKay, A Model for the Evolution of CO2 on Mars, *Icarus, 109,* 102-120, 1994.

Hapke, B., *Theory of Reflectance and Emittance Spectroscopy*, pp. 318-324, Cambridge Univ. Press, 1993.

Hargraves, R. B., D. W. Collinson, R. E. Arvidson, and C. R. Spitzer, The Viking Magnetic Properties Experiment: Primary Mission Results, *JGR, 82*, 4547-4558, 1977.

Houck, J.R., J.B. Pollack, C. Sagan, D. Schaack, and J.A. Decker Jr., High Altitude Infrared Spectroscopic Evidence for Bound Water on Mars, *Icarus, 18*, 470-480, 1973.

Huguenin, R. L., Formation of Goethite and Hydrated Clay Minerals on Mars, *JGR, 79*, 3895-3905, 1974.

Huguenin, R. L., Photo-stimulated Oxidation of Magnetite: 1. Kinetics and Alteration Phase Identification, *JGR, 78*, 8481-8493, 1973a.

Huguenin, R. L., Photo-stimulated Oxidation of Magnetite: 2. Mechanism, *JGR, 78*, 8495-8506, 1973b.

Hunten, D. M., Possible Oxidant Sources in the Atmosphere and Surface of Mars, *J. Mol. Evol., 14,* 71-78, 1979.

Hviid, S. F., M. B. Madsen, H. P. Gunnlaugsson, W. Goetz, J. M. Knudsen, R. B. Hargraves, P. Smith, D. Britt, A. R. Dinesen, C. T. Mogensen, M. Olsen, C. T. Pedersen, and L. Vistisen, Magnetic Properties Experiments on the Mars Pathfinder Lander: Preliminary Results, *Science, 278,* 1768-1770, 1997.

Ingersoll, A.P., Mars: Occurrence of Liquid Water, *Science, 168*, 972-973, 1970.

Jakosky, B. M, A. P. Zent, and R. W. Zurek, The Mars Water Cycle: Determining the Role of Exchange with Regolith, *Icarus, 130*, 87-95, 1997.

Jakosky, B.M., The Seasonal Cycle of Water on Mars, *Space Science Reviews, 41*, 131-200, 1985.

Kortum, G. *Reflectance Spectroscopy,* Springer-Verlag New York Inc., 1969.

Kuhn, W. R. and S. K. Atreya, Solar Radiation Incident on the Martian Surface, *J. of Molecular Evolution, 14,* 57-64, 1979.

Lastovickova, M. and V. Kropacek, Electrical Conductivity of Fe-Ti-O Minerals in Connection with Oxidation Processes, *J. Geomag. Geoelectr., 35*, 777-786, 1983.

Levin, G. V. and P. A. Straat, Recent Results from the Viking Labeled Release Experiment on Mars, *J. Geophys. Res., 82,* 4663-4667, 1977.

Madey, T. E., History of Desorption Induced by Electronic Transitions, *Surface Science, 299/300*, 824-836, 1994.

Manning, C., J. Lamb, R. Williams, F. Pool, Mars Oxidant Experiment (MOx) Instrument Fabrication Overview and Films Report, JPL internal report, 1997.

McCord, T. B., R. N. Clark, and R. B. Singer, Mars: Near-Infrared Spectral Reflectance of Surface Regions and Compositional Implications, *J. Geophys. Res., 87*, 3021-3032, 1982.

McKay, C. P. and S. S. Nedell, Carbonates in the Valles Marineris, *Icarus, 73,* 142-148, 1988.

Moroz, V.I., The Infrared Spectrum of Mars (1.1 - 4.1 μm), *Astronomicheskii zhurnal, 41*, 350, 1964.

Morris, R. L. and H. V. Lauer, Jr., The Case Against UV Photo-stimulated Oxidation of Magnetite, *Geophys. Res. Lett., 7,* 605-608, 1980.

Morris, R. V. Personal communications. LPSC 1998.

Morris, R. V., and H. V. Lauer, Jr., Stability of Goethite and Lepidocrocite to Dehydration by UV Radiation: Implications for their Occurrence on the Martian Surface, *JGR, 100,* 10893-10899, 1981.

Morris, R.V., H.V. Lauer, Jr., J.L. Gooding, and W.W. Mendell, Spectral Evidence and Implications for the Occurrence of Aluminous Iron Oxides on Mars, *LPSC XIV*, 526-527 (abstract), 1983.

Morris, R.V., J.L. Gooding, H.V. Lauer, Jr., R.B. Singer, Origins of Marslike Spectral and Magnetic Properties of a Hawaiian Palagonitic Soil, *J. Geophys. Res., 95*, 14,427-14,434, 1990.

Muhkin, L. M., A. P. Koscheev, Y. P. Dikov, J. Huth, and H. Wanke, Experimental Simulations of the Photodecomposition of Carbonates and Sulphates on Mars, *Nature, 379*, 141-143, 1996.

Murchie, S., J. Mustard, J. Bishop, J. Head, C. Pieters, and S. Erard, Spatial Variations in the Spectral Properties of Bright Regions on Mars, *Icarus, 105*, 454-468, 1993.

Murchie, S., L. Kirkland, S. Erard, J. Mustard, and M. Robinson, NIR Spectral Variations on Mars from ISM Imaging Spectrometer Data: Evidence for Lithological Variations of the Surface Layer, submitted to *Icarus*, 1997.

Mustard, J.F. and J.F. Bell III, New Composite Reflectance Spectra of Mars from 0.4 to 3.14 μm, *Geophys. Res. Lett, 21*, 353-356, 1994.

Mustard, J.F., S. Erard, J.P. Bibring, J.W. Head, S. Hurtrez, Y. Langevin, C.M. Pieters, and C.J. Sotin, The Surface of Syrtis Major: Composition of the Volcanic Substrate and Mixing with Altered Dust and Soil, *J. Geophys. Res., 98*, 3387-3400, 1993.

Newsom, H. E., Hydrothermal Alteration of Impact Melt Sheets with Implications for Mars, *Icarus, 44,* 207-216, 1980.

Oyama, V. I. and B. J. Berdahl, The Viking Gas Exchange Experiment Results from Chryse and Utopia Surface Samples, *J. Geophys. Res., 82*, 4669-4676, 1977.

Paige, D. A., and K. D. Keegan, Thermal and Albedo Mapping of the Polar Regions of Mars using Viking Thermal Mapper Observations, *J. Geophys. Res., 99,* 25,993-26,013, 1994.

Palluconi, F.D. and H.H. Kieffer, Thermal Inertia Mapping of Mars from 60°S to 60°N, *Icarus, 45*, 415-426, 1981.

Pimentel, G.C., P.B. Forney, and K.C. Herr, Evidence about Hydrate and Solid Water in the Martian Surface from the 1969 Mariner Infrared Spectrometer, *J. Geophys. Res., 79*, 1623-1634, 1974.

Pollack, J. B., J. F. Kasting, S. M. Richardson, K. Poliakoff, The Case for a Wet, Warm Climate on Early Mars, *Icarus, 71,* 203-224, 1987.

Pollack, J. B., R. N. Wilson, and G. G. Goles, A Re-Examination of the Stability of Goethite on Mars, *JGR, 75,* 7491-7500, 1970.

Pollack, J.B., D.S. Colburn, F.M. Flasar, R. Kahn, C.E. Carlston, and D.C. Pidek, Properties and Effects of Dust Particles Suspended in the Martian Atmosphere, *J. Geophys. Res., 84*, 2929-2945, 1979.

Sharp, R.P. and M.C. Malin, Surface Geology from Viking Landers on Mars: A Second Look, *GSA Bulletin, 95*, 1398-1412, 1984.

Sharp, R.P., Kelso Dunes, Mojave Desert, California, *GSA Bulletin, 77,* 1045-1074, 1966.

Singer, R.B., Spectral Evidence for the Mineralogy of High-Albedo Soils and Dust on Mars, *J. Geophys. Res., 87*, 10,159-10,168, 1982.

Sinton, W.M., On the Composition of Martian Surface Materials, *Icarus, 6*, 222-228, 1967.

Smith, P. H., J. F. Bell III, N. T. Bridges, D. T. Britt, L. Gaddis, et al., Results from the Mars Pathfinder Camera, *Science, 278*, 1758-1765, 1997.

Soderblom, L. A. and D. B. Wenner, Possible Fossil H2O Liquid-Ice Interfaces in the Martian Crust, *Icarus, 34,* 622-637, 1978.

Soderblom, L.A., The Composition and Mineralogy of the Martian Surface from Spectroscopic Observations: 0.3 μm to 50 μm, in *Mars*, edited by H.H.

Kieffer, B.M. Jakosky, C.W. Snyder, and M.S. Matthews, pp. 557-593, Univ. of Ariz. Press, Tucson, 1992.

Soffen, G. A., The Viking project, *J. Geophys. Res., 82,* 3959-3970, 1977.

Stoker, C. R. and M. A. Bullock, Organic Degradation under Simulated Martian Conditions, *J. Geophys. Res., 102,* 10,881- 10,888, 1997.

Toulmin, P., III, A.K Baird, B.C. Clark, K. Keil, H.J. Rose, Jr., R.P. Christian, P.H. Evans, and W.C. Kelliher, Geochemical and Mineralogical Interpretation of the Viking Inorganic Chemical Results, *J. Geophys. Res., 82,* 4625-4634, 1977.

Van der Marel, H.W. and H. Beutelspacher, *Atlas of Infrared Spectroscopy of Clay Minerals and their Admixtures*, pp. 249-253, Elsevier Scientific Publishing Co., 1976.

Wagner, C. D., W. M. Riggs, L. E. Davis, J. F. Moulder, and G. E. Muilenberg (editor), Handbook of X-Ray Photoelectron Spectroscopy, Perkin-Elmer Physical Electronics Division, 1978.

Ward, W. R., B. C. Murray, and M. C. Malin, Climatic Variations on Mars, 2. Evolution of Carbon Dioxide Atmosphere and Polar Caps, *J. Geophys. Res., 79,* 3387-3395, 1974.

Weast, R. C. and M. J. Astle, eds. *CRC Handbook of Chemistry and Physics*, CRC Press, Inc., Boca Raton, Florida, p. F-135, 1981.

Westley, M. S., R. A. Baragiola, R. E. Johnson, and G. A. Baratta, Ultraviolet Photodesorption from Water Ice, *Planet. Space Sci., 43*, 1311-1315, 1995.

Yen, A. S., B. C. Murray, and G. R. Rossman, Water Content of the Martian Soil: Laboratory Simulations of Reflectance Spectra, *J. Geophys. Res.*, in press.

Zent, A. P. and C. P. McKay, The Chemical Reactivity of the Martian Soil and Implications for Future Missions, *Icarus, 108,* 146-157, 1994.

Zent, A. P., R. M. Haberle, H. C. Houben, and B. M. Jakosky, A Coupled Subsurface-Boundary Layer Model of Water on Mars, *JGR, 98,* 3319-3337, 1993.

Zent, A.P. and R.C. Quinn, Measurement of H_2O Adsorption Under Mars-like Conditions: Effects of Adsorbent Heterogeneity, *J. Geophys. Res., 102*, 9085-9095, 1997.

Zolotov, M.Y., Y.I. Sidorov, V.P. Volkov, M.V. Borisov, and I.L. Khodakovsky, Mineral Composition of Martian Regolith: Thermodynamic Assessment, *LPSC XIV*, 883-334, 1983.